UNIVERSITÀ DI PARMA

UNIVERSITÀ DEGLI STUDI DI PARMA

DOTTORATO DI RICERCA IN MATEMATICA

CICLO XXXV

Swarm and consensus based methods for global optimization: mean-field convergence and applications to machine learning

---

Coordinatore:
Prof. Alessandra Lunardi

Tutore:
Prof. Lorenzo Pareschi

Dottoranda: **Dott.ssa Sara Grassi**

Anni Accademici 2019/2020 - 2021/2022

Acknowledgement

I express my sincere thanks to the University of Ferrara and especially to Prof. Lorenzo Pareschi, who supervised me during my PhD and introduced me to the wonderful research topic of swarm intelligence and consensus-based optimization, which led to the writing of two articles and a survey in collaboration with Prof. Lorenzo Pareschi, Prof. Hui Huang, Prof. Jinniao Qiu and Dr. Giacomo Borghi. I also take this opportunity to thank Giacomo for his support and collaboration in both research and teaching activities. I am very grateful to my family for being there for me in times of distress and always supporting me. I also thank the University of Parma and the Emilia Romagna region for financially supporting my PhD and finally Prof. Alessandra Lunardi for her coordination work over these three years. It has been a pleasure to collaborate with each of you.

Abstract

High dimensional optimization problems with a non-convex cost function are a popular topic in various disciplines today ranging from signal/image processing to machine learning. In addition to the well-known gradient based methods, another popular class of methods for dealing with such large scale optimization problems is the so-called metaheuristics. In this thesis, we will focus on a subclass of metaheuristic methods based on the notion of *swarm intelligence*. More precisely, we will consider particle swarm optimization (PSO) and consensus-based optimization (CBO) methods, i.e. two methods that exploit the collective iterations between a number of agents populating the domain of the cost function to be minimized. Each agent balances the tendency to explore the search space and the tendency to share position (and velocity) information. While the CBO method have been formulated in terms of a system of first-order stochastic differential equations (SDEs), in this thesis we introduce a novel formulation for the PSO method through a second-order system of SDEs. This allows us not only to design more general PSO methods with better performances, but also to rigorously study, at the cost of mild assumptions on the cost function, its mean-field convergence and small inertia limits, thus providing a robust mathematical theory and clarifying the relationships between the two methods. As a side result of our analysis, we derive a novel consensus based method with memory effects, which keeps track of the best position each particle has encountered throughout its history. We then further discuss implementation aspects, trying to improve numerical performance with the introduction of a random selection technique which greatly improve the efficiency of the methods. We demonstrate the convergence of the solution to the global minimizer even in this latter case. In addition to common benchmark problems we apply the resulting algorithms to three important application problems: image segmentation, function approximation and character classification on the MNIST dataset.

Table of Contents

1 Introduction **1**

2 From particle swarm optimization to consensus based optimization **7**

2.1 Stochastic differential models for particle swarm optimization 7

2.1.1 The original PSO method 8

2.1.2 The stochastic differential PSO system 9

2.1.3 Stochastic differential PSO model with inertia 10

2.2 Mean-field description of particle swarm optimization 11

2.2.1 Regularized PSO dynamic without memory effects 12

2.2.2 Regularized PSO dynamic with memory and local best 14

2.3 Small inertia limit of particle swarm optimization 15

2.3.1 The case without memory effects 15

2.3.2 The general case with memory 18

2.4 Numerical examples 19

2.4.1 Validation of the mean field limit 20

2.4.2 Numerical small inertia limit 28

2.4.3 Comparison on high dimensional test cases 31

2.5 Concluding remarks 38

3 Theoretical analysis: mean-field convergence and small inertia limit **39**

3.1 Mean-field limit of particle swarm optimization 39

3.1.1 Theoretical analysis on PSO dynamics without memory effects . 40

3.1.2 Theoretical analysis on PSO dynamic with memory and local best 48

3.2 Zero-inertia limit and consensus-based optimization 49

3.2.1 The case without memory effects 50

3.2.2 The general case with memory 62

3.3 Convergence to the global minimum 64

3.4 Concluding remarks 72

4 Consensus based optimization with memory and random selection 73
4.1 Consensus-based optimization with memory effects 73
4.1.1 Particles update rule 74
4.1.2 Random selection strategy 75
4.1.3 Comparison with CBO and PSO 77
4.2 Numerical results 78
4.3 Tests on benchmark problems 79
4.4 Theoretical analysis 83
4.4.1 Mean-field approximation 84
4.4.2 Convergence in mean-field law 86
4.4.3 Random selection analysis 89
4.5 Proofs 91
4.5.1 Notation and auxiliary lemmas 91
4.5.2 Proof of Proposition 4.4.1 93
4.5.3 Proof of Theorem 4.1 95
4.5.4 Proof of Proposition 4.4.2 and Theorem 4.2 98
4.6 Concluding remarks 103

5 Applications to image segmentation and machine learning 104
5.1 Image segmentation 105
5.2 Approximating functions with NN 108
5.3 Application on MNIST dataset 109
5.4 Concluding remarks 115

A Appendices 117
A1 Benchmark functions 117

Chapter 1

Introduction

One of the main challenges in various disciplines such as science, engineering, economics, and even medicine is how to deal with the global optimization of a high dimensional problem in which you provide a representation of it through a mathematical model and then look for an optimal value for a non convex cost function that describes it. In the literature, the most popular optimization problems are related to operation research, such as the traveling salesman problem (TSP) [72] and the knapsack problem [31], to signal and image processing, such as compression, denoising, segmentation [6] problems and more recently to machine and deep learning [11]. For the sake of simplicity, we will concentrate in the course of this thesis exclusively on finding the minimums, turning the eventual maximization of a cost function $\mathcal{F}$ into the equivalent minimization of $-\mathcal{F}$. More specifically we are interested in finding:

$$x^* \in \operatorname*{argmin}_{x \in \mathbb{R}^d} \mathcal{F}(x)\,, \tag{1.1}$$

where $\mathcal{F}(x) : \mathbb{R}^d \to \mathbb{R}$ is a given continuous, high-dimensional, non convex (possibly non smooth) cost function. In particular, both statistical estimation and machine learning consider the problem of minimizing an objective function in the form of a sum [11, 44, 98]

$$\mathcal{F}(x) = \frac{1}{n} \sum_{i=1}^{n} \mathcal{F}_i(x). \tag{1.2}$$

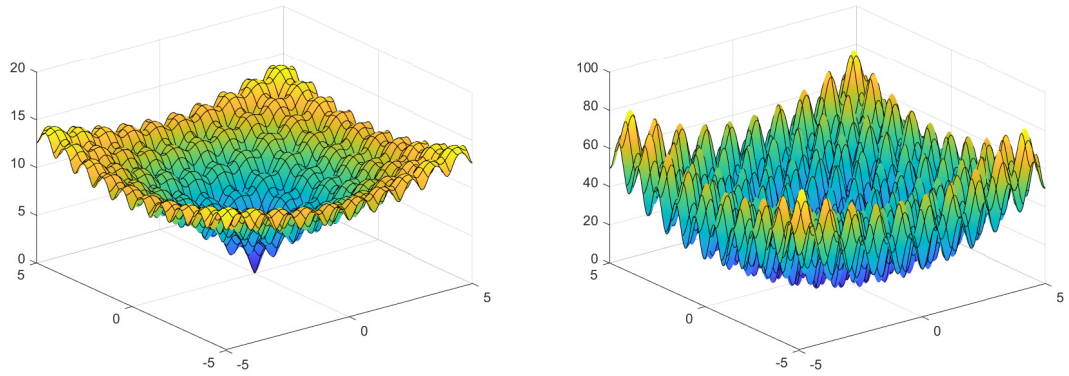

Figure 1.1: Examples of benchmark functions for global optimization in two dimensions: Ackley function (left) and Rastrigin function (right).

Gradient methods have dominated for years, especially in applications, due to their simplicity and the fact that in a century since their first formulations, it has been possible to work on their mathematical and algorithmic enhancements. This type of methods relies on improving the initial solution of the algorithm through several steps (in the gradient descent direction) rather than randomly exploring the domain or search space. For example, the *steepest gradient descent* works starting from a value x_0, in the neighborhood of which the cost function $\mathcal{F}$ must be differentiable and getting values $x_1, x_2, x_3, \ldots$ step by step, following:

$$x_{n+1} = x_n - \gamma \nabla \mathcal{F}(x_n), \tag{1.3}$$

where $\mathcal{F}(x_n) \geq \mathcal{F}(x_{n+1}),\ n = 1, 2, 3, \ldots$ and $\gamma \in \mathbb{R}_+$ is called learning rate and usually changes at each iteration. However, gradient methods can have some drawbacks, for example they encounter difficulties when approached to non-differentiable problems, which will have to be reformulated or replaced by a more tractable approximation, at the cost of loss of accuracy. Other disadvantages are the computation of the gradient that sometimes becomes very expensive in terms of time and memory and the lack of convergence proofs towards a global minimizer for non convex problems.

On the other side, a different approach to global optimization problems is based on metaheuristics [3, 7, 69, 78]. These algorithms are inspired by some analogies with the physical nature and do not require the computation of gradients of the cost function (derivative-free optimization methods). For example in *simulated annealing* [1, 55, 68] we compare the process of solving a combinatorial optimization problem, where we iteratively move from one admissible solution to another, gradually improving the objective function, to the process by which a gas, as it cooled down, moves into configurations with progressively lower energy content or in *genetic algorithms* [54], where a set of

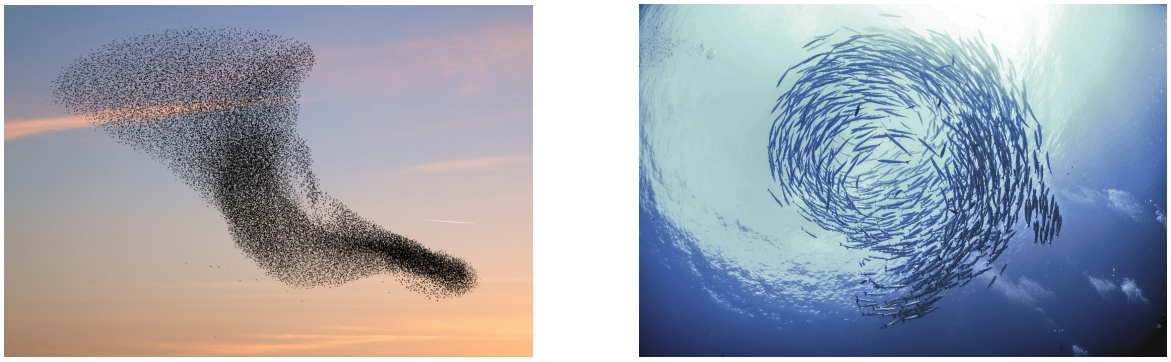

Figure 1.2: Metaheuristic optimization methods are inspired by nature, as in the collective behavior of flocks of birds (left) or schools of fish (right)[1].

eligible solutions is seen as a set of individuals in a population that, by mating and combining with each other, produce new solutions that may result better than those from which they were generated. Other examples of metaheuristics are given by *evolutionary programming* [38], *Metropolis-Hastings sampling algorithm* [53], *ant colony optimization* [33]. In general, these types of algorithms try to combine two important aspects such as the exploitation of acquired knowledge about the solution with consequent alignment towards the optimal directions and the simultaneous exploration of the search domain, in order to archive global optimal solutions within acceptable search time at reasonable computational cost [75, 80]. Despite the simplicity, most metaheuristics can not be analyzed rigorously as they lack a formal mathematical description [8, 17, 85, 89, 100, 105]. Unlike gradient-based methods in a convex search space, meta-heuristic methods do not necessarily guarantee to find global optimal solutions, but are capable of finding many good solutions that are sometimes sufficient in practical applications.

In this thesis we will focus on metaheuristic methods based on the notion of *swarm intelligence*, a category of metaheuristics initially proposed to model the intelligent behaviour of flocks of birds or fish schools [13, 25, 29, 77, 92] and of which the eldest is probably the *particle swarm optimization* (PSO) method [65, 67, 90]. As a particle-based stochastic optimization algorithm, the PSO has attracted a great deal of attention from the scientific community, producing a huge number of variants of the standard method with the main goal to improve the algorithm performances [36, 66, 79, 86, 90]. One consequence of this is that nowadays the method is available in several programming language libraries. The algorithm explores the search space thanks to a population of particles (agents) interacting with each other and updating at each iteration their position and velocity. Thus, from the theoretical point of view, one can take ad-

[1]Images from https://www.flickr.com (left) and https://www.gettyimages.com (right)

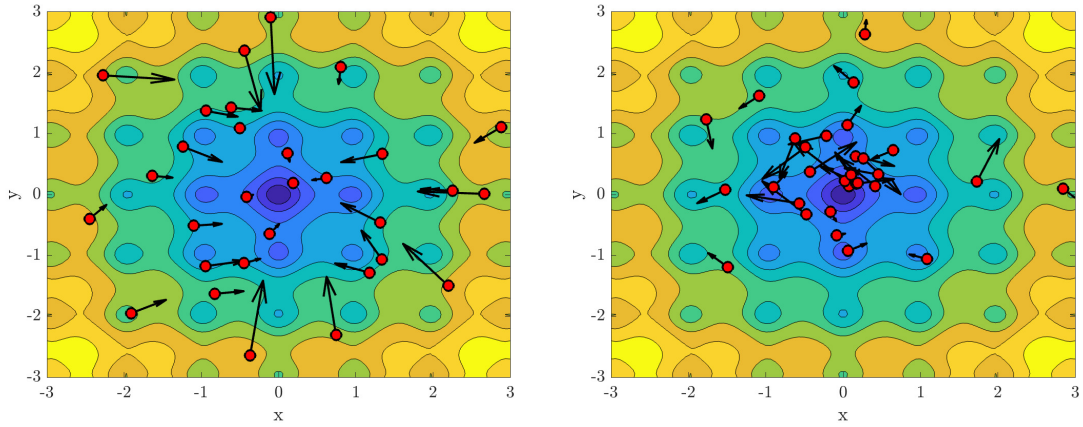

Figure 1.3: Swarm minimization process for the two-dimensional Ackley function. The vectors represent the direction and intensity of the velocity of the agents, which increases when far from the global optimum and decreases when close to it.

vantage of the fact that PSO is inspired by classical second order Newtonian dynamics of particle systems. This allows approaches derived from statistical mechanics and mean-field theory to be adapted to the study of the system properties in the limit of a large number of particles [12, 18, 19, 48, 58, 61, 62, 93]. Despite its apparent simplicity, PSO presents formidable challenges for those interested in understanding swarm intelligence through theoretical analysis and to date a fully complete mathematical theory for particle swarm optimization is still lacking.

Analogies with mean-field dynamics in consensus formation have recently inspired Consensus-based Optimization (CBO) methods, a novel class of particle based methods for global optimization *consensus-based optimization* (see [20, 23, 39, 40, 51, 83, 95, 96]). In contrast to classic metaheuristic methods typically formulated through a discrete sequence of operations and for which it is quite difficult to provide rigorous convergence to global minimizers, CBO-like methods, thanks to their formulation through stochastic differential equations (SDE) permit to exploit mean-field techniques to prove global convergence for a large class of optimization problems[20, 23, 40, 41]. On the other hand, CBO methods seem to be powerful and robust enough to tackle many interesting high dimensional non-convex optimization problems of interest in machine learning and sampling [9, 22, 23, 24, 40, 41, 49]. Global optimization methods with similar features, but based on Kuramoto-Vicseck dynamics constrained to hypersurfaces [39, 40, 41], on binary Boltzmann dynamics [9] or that exploit the particle memory to address the global search [14] have been introduced and studied recently. We mention also the recent extensions of CBO methods to constrained optimization problems [16] and multi-objective optimization [15].

Contribution

In this thesis, we discuss the construction of a robust mathematical theory for generalized PSO methods based on a continuous description of their dynamics and show their close relationship with CBO methods. The derivation of CBO methods as the low inertia limit of generalized PSO is shown also analytically. In addition, we focus on the development and analysis of a novel CBO method (CBO-ME) that exploits agent memory and random selection to increase algorithmic performance in solving high-dimensionality problems. Several applications are also reported. The thesis is self-contained, based on the publications [50], [49] and [14] and is organized as follows:

In **Chapter 2**, we construct a robust mathematical theory for PSO methods based on a continuous description of their dynamics. The presence of memory effects makes the interpretation in terms of differential equations particularly challenging and requires the introduction of an additional state variable to account for the memory of the individual agent. The resulting PSO dynamics is then described by a system of second-order stochastic differential equations (SDEs) using both global best and local best search. This paves the way for a rigorous mathematical treatment of PSO, since, similarly to CBO methods, it is possible to introduce a regularized global best based on the Laplace principle [20, 83], which permits in the mean-field limit to derive, on a formal level, the corresponding Vlasov-Fokker-Planck equation [8, 48, 62, 93]. Thanks to the new mathematical formalism we next consider the behaviour of PSO methods in the small inertia limit, analogous to what has been done in other contexts for nonlinear systems of Vlasov-Fokker-Planck type [3, 34], and show the close relationship between PSO and CBO. Several numerical examples, validating the mean-field approximation and the small inertia limit are also included at the end of the chapter. The results of this chapter are contained in reference [50].

In **Chapter 3**, we provide a robust mathematical theory for the formulation of PSO methods described by second order systems of SDEs, as derived in Chapter 2, and their convergence to the global minimum [27, 57, 59, 60]. We show how, through the use of mean-field techniques, it is possible to derive in the limit of large particles number the corresponding mean-field PSO description based on Vlasov-Fokker-Planck type equations. Therefore, in the zero inertia limit, we will analyze the corresponding macroscopic hydrodynamic equations, showing that they generalize the consensus-based optimization (CBO) methods. Rigorous results concerning the mean-field limit, the zero-inertia limit, and the convergence of the mean-field PSO method towards the global minimum are provided. Results of the chapter are based on the paper [49].

In **Chapter 4**, we discuss improvements of the consensus-based optimization method with memory effects (CBO-ME), derived as the low inertia limit of PSO, in which the consensus point is calculated on the best positions obtained by individual particles throughout their history and not only on the positions at the current iteration. In particular, the method is enhanced by introducing a *random selection technique* [71, 91] as the variance decreases in order to speed up the convergence and reduce memory usage. The use of a random selection does not alter the particle distribution and permits to extend also to the present case the rigorous mathematical analysis that lead to mean field convergence. Several tests on benchmark functions (see Appendix (A1)) are reported to compare the performance of CBO-ME to that achieved with classical CBO and a standard implementation of PSO and to verify the speed up obtained through the random selection techniques. Theoretical convergence guarantees and analysis of the random selection strategy are also reported. The results of this chapter are contained in reference [14].

In **Chapter 5** we employ CBO-ME as a gradient free technique to approach some well-known high-dimensional applied optimization problems from image segmentation and machine learning. In this section we incorporate both algorithmic speed-up techniques and adaptive computation of the parameters. First we consider a image segmentation problem using multi-thresholding [97], then we train a Neural Network (NN) architecture to approximate functions [24] and, finally, perform image classification on MNIST database of handwritten digits [9, 23, 43, 87]. The numerical results are contained in reference [14].

Chapter 2

From particle swarm optimization to consensus based optimization

In this chapter, starting from a continuous description based on stochastic differential equations of the popular particle swarm optimization (PSO) process for solving global optimization problems, we derive in the large-particle limit the corresponding mean-field approximation based on Vlasov-Fokker-Planck type equations. The introduction of an additional differential equation describing the evolution of the local best position overcomes the limitation of keeping track of the past best positions of each particle. A regularization process for the global best allows the respective mean-field description to be formally derived. Subsequently, in the limit of small inertia, we calculate the corresponding macroscopic hydrodynamic equations that clarify the link with consensus-based optimization (CBO) methods. Several numerical examples illustrate the mean-field process, the small inertia limit and the potential of this general class of global optimization methods. We leave a careful theoretical treatment of the arguments here presented to Chapter 3.

2.1 Stochastic differential models for particle swarm optimization

In the sequel we consider the optimization problem (1.1) solved by means of classical particle swarm optimization. The PSO algorithm, originally introduced by Kennedy, Eberhart and Shi [65, 67, 90], solves the minimization problem by starting from a population of candidate solutions, represented by particles, and moving these particles in the search space according to simple mathematical relationships on particle position and speed. The movement of each particle is influenced by its best known local position,

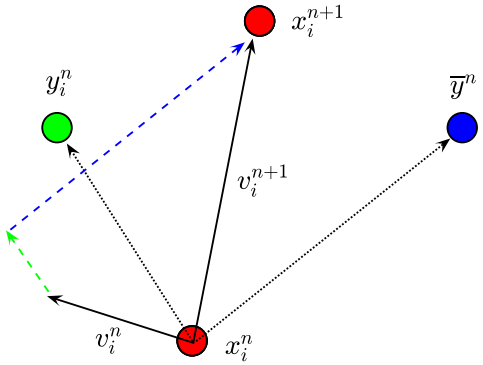

Figure 2.1: Particle dynamics in the standard PSO model (2.1). Green and blue dashed arrows denote the influence of the local best and global best, respectively.

but it is also driven to the best known position in the search space, which is updated when the particles find better positions.

2.1.1 The original PSO method

The method is based on introducing N particles with position $x_i \in \mathbb{R}^d$ and speed $v_i \in \mathbb{R}^d$, $i = 1, \dots, N$. The particle positions and velocities, starting with an initial x_i^0 and v_i^0 assigned, are updated according to the following rule for $n \geq 0$

$$\begin{aligned} x_i^{n+1} &= x_i^n + v_i^{n+1}, \\ v_i^{n+1} &= v_i^n + c_1 R_1^n \left(y_i^n - x_i^n\right) + c_2 R_2^n \left(\overline{y}^n - x_i^n\right), \end{aligned} \tag{2.1}$$

where $c_1, c_2 \in \mathbb{R}$ are the *acceleration coefficients*, y_i^n is the *local best* position found by the i particle up to that iteration, and $\overline{y}^n$ is the *global best* position found among all the particles up to that iteration. The terms R_1^n and R_2^n denote two d-dimensional diagonal matrices with random numbers uniformly distributed in $[0, 1]$ on their diagonals. These numbers are generated at each iteration and for each particle. Typically, the values of x_i and v_i are restricted within a specific search domain $X = [X_{min}, X_{max}]^d$ and $V = [-V_{max}, V_{max}]^d$.

By replacing the second equation in the first one and using the fact that in the previous step $x_i^n = x_i^{n-1} + v_i^n$, we get a model based on a single two-level recursive equation for the particle positions

$$x_i^{n+1} = 2x_i^n - x_i^{n-1} + c_1 R_1^n \left(y_i^n - x_i^n\right) + c_2 R_2^n \left(\overline{y}^n - x_i^n\right). \tag{2.2}$$

There are several ways to define the functions y_i^n and $\overline{y}^n$. In the original PSO method,

these are defined by the following relationships

$$\begin{aligned} y_i^0 &= x_i^0, \\ y_i^{n+1} &= \begin{cases} y_i^n & \text{if } \mathcal{F}(x_i^{n+1}) \geq \mathcal{F}(x_i^n), \\ x_i^{n+1} & \text{if } \mathcal{F}(x_i^{n+1}) < \mathcal{F}(x_i^n); \end{cases} \\ \overline{y}^0 &= \operatorname{argmin}\{\mathcal{F}(x_1^0), \mathcal{F}(x_2^0), \ldots, \mathcal{F}(x_N^0)\}, \\ \overline{y}^{n+1} &= \operatorname{argmin}\{\mathcal{F}(x_1^{n+1}), \mathcal{F}(x_2^{n+1}), \ldots, \mathcal{F}(x_N^{n+1}), \mathcal{F}(\overline{y}^n)\}. \end{aligned} \tag{2.3}$$

2.1.2 The stochastic differential PSO system

In order to derive a time continuous version of the discrete PSO method (2.1), we rewrite it in the form

$$\begin{aligned} x_i^{n+1} &= x_i^n + v_i^{n+1}, \\ v_i^{n+1} &= v_i^n + \frac{c_1}{2}\left(y_i^n - x_i^n\right) + \frac{c_2}{2}\left(\overline{y}^n - x_i^n\right) + \frac{c_1}{2}\widetilde{R}_1\left(y_i^n - x_i^n\right) + \frac{c_2}{2}\widetilde{R}_2\left(\overline{y}^n - x_i^n\right), \end{aligned} \tag{2.4}$$

where $\widetilde{R}_k = (2R_k - 1)$, $k = 1, 2$. We can interpret (2.4) as a semi-implicit time discretization method for SDEs of time stepping $\Delta t = 1$ where the implicit Euler scheme has been used for the first equation and the Euler-Maruyama method is used for the second one. Note that, the particular distribution of the random noise will not change the corresponding stochastic differential system provided the noise has the same mean value and variance. In the case of the PSO model (2.4), since the random terms are uniformly distributed in $[-1, 1]$, the mean value is 0 and the corresponding variance $1/3$.

We can then write its time continuous formulation as a second order system of SDEs in Itô form

$$\begin{aligned} dX_t^i &= V_t^i dt, \\ dV_t^i &= \lambda_1\left(Y_t^i - X_t^i\right)dt + \lambda_2\left(\overline{Y}_t - X_t^i\right)dt \\ &\quad + \sigma_1 D(Y_t^i - X_t^i)dB_t^{1,i} + \sigma_2 D(\overline{Y}_t - X_t^i)dB_t^{2,i}, \end{aligned} \tag{2.5}$$

with

$$\lambda_k = \frac{c_k}{2}, \quad \sigma_k = \frac{c_k}{2\sqrt{3}}, \quad k = 1, 2 \tag{2.6}$$

and

$$D(X_t) = \operatorname{diag}\left\{(X_t)_1, (X_t)_2, \ldots, (X_t)_d\right\}, \tag{2.7}$$

a d-dimensional diagonal matrix. In (2.5) the vectors $B_t^{k,i} = \left((B_t^{k,i})_1, (B_t^{k,i})_2, \ldots, (B_t^{k,i})_d\right)^T$, $k = 1, 2$ denote d independent 1-dimensional Brownian motions and depend on the i-th

particle.

One critical aspect is the definition of the best positions Y_t^i and $\overline{Y}_t$ which in the PSO method make use of the past history of the particles. In [36] the authors observed that the local best can be rewritten as

$$y_i^{n+1} = y_i^n + \frac{1}{2}\left(x_i^{n+1} - y_i^n\right) S(x_i^{n+1}, y_i^n),$$

where

$$S(x, y) = \left(1 + \operatorname{sgn}\left(\mathcal{F}(y) - \mathcal{F}(x)\right)\right). \tag{2.8}$$

Therefore, for a positive constant ν we can approximate the above equation with the following differential system

$$dY_t^i = \nu\left(X_t^i - Y_t^i\right) S(X_t^i, Y_t^i)dt, \tag{2.9}$$

with $Y_0^i = X_0^i$ and consequently define

$$\overline{Y}_t = \operatorname{argmin}\left\{\mathcal{F}(Y_t^1), \mathcal{F}(Y_t^2), \ldots, \mathcal{F}(Y_t^N)\right\}. \tag{2.10}$$

Note that, equation (2.9) does not describe the evolution of the local best, but rather a time continuous approximation of its evolution.

2.1.3 Stochastic differential PSO model with inertia

To optimize the search algorithm, the value $c_k = 2$, $k = 1, 2$ was adopted in early PSO research. This value, which corresponds to $\lambda_k = 1$ and $\sigma_k = 1/\sqrt{3}$, $k = 1, 2$ in the SDEs form, however, leads to unstable dynamics with particle speed increase without control. The use of hard bounds on velocity in $[-V_{\max}, V_{\max}]^d$ is one way to control the velocities. However, the value of $V_{\max}$ is problem-specific and difficult to determine. For this reason, the PSO model has been considered with a modified term which reads as [90]

$$\begin{aligned} x_i^{n+1} &= x_i^n + v_i^{n+1}, \\ v_i^{n+1} &= m v_i^n + c_1 R_1^n \left(y_i^n - x_i^n\right) + c_2 R_2^n \left(\overline{y}^n - x_i^n\right), \end{aligned} \tag{2.11}$$

where $m \in (0, 1]$ is the inertia weight. The above system can be rewritten as

$$\begin{aligned} x_i^{n+1} &= x_i^n + v_i^{n+1}, \\ m v_i^{n+1} &= m v_i^n - (1 - m) v^{n+1} + c_1 R_1^n \left(y_i^n - x_i^n\right) + c_2 R_2^n \left(\overline{y}^n - x_i^n\right). \end{aligned} \tag{2.12}$$

In this case, we can interpret the second equation as a semi-implicit Euler-Maruyama method, that is implicit in v_i and explicit in x_i, hence the corresponding SDEs system reads

$$\begin{aligned} dX_t^i &= V_t^i dt, \\ m dV_t^i &= -\gamma V_t^i dt + \lambda_1 \left(Y_t^i - X_t^i\right) dt + \lambda_2 \left(\overline{Y}_t - X_t^i\right) dt \\ &+ \sigma_1 D(Y_t^i - X_t^i) dB_t^{1,i} + \sigma_2 D(\overline{Y}_t - X_t^i) dB_t^{2,i}, \end{aligned} \tag{2.13}$$

where $\gamma = (1 - m) \geq 0$. Thus, the constant γ acts effectively as a friction coefficient, and can be related to the viscosity of the medium in which particles move. The viscosity is a physical quantity that measures the resistance of a fluid to flowing; it increases with increasing friction force and essentially delays the particle motion. System (2.13) is reminescent of other second order stochastic particle system with inertia [3, 34]. However, note that here, the inertia weight m and the friction coefficient γ are not independent, since when the inertia decreases the viscosity term increases.

In practice, in the PSO method (2.11) the parameter γ is often initially set to some low value, which corresponds to a system where particles move in a low viscosity medium and perform extensive exploration, and gradually increased to a higher value closer to one, where the system is more dissipative and would more easily concentrate into local minima. Most PSO approaches, nowadays, are based on (2.11) (or some variant) which is usually referred to as canonical PSO method to distinguish it from the original PSO method (2.1) (see [86]). Similarly we will refer to (2.5)-(2.9) as the original stochastic differential PSO (SD-PSO) system and to (2.13)-(2.9) as the canonical SD-PSO system. We emphasize that these stochastic systems, when discretized according to the methods described above (namely implicit in V_t^i and explicit in X_t^i) and with the choice $\Delta t = 1$ correspond to the original discrete PSO methods. From the previous formulations, in classical PSO, since the components governing the two behaviors are closely linked by the c_k parameters, increasing the alignment toward the minimum also means increasing the stochasticity of the system. In CBO this does not happen, since λ_k and σ_k, which govern exploration and explotation, are independent of each other.

2.2 Mean-field description of particle swarm optimization

In this section we introduce a modified version of the canonical stochastic differential PSO system for which we can formally compute its mean field limit. We first consider

the case in absence of memory effects and then we extend the results to the general case.

2.2.1 Regularized PSO dynamic without memory effects

To simplify the mathematical description, let us consider a PSO approach where the dynamic is instantaneous without memory of the local best positions and the global best has been regularized as in [83]. The corresponding second order system of SDEs takes the form

$$\begin{aligned} dX_t^i &= V_t^i dt, \\ m dV_t^i &= -\gamma V_t^i dt + \lambda \left(X_t^\alpha - X_t^i\right) dt + \sigma D(X_t^\alpha - X_t^i) dB_t^i, \end{aligned} \tag{2.14}$$

where X_t^α is the weighted average

$$X_t^\alpha = \frac{1}{N^\alpha} \sum_{i=1}^N X_t^i \omega_\alpha(X_t^i), \quad N^\alpha = \sum_{i=1}^N \omega_\alpha(X_t^i), \quad \omega_\alpha(X_t) := e^{-\alpha \mathcal{F}(X_t)}. \tag{2.15}$$

The choice of the weight function ω_α in (2.15) comes from the well-known Laplace principle [32], a classical result in large deviation theory, which states that for any probability measure $\rho \in \mathcal{P}(\mathbb{R}^d)$ compactly supported, it holds

$$\lim_{\alpha \to \infty} \left(-\frac{1}{\alpha} \log \left(\int_{\mathbb{R}^d} e^{-\alpha \mathcal{F}(x)} d\rho(x) \right) \right) = \inf_{x \in \mathrm{supp}(\rho)} \mathcal{F}(x). \tag{2.16}$$

Therefore, for large values of $\alpha \gg 1$ the regularized global best $X_t^\alpha \approx \overline{X}_t$, where

$$\overline{X}_t = \mathrm{argmin} \left\{ \mathcal{F}(X_t^1), \mathcal{F}(X_t^2), \dots, \mathcal{F}(X_t^N) \right\}.$$

We emphasize that the stochastic particle system (2.14) has locally Lipschitz coefficients, thus it admits strong solutions and pathwise uniqueness holds up to any finite time $T > 0$, see [25, 35]. The above system of SDEs in the sequel is considered in a general setting, without necessarily satisfying the PSO constraint (2.6).

Thanks to the smoothness of the right-hand side in (2.14), we can formally derive the mean-field description of the microscopic system (see [48, 62]). Introducing the N-particle probability density

$$f^{(N)}(x_1, \dots, x_N, v_1, \dots, v_N, t),$$

we consider the dynamics of the first marginal

$$f_1^{(N)}(x_1, v_1, t) = \int f^{(N)}(x_1, \dots, x_N, v_1, \dots, v_N, t)\, d\Omega_1,$$

where $d\Omega_1 = dx_2 \dots dx_N\, dv_2 \dots dv_N$ is the volume element, and make the so-called propagation of chaos assumption on the marginals. More precisely, one assumes that for $N \gg 1$ sufficiently large the N-particle probability density $f^{(N)} \approx f^{\otimes N}$, i.e. the random pairs (X_1, V_1), …, (X_N, V_N) are approximatively independent and each with the same distribution $f(x, v, t)$. As a consequence

$$X_t^\alpha \approx X^\alpha(\rho) = \frac{\int_{\mathbb{R}^d} x\omega_\alpha(x)\rho(x,t)\, dx}{\int_{\mathbb{R}^d} \omega_\alpha(x)\rho(x,t)\, dx}, \qquad \rho(x,t) = \int_{\mathbb{R}^d} f(x,v,t)\, dv, \tag{2.17}$$

and the evolution of the distribution $f(x, v, t)$ obeys the nonlinear Vlasov-Fokker-Planck equation

$$\partial_t f + v \cdot \nabla_x f = \nabla_v \cdot \left(\frac{\gamma}{m} v f + \frac{\lambda}{m}(x - X^\alpha(\rho)) f + \frac{\sigma^2}{2m^2} D(x - X^\alpha(\rho))^2 \nabla_v f \right) \tag{2.18}$$

where we used the identity

$$\sum_{k=1}^{d} \frac{\partial^2}{\partial v_k^2} \left((x - X^\alpha(\rho))_k^2 f \right) = \nabla_v \cdot \left(D(x - X^\alpha(\rho))^2 \nabla_v f \right)$$

with $D(x - X^\alpha(\rho))^2$ the diagonal matrix given by the square of $D(x - X^\alpha(\rho))$. Equation (2.18) represents the mean-field PSO (MF-PSO) model without local best and should be accompanied by initial (and boundary) data, and normalization

$$\int_{\mathbb{R}^d \times \mathbb{R}^d} f(x, v, t)\, dx\, dv = 1.$$

We refer to [12, 21, 48, 61, 93] and the references therein, for more details and rigorous results about mean-field models of Vlasov-Fokker-Planck type. Note, however, that the presence of $\overline{X}^\alpha(\rho)$ makes the Vlasov-Fokker-Planck equation nonlinear and nonlocal. This is nonstandard in the literature and raises several analytical and numerical questions (see [20, 40]).

2.2.2 Regularized PSO dynamic with memory and local best

We consider the second order system of SDEs corresponding to the canonical PSO method where the global best and local best have been regularized as follows

$$\begin{aligned} dX_t^i &= V_t^i dt, \\ dY_t^i &= \nu \left(X_t^i - Y_t^i\right) S^\beta(X_t^i, Y_t^i) dt, \\ m dV_t^i &= -\gamma V_t^i dt + \lambda_1 \left(Y_t^i - X_t^i\right) dt + \lambda_2 \left(Y_t^\alpha - X_t^i\right) dt \\ &\quad + \sigma_1 D(Y_t^i - X_t^i) dB_t^{1,i} + \sigma_2 D(Y_t^\alpha - X_t^i) dB_t^{2,i}, \end{aligned} \tag{2.19}$$

where, similarly to the previous case, we introduced the following regularization of the global best position

$$Y_t^\alpha = \frac{\sum_{i=1}^N Y_t^i \omega_\alpha(Y_t^i)}{\sum_{i=1}^N \omega_\alpha(Y_t^i)}, \qquad \omega_\alpha(Y_t) := e^{-\alpha \mathcal{F}(Y_t)}. \tag{2.20}$$

Furthermore, in the right hand side of (2.19) we have replaced the $\mathrm{sgn}(x)$ function with a sigmoid, for example the hyperbolic tangent $\tanh(\beta x)$ for $\beta \gg 1$, and consider $S^\beta(y,x) = 1 + \tanh\left(\beta(\mathcal{F}(y) - \mathcal{F}(x))\right)$. Thanks to these regularizations, also the stochastic particle system (2.19) has locally Lipschitz coefficients and therefore it admits strong solutions and pathwise uniqueness holds for any finite time $T > 0$. Even in this case, the system of SDEs (2.19) is generalized without restricting the search parameters to the PSO constraint (2.6).

In order to derive a mean field description of system (2.19), we must introduce an additional dependence from the memory variables in the N-particle probability density

$$f^{(N)}(x_1, \dots, x_N, y_1, \dots, y_N, v_1, \dots, v_N, t),$$

and consider the dynamics of the first marginal

$$f_1^{(N)}(x_1, y_1, v_1, t) = \int_{\mathbb{R}^d} f^{(N)}(x_1, \dots, x_N, y_1, \dots, y_N, v_1, \dots, v_N, t)\, d\Omega_1,$$

where now $d\Omega_1 = dx_2 \dots dx_N\, dy_2 \dots dy_N\, dv_2 \dots dv_N$ is the volume element. Again assuming propagation of chaos, namely that for sufficiently large $N \gg 1$ the N- particle probability density factorizes $f^{(N)} \approx f^{\otimes N}$, i.e the random triples (X_t^i, Y_t^i, V_t^i) are independent and with the same distribution $f(x,y,v,t)$, we have

$$Y_t^\alpha \approx Y^\alpha(\overline{\rho}) = \frac{\int_{\mathbb{R}^d} y\, \omega_\alpha(y) \overline{\rho}(y,t)\, dy}{\int_{\mathbb{R}^d} \omega_\alpha(y) \overline{\rho}(y,t)\, dy}, \qquad \overline{\rho}(y,t) = \int_{\mathbb{R}^d \times \mathbb{R}^d} f(x,y,v,t)\, dx\, dv. \tag{2.21}$$

Additionally, the distribution $f(x, y, v, t)$ satisfies the nonlinear Vlasov-Fokker-Planck equation

$$\begin{aligned}\partial_t f + v \cdot \nabla_x f + \nabla_y \cdot \left(\nu(x-y) S^\beta(x,y) f\right) = \\ \nabla_v \cdot \left(\frac{\gamma}{m} v f + \frac{\lambda_1}{m}(x-y) f + \frac{\lambda_2}{m}(x - Y^\alpha(\overline{\rho})) f \right. \\ \left. + \left(\frac{\sigma_2^2}{2m^2} D(x - Y^\alpha(\overline{\rho}))^2 + \frac{\sigma_1^2}{2m^2} D(x-y)^2 \right) \nabla_v f \right).\end{aligned} \tag{2.22}$$

For consistency, initially we assume $f(x, y, v, 0) = f_0(x, y, v)$ with $f_0(x, y, v)$ compactly supported and $f_0(x, y, v) \neq 0$ only for $x = y$. As already mentioned, the rigorous proof of the mean-field limit is an open problem for these interacting particle systems due to the nonlinear terms and the difficulty of managing the multiplicative noise in (2.14) and (2.19). We refer to Chapter 3 of the thesis for more details on the theoretical aspects.

2.3 Small inertia limit of particle swarm optimization

In this section we consider the asymptotic behavior of the previous Vlasov-Fokker-Planck equations modelling the PSO dynamic in the small inertia limit. We will derive the corresponding macroscopic equations which permit to recover the recently introduced consensus based optimization (CBO) methods [23]. We refer to [26, 34] for a theoretical background concerning the related problem of the overdamped limit of nonlinear Vlasov-Fokker-Planck systems.

2.3.1 The case without memory effects

Let us first consider the simplified setting in absence of local best. To illustrate the limiting procedure, let us observe that for small values of $m \ll 1$ from the second equation in (2.14) we formally get

$$V_t^i dt = \lambda \left(\overline{X}_t^\alpha - X_t^i \right) dt + \sigma D(\overline{X}_t^\alpha - X_t^i) dB_t^i,$$

where we used the fact that $\gamma = 1 - m \approx 1$. Substituting the above identity into the first equation in (2.14) gives the first order CBO dynamic [23]

$$dX_t^i = \lambda \left(\overline{X}_t^\alpha - X_t^i \right) dt + \sigma D(\overline{X}_t^\alpha - X_t^i) dB_t^i. \tag{2.23}$$

Therefore, the CBO models based on a multiplicative noise can be understood as reduced order approximations of canonical SD-PSO dynamics. Note, however, that in (2.23) the values of λ and σ are independent and does not necessarily satisfy the PSO constraints (2.6).

In the sequel we will develop these arguments in the case of the nonlinear Vlasov-Fokker-Planck equation (2.18) describing the mean-field limit dynamic associated to (2.14). For notation clarity we denote the small inertia value $m = \varepsilon > 0$ in (2.18),

In the sequel we will develop these arguments in the case of the nonlinear Vlasov-Fokker-Planck equation (2.18) describing the mean-field limit dynamic associated to (2.14). For notation clarity we denote the small inertia value $m = \varepsilon > 0$ in (2.18), and re-write the scaled Vlasov-Fokker-Planck system in the form

$$\partial_t f + v \cdot \nabla_x f + \frac{1}{\varepsilon} \nabla_v \cdot (-\varepsilon v f + \lambda (X^\alpha(\rho) - x) f) = L_\varepsilon(f) \tag{2.24}$$

where we used the fact that $\gamma = 1 - \varepsilon$ and define

$$\begin{aligned} L_\varepsilon(f) &= \frac{1}{\varepsilon} \nabla_v \cdot \left(v f + \frac{\sigma^2}{2\varepsilon} D (x - X^\alpha(\rho))^2 \nabla_v f \right) \\ &= \frac{1}{\varepsilon} \sum_{j=1}^d \frac{\sigma^2}{2} (x_j - X_j^\alpha(\rho))^2 \frac{\partial}{\partial v_j} \left(\frac{2 f v_j}{\sigma^2 (x_j - X_j^\alpha(\rho))^2} + \frac{1}{\varepsilon} \frac{\partial f}{\partial v_j} \right). \end{aligned}$$

Let us now introduce the local Maxwellian with unitary mass and zero momentum

$$\begin{aligned} \mathcal{M}_\varepsilon(x, v, t) &= \prod_{j=1}^d M_\varepsilon(x_j, v_j, t), \\ M_\varepsilon(x_j, v_j, t) &= \frac{\varepsilon^{1/2}}{\pi^{1/2} \sigma |x_j - X_j^\alpha(\rho)|} \exp\left\{ - \frac{\varepsilon v_j^2}{\sigma^2 (x_j - X_j^\alpha(\rho))^2} \right\}, \end{aligned}$$

then we have

$$L_\varepsilon(f) = \frac{1}{\varepsilon^2} \sum_{j=1}^d \frac{\sigma^2}{2} (x_j - X_j^\alpha(\rho))^2 \frac{\partial}{\partial v_j} \left(f \frac{\partial}{\partial v_j} \log \left(\frac{f}{M_\varepsilon(x_j, v_j, t)} \right) \right).$$

Therefore $L_\varepsilon(f)$ is of order $1/\varepsilon^2$ and we can write for small values of $\varepsilon \ll 1$

$$f(x, v, t) = \rho(x, t) \mathcal{M}_\varepsilon(x, v, t). \tag{2.25}$$

Let us now integrate equation (2.24) with respect to v, we get

$$\begin{aligned}\frac{\partial \rho}{\partial t} + \nabla_x \cdot (\rho u) &= 0\\ \frac{\partial \rho u}{\partial t} + \int_{\mathbb{R}^d} v\,(v \cdot \nabla_x f)\; dv &= \frac{1-\varepsilon}{\varepsilon}\rho u + \frac{1}{\varepsilon}\lambda(X^\alpha(\rho) - x)\rho\end{aligned}$$

where

$$\rho u = \int_{\mathbb{R}^d} f(x,v,t) v\, dv.$$

Now assuming (2.25) we can compute for $\varepsilon \ll 1$ the i-th component as

$$\begin{aligned}\int_{\mathbb{R}^d} v_i\,(v \cdot \nabla_x\,(\rho(x,t)\mathcal{M}_\varepsilon(x,v,t)))\; dv &= \sum_{j=1}^d \frac{\partial}{\partial x_j}\left(\rho(x,t)\int_{\mathbb{R}^d} v_i(v_j \mathcal{M}_\varepsilon(x,v,t))\, dv\right)\\ &= \frac{\partial}{\partial x_i}\left(\rho(x,t)\int_{\mathbb{R}} v_i^2 M_\varepsilon(x_i,v_i,t)\, dv_i\right)\\ &= \frac{\sigma^2}{2\varepsilon}\frac{\partial}{\partial x_i}\left(\rho(x,t)(x_i - X_i^\alpha(\rho))^2\right)\end{aligned}$$

which provides the second order macroscopic model

$$\begin{aligned}\frac{\partial \rho}{\partial t} + \nabla_x \cdot (\rho u) &= 0\\ \frac{\partial (\rho u)_i}{\partial t} + \frac{\sigma^2}{2\varepsilon}\frac{\partial}{\partial x_i}\left(\rho(x,t)(x_i - X_i^\alpha(\rho))^2\right) &= -\frac{1-\varepsilon}{\varepsilon}(\rho u)_i + \frac{1}{\varepsilon}\lambda(X_i^\alpha(\rho) - x_i)\rho.\end{aligned} \tag{2.26}$$

Formally, as $\varepsilon \to 0$, from the second equation in (2.26) we get

$$(\rho u)_i = \lambda(X_i^\alpha(\rho) - x_i)\rho - \frac{\sigma^2}{2}\frac{\partial}{\partial x_i}\left(\rho(x,t)(x_i - X_i^\alpha(\rho))^2\right),$$

which substituted in the first equation yields the mean-field CBO system [23]

$$\frac{\partial \rho}{\partial t} + \nabla_x \cdot \lambda(X^\alpha(\rho) - x)\rho = \frac{\sigma^2}{2}\sum_{j=1}^d \frac{\partial^2}{\partial x_j^2}\left(\rho(x,t)(x_j - X_j^\alpha(\rho))^2\right). \tag{2.27}$$

Therefore, in the small inertia limit we expect the macroscopic density in the PSO system (2.18) to be well approximated by the solution of the CBO equation (2.27). We remark that this is not the case for the original CBO method proposed in [83] where the noise is not in component-wise form.

2.3.2 The general case with memory

Next, we consider the same small inertia scaling in the general case with dependence from the local best. Again, we can first illustrate the result by considering the behaviour for $m \ll 1$ of the SD-PSO system (2.19). We formally get from the third equation

$$V_t^i dt = \lambda_1 \left(Y_t^i - X_t^i\right) dt + \lambda_2 \left(Y_t^\alpha - X_t^i\right) dt + \sigma_1 D(Y_t^i - X_t^i) dB_t^{1,i} + \sigma_2 D(Y_t^\alpha - X_t^i) dB_t^{2,i},$$

which inserted into the first equation in (2.19) corresponds to a novel first order CBO dynamic with local best

$$\begin{aligned} dX_t^i &= \lambda_1 \left(Y_t^i - X_t^i\right) dt + \lambda_2 \left(Y_t^\alpha - X_t^i\right) dt \\ &+ \sigma_1 D(Y_t^i - X_t^i) dB_t^{1,i} + \sigma_2 D(Y_t^\alpha - X_t^i) dB_t^{2,i}, \\ dY_t^i &= \nu \left(X_t^i - Y_t^i\right) S^\beta(X_t^i, Y_t^i) dt. \end{aligned} \tag{2.28}$$

In contrast with the model recently introduced in [96] the above first order CBO method avoids backward time integration through the use of an additional differential equation. We remark that at the SDEs level, by analogous arguments as the one presented in this thesis, in principle even the CBO model [96] can be derived as the small inertia limit of the corresponding PSO model where memory effects are modeled as in [96].

Concerning the corresponding MF-PSO limit we can essentially perform analogous computations as in the previous section. Thus, after setting $m = \varepsilon > 0$ we consider the scaled system

$$\begin{aligned} &\partial_t f + v \cdot \nabla_x f + \nabla_y \cdot \left(\nu(x-y) S^\beta(x,y) f\right) \\ &\qquad + \frac{1}{\varepsilon} \nabla_v \cdot (-\varepsilon v f + \lambda_1 (y-x) f + \lambda_2 (Y^\alpha(\overline{\rho}) - x) f) = L_\varepsilon(f), \end{aligned} \tag{2.29}$$

where now

$$\begin{aligned} L_\varepsilon(f) &= \frac{1}{\varepsilon} \nabla_v \cdot \left(v f + \frac{\sigma_2^2}{2\varepsilon} D(x - Y^\alpha(\overline{\rho}))^2 \nabla_v f + \frac{\sigma_1^2}{2\varepsilon} D(x-y)^2 \nabla_v f \right) \\ &= \frac{1}{2\varepsilon} \sum_{j=1}^d \Sigma(x_j, y_j, t)^2 \frac{\partial}{\partial v_j} \left(\frac{2 f v_j}{\Sigma(x_j, y_j, t)^2} + \frac{1}{\varepsilon} \frac{\partial f}{\partial v_j} \right) \end{aligned}$$

and we use the notation

$$\Sigma(x_j, y_j, t)^2 = \sigma_2^2 (x_j - Y_j^\alpha(\overline{\rho}))^2 + \sigma_1^2 (x_j - y_j)^2.$$

Then, introducing the local Maxwellian

$$\mathcal{M}_\varepsilon(x,y,v,t) = \prod_{j=1}^{d} M_\varepsilon(x_j,y_j,v_j,t),$$
$$M_\varepsilon(x_j,y_j,v_j,t) = \frac{\varepsilon^{1/2}}{\pi^{1/2}|\Sigma(x_j,y_j,t)|}\exp\left\{-\frac{\varepsilon v_j^2}{\Sigma(x_j,y_j,t)^2}\right\},$$

with unitary mass and zero momentum we have

$$L_\varepsilon(f) = \frac{1}{2\varepsilon^2}\sum_{j=1}^{d}\Sigma(x_j,y_j,t)^2\frac{\partial}{\partial v_j}\left(f\frac{\partial}{\partial v_j}\log\left(\frac{f}{M_\varepsilon(x_j,y_j,v_j,t)}\right)\right).$$

We can thus write for $\varepsilon \ll 1$

$$f(x,y,v,t) = \rho(x,y,t)\mathcal{M}_\varepsilon(x,y,v,t), \tag{2.30}$$

and after integrating (2.29) with respect to v and using the approach (2.30), we get the second order macroscopic model

$$\begin{aligned}
&\frac{\partial\rho}{\partial t} + \nabla_x\cdot(\rho u) + \nabla_y\cdot\left(\nu(x-y)S^\beta(x,y)\rho\right) = 0\\
&\qquad\frac{\partial(\rho u)_i}{\partial t} + \frac{\sigma^2}{2\varepsilon}\frac{\partial}{\partial x_i}\left(\rho(x,t)\Sigma(x_i,y_i,t)^2\right) =\\
&\qquad\qquad = -\frac{1-\varepsilon}{\varepsilon}(\rho u)_i + \frac{1}{\varepsilon}\left(\lambda_1(y_i-x_i) + \lambda_2(Y_i^\alpha(\overline{\rho})-x_i)\right)\rho.
\end{aligned} \tag{2.31}$$

Formally, as $\varepsilon\to 0$, the above system reduces to a novel mean-field CBO system with local best

$$\begin{aligned}
&\frac{\partial\rho}{\partial t} + \nabla_x\cdot\left(\lambda_1(y-x) + \lambda_2(Y^\alpha(\overline{\rho})-x)\right)\rho + \nabla_y\cdot\left(\nu(x-y)S^\beta(x,y)\rho\right)\\
&\qquad = \frac{1}{2}\sum_{j=1}^{d}\frac{\partial^2}{\partial x_j^2}\left(\rho(x,t)\left(\sigma_1^2(x_j-y_j)^2 + \sigma_2^2(x_j - Y_j^\alpha(\overline{\rho}))^2\right)\right).
\end{aligned} \tag{2.32}$$

2.4 Numerical examples

In this section we present several numerical tests in order to verify the validity of the previous theoretical analysis, namely the mean field limit and the small inertial limit, and to analyze the performance of the methods based on SD-PSO against various prototype global optimization functions.

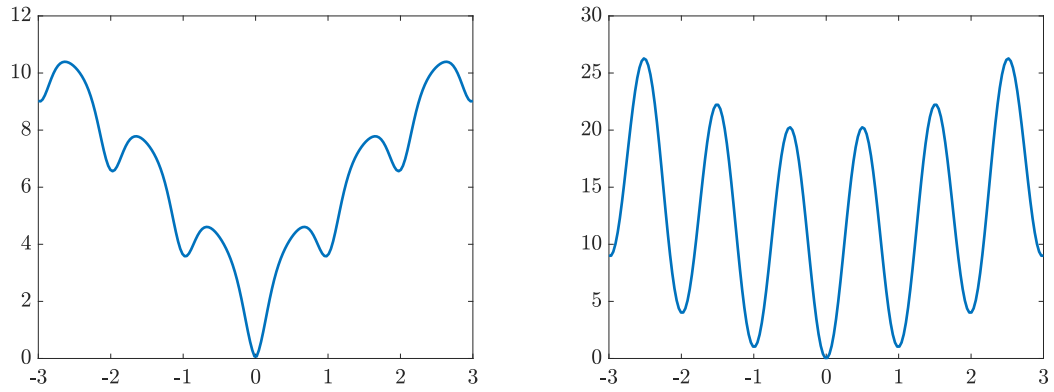

(a) Ackley (b) Rastrigin

Figure 2.2: One-dimensional Ackley and Rastrigin functions in the interval $[-3, 3]$ with global minimum in the origin.

2.4.1 Validation of the mean field limit

In the following we present three numerical test cases to validate the mean field limit process in one dimension by considering as prototype functions for global optimization the Ackley function (A.1) and the Rastrigin function (A.3). Both functions have multiple local minima that can easily trap the particle dynamics (see Figure 2.2) and have been used recently to test consensus based particle optimizers [23, 39, 83].

First we have considered the case without memory effect formulated by the SD-PSO system (2.14) that uses only the action of the global best compared to the solution obtained using the mean field limit (2.18). The particle system (2.14) is solved by

$$\begin{aligned} X_i^{n+1} &= X_i^n + \Delta t\, V_i^{n+1}, \\ mV_i^{n+1} &= mV_i^n - \gamma\Delta t\, V_i^{n+1} + \lambda\Delta t\,(X_\alpha^n - X_i^n) \\ &+ \sigma\sqrt{\Delta t}\, D(X_\alpha^n - X_i^n)\, \vartheta_i^n, \end{aligned} \tag{2.33}$$

where $\vartheta_i \sim \mathcal{N}(0,1)$ and the last equation can be rewritten as

$$V_i^{n+1} = \left(\frac{m}{m+\gamma\,\Delta t}\right) V_i^n + \frac{\lambda\,\Delta t}{m+\gamma\,\Delta t}(X_\alpha^n - X_i^n) + \frac{\sigma\,\sqrt{\Delta t}}{m+\gamma\,\Delta t} D(X_\alpha^n - X_i^n)\,\vartheta_i^n.$$

The corresponding MF-PSO limit (2.18) has been discretized using a dimensional splitting where the transport part is solved through a second order backward semi-Lagrangian method and the remaining Fokker-Planck term is discretized using an implicit central scheme. The introduction of an implicit method permits to avoid restrictive CFL conditions [28] and to obtain second order accuracy in space and velocity.

In the second and third test cases we introduced the memory variable, initially with the action of the local best only, and then with both local and global dynamics. In this case, the SD-PSO system (2.19) is solved by

$$\begin{aligned} Y_i^{n+1} &= Y_i^n + \nu\ \Delta t \left(X_i^{n+1} - Y_i^n\right) S^\beta(X_i^{n+1}, Y_i^n), \\ X_i^{n+1} &= X_i^n + \Delta t\ V_i^{n+1}, \\ V_i^{n+1} &= \left(\frac{m}{m+\gamma\ \Delta t}\right) V_i^n + \frac{\lambda_1\ \Delta t}{m+\gamma\ \Delta t}\,(Y_i^n - X_i^n) + \frac{\lambda_2\ \Delta t}{m+\gamma\ \Delta t}\,(Y_\alpha^n - X_i^n) \\ &\quad \frac{\sigma_1\ \sqrt{\Delta t}}{m+\gamma\ \Delta t} D(Y_i^n - X_i^n)\ \vartheta_{1,i}^n + \frac{\sigma_2\ \sqrt{\Delta t}}{m+\gamma\ \Delta t} D(Y_\alpha^n - X_i^n)\ \vartheta_{2,i}^n, \end{aligned} \tag{2.34}$$

where $\vartheta_{1,i},\ \vartheta_{2,i} \sim \mathcal{N}(0,1)$. Note that, the above discretization is equivalent to the discrete PSO system (2.11) under assumptions (2.6) for $\Delta t = 1$, $\nu = 0.5$, and taking the limit $\alpha,\ \beta \to \infty$ so that Y_i^n, Y_α^n match the local and global best definitions in (2.3). The limiting MF-PSO equation (2.22) is solved by a further dimensional splitting where the additional memory term is discretized using a Lax-Wendroff method that permits to achieve overall second order accuracy. We mention here that we tested also various other approaches for the discretization of the differential memory term. However, in our numerical results we have found essential for the accuracy of the mean-field solution in presence of local best, to discretize the differential term modeling particles' memory using a second order low dissipative scheme. Finally, concerning the time approximation, we implemented both conventional splitting as well as second order Strang splitting without noticing relevant differences in the results. We also tested several set of parameters and initial data (uniform, Gaussian) without observing significant changes with respect to the selection of results reported in the sequel.

In all test cases we used $N = 5\times10^5$ particles, a mesh size for the mean field solver of 90×120 points for $(x,v) \in [-3,3]\times[-4,4]$, and whenever present, the mesh and domain size in y have been taken identical to those in x. The choice of the particle number was based on having a good compromise between the convergence to the mean-field limit and the possibility to still visually distinguish the two solutions in the figures. In the deterministic discretization the boundary conditions have been implemented assuming $f(x,v,t) = 0$ or $f(x,y,v,t) = 0$ outside the computational domain whereas no boundary conditions have been applied to the particle dynamics.

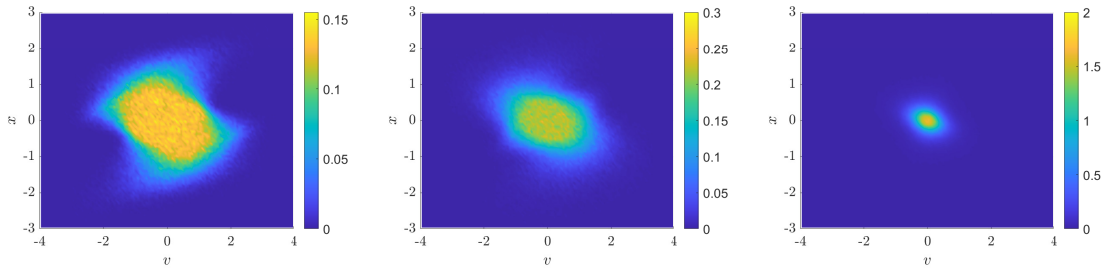

(a) Particle solution, $t = 0.5$ (b) Particle solution, $t = 1$ (c) Particle solution, $t = 3$

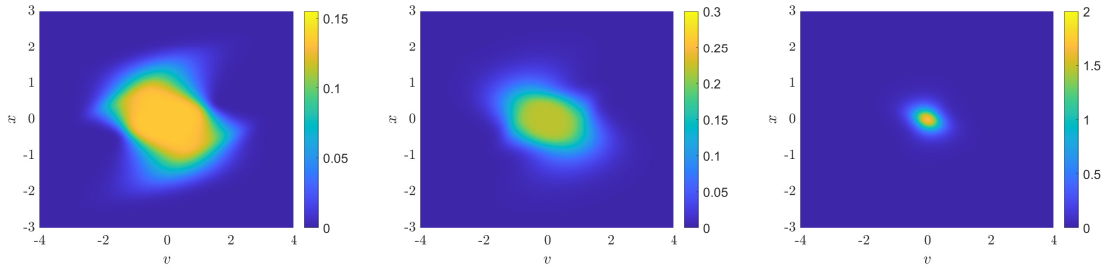

(d) Mean-field solution, $t = 0.5$ (e) Mean-field solution, $t = 1$ (f) Mean-field solution, $t = 3$

Figure 2.3: Case #1 (no memory). Optimization of the one-dimensional Ackley function with minimum in $x = 0$. First row: solution of the SD-PSO system (2.14). Second row: solution of the MF-PSO limit (2.18).

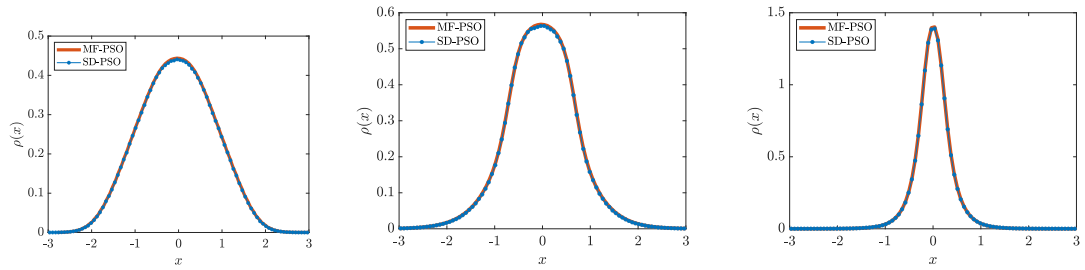

(a) $\rho(x,t)$, $t = 0.5$ (b) $\rho(x,t)$, $t = 1$ (c) $\rho(x,t)$, $t = 3$

Figure 2.4: Case #1 (no memory). Evolution of the density $\rho(x,t)$ of the SD-PSO system (2.14) and the MF-PSO limit (2.18) for the one-dimensional Ackley function with minimum in $x = 0$.

Case #1: MF-PSO without memory effects

We consider the optimization process of the Ackley function with global minimum in the origin $x = 0$. Here we report the results obtained with

$$\gamma = 0.5, \quad \lambda = 1, \quad \sigma = 1/\sqrt{3}, \quad \alpha = 30. \tag{2.35}$$

Note that, the values of λ and σ are compatible with the usual choice $c_k = 2$ in (2.6). In Figure 2.3 we report the contour plots of the evolution, at times $t = 0.5$,

$t = 1$ and $t = 3$, of the particle distribution computed through (2.33) and by the direct discretization of the mean-field equation (2.18). The initial distribution is taken uniform in all simulations.

To emphasize the good agreement between the results obtained from the resolution of the large particle limit of the SD-PSO model and the results of its corresponding MF-PSO, in Figure 2.4 we report the evolution in time of the marginal density $\rho(x,t) = \int_{\mathbb{R}^d} f(x,v,t)\,dv$. The convergence towards a Dirac delta centered in the origin is very similar in both dynamics.

In Figures 2.5 and 2.6 we report the same results but applied to the Ackley function with minimum in $x = 1$. Even in this case the plot of the density in Figure 2.6 show the excellent agreement between the stochastic differential system and the mean-field limit. It is interesting to note that the particle distribution evolves asymmetrically in this case and initially exceed the value $x = 1$ before moving backward to reach the global minimum.

Case #2: MF-PSO with memory and only local best dynamics

In the second test case we introduce the dependence from the memory variable and report a comparison between the solution of the discretized stochastic particle model (2.35) and the solver of the mean field limit (2.22) where we assume $\lambda_2, \sigma_2 = 0$, namely only the local best is present. The same parameters (2.35) have been used together with $\beta = 30$ and $\nu = 0.5$ for the local best. Initially the local best values are assumed to be equal to the particle positions.

In Figures 2.7 and 2.9 we report the contour plots of the particle solution and the mean-field solution for the one-dimensional Ackley and Rastrigin functions with minimum in $x = 0$ and using an uniform initial data. The final simulation time now is $t = 6$. We can note that in the presence of local best only, the particles tend to return to their local best position creating a "memory effect" that leads them to concentrate not only in the global minimum but also in the local minima. For large times we obtain a sequence of particle peaks with zero speed exactly in the positions of the local minima. Thus the dynamic allows us to identify each type of minimum present in the functions.

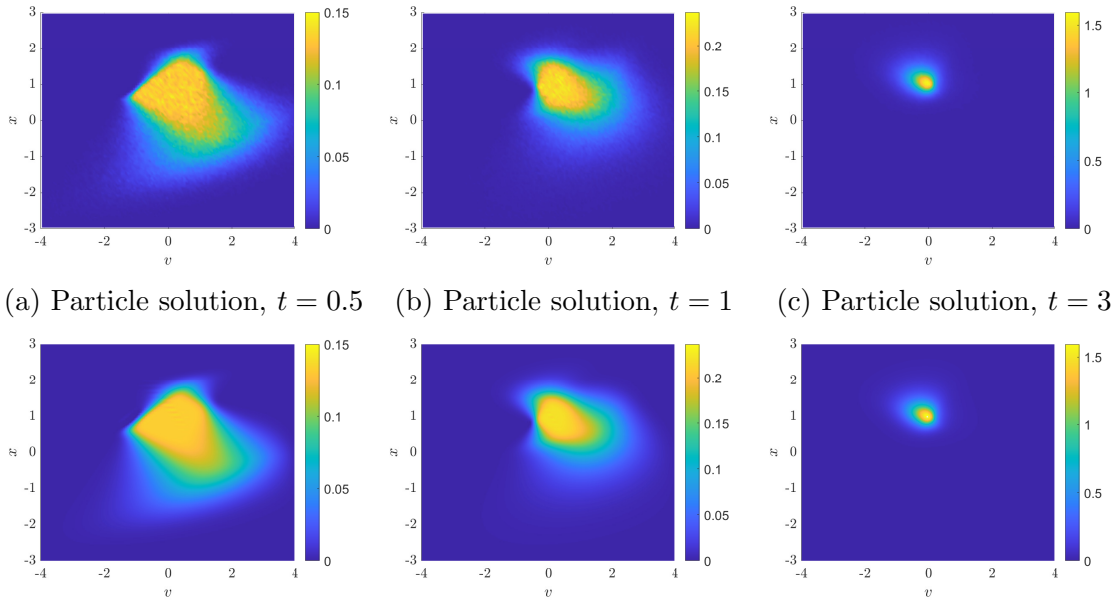

(a) Particle solution, $t = 0.5$ (b) Particle solution, $t = 1$ (c) Particle solution, $t = 3$

(d) Mean-field solution, $t = 0.5$ (e) Mean-field solution, $t = 1$ (f) Mean-field solution, $t = 3$

Figure 2.5: Case #1 (no memory). Optimization of the one-dimensional Ackley function with minimum in $x = 1$. First row: solution of the SD-PSO system (2.14). Second row: solution of the MF-PSO limit (2.18).

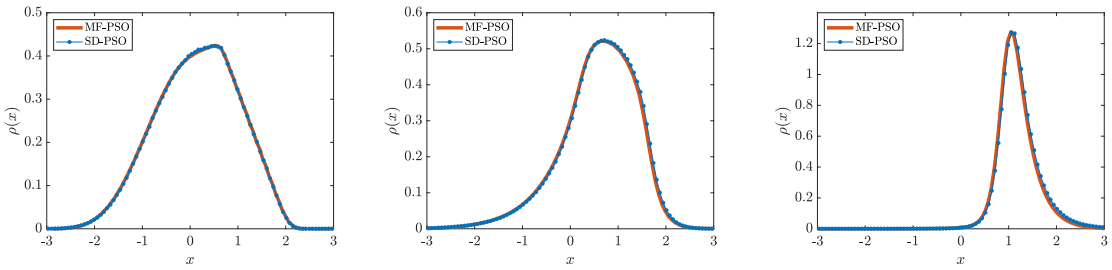

(a) $\rho(x,t)$, $t = 0.5$ (b) $\rho(x,t)$, $t = 1$ (c) $\rho(x,t)$, $t = 3$

Figure 2.6: Case #1 (no memory). Evolution of the density $\rho(x,t)$ of the SD-PSO system (2.14) and the MF-PSO limit (2.18) for the one-dimensional Ackley function with minimum in $x = 1$.

This effect can be better appreciated if one compares the explicit form of the one-dimensional Ackley and Rastrigin function in Figure 2.2 and the corresponding density plots (approximated by simple histogram reconstruction) of the particle minimizer in Figures 2.8 and 2.10. It is interesting to point out that from a computational point of view solving the mean field equation (2.22) in this setting (presence of local best only) has proved to be quite challenging due to the high dimensionality and the importance of avoiding dissipative effects in the discretization of memory terms to preserve the peaks structure in the asymptotic numerical solution. Second order schemes for the discretization of the mean-field equation are essential in this case to resolve correctly

the structure of the solution. One can appreciate the good agreement between the particle and mean-field solutions in Figures 2.8 and 2.10.

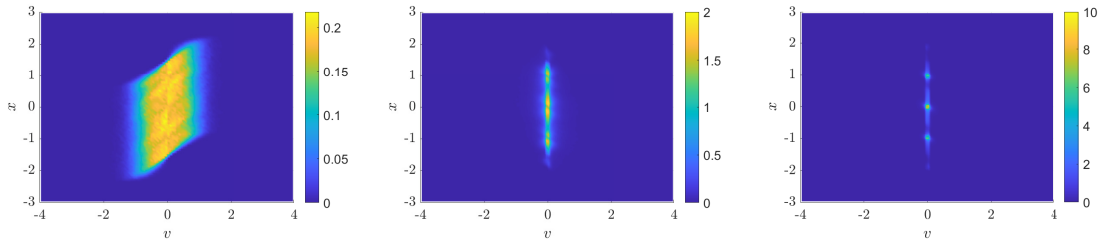

(a) Particle solution, $t = 0.5$ (b) Particle solution, $t = 3$ (c) Particle solution, $t = 6$

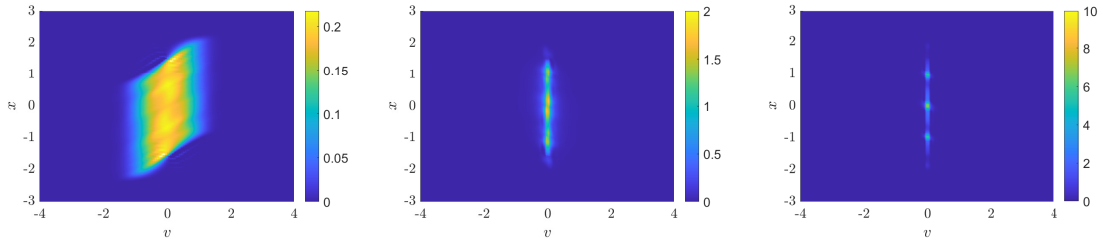

(d) Marginal $\rho(x, v, t)$, $t = 0.5$ (e) Marginal $\rho(x, v, t)$, $t = 3$ (f) Marginal $\rho(x, v, t)$, $t = 6$

Figure 2.7: Case #2 (local best only). Optimization of the one-dimensional Ackley function with minimum in $x = 0$. First row: solution of the SD-PSO system (2.19). Second row: solution of the MF-PSO limit (2.22).

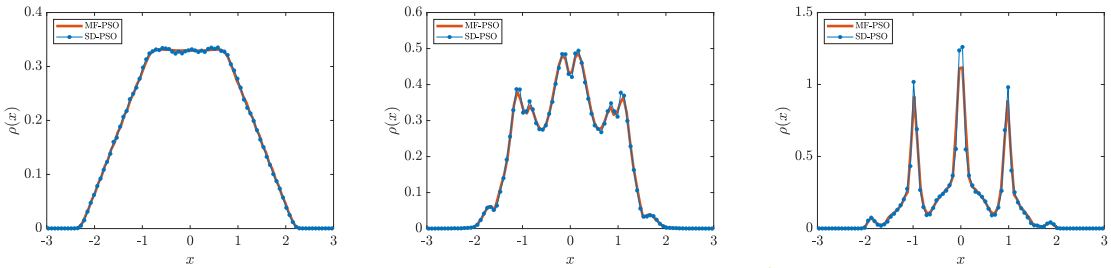

(a) $\rho(x, t)$, $t = 0.5$ (b) $\rho(x, t)$, $t = 3$ (c) $\rho(x, t)$, $t = 6$

Figure 2.8: Case #2 (local best only). Evolution of the density $\rho(x, t)$ of the SD-PSO system (2.19) and the MF-PSO limit (2.22) for the one-dimensional Ackley function with minimum in $x = 0$.

Case #3: MF-PSO with memory, general case

In the last test case we repeat the previous scenario by adding the action of the global best with the same weight as the local best. Therefore, we take $\lambda_1 = \lambda_2 = 1$, $\sigma_1 = \sigma_2 = 1/\sqrt{3}$ and the same parameters in (2.35) in our numerical experiments.

In Figures 2.11 and 2.13 we report the contour plots of the solutions obtained with

the discretized stochastic particle system (2.35) and the deterministic solver of the mean field equation (2.22). One can immediately observe that the local minima effect disappears and the systems converge consistently towards the global minima for both the Ackley and the Rastrigin functions. The good agreement between the particle and the mean-field solutions, as before, is emphasized by the density plots in Figures 2.12 and 2.14. Note that, by comparing the results in Figure 2.12 and those in Figure 2.4 obtained by solving the same problem in absence of memory terms and presence of global best only, at the same time instants, a faster convergence towards the global minimum is observed in Figure 2.12 thanks to the inclusion of the memory effects in the dynamic.

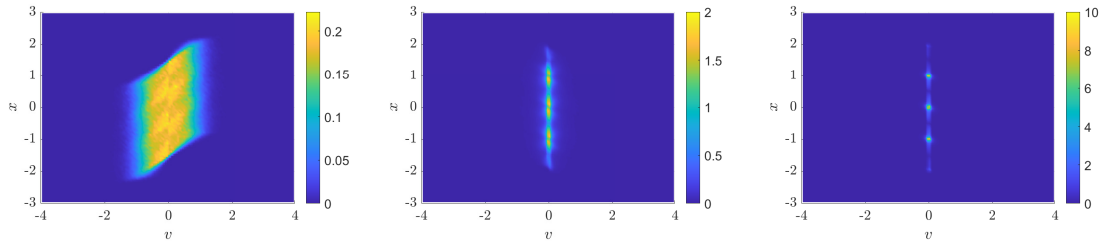

(a) Particle solution, $t = 0.5$ (b) Particle solution, $t = 3$ (c) Particle solution, $t = 6$

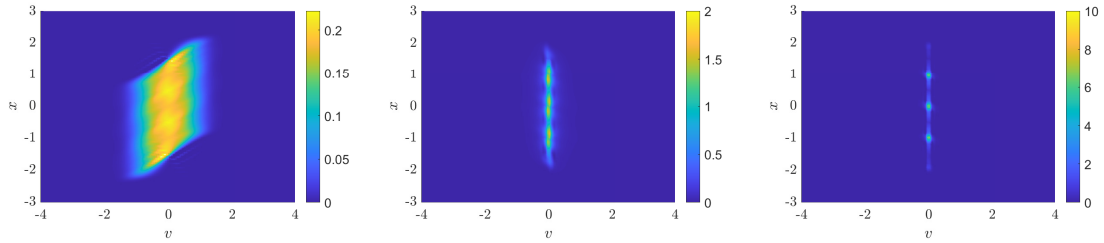

(d) Marginal $\rho(x, v, t)$, $t = 0.5$ (e) Marginal $\rho(x, v, t)$, $t = 3$ (f) Marginal $\rho(x, v, t)$, $t = 6$

Figure 2.9: Case #2 (local best only). Optimization of the one-dimensional Rastrigin function with minimum in $x = 0$. First row: solution of the SD-PSO system (2.19). Second row: solution of the MF-PSO limit (2.22).

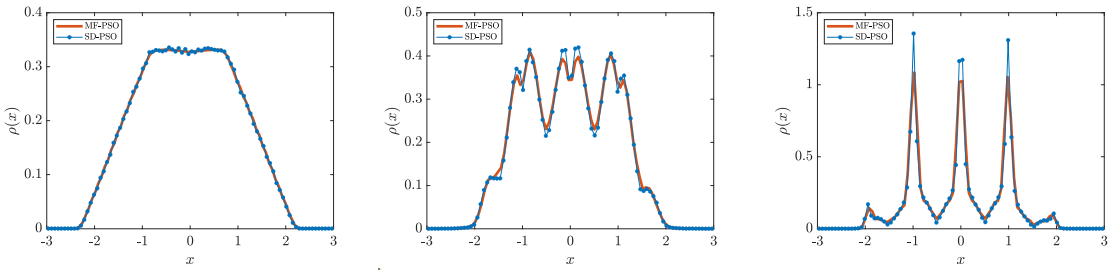

(a) $\rho(x, t)$, $t = 0.5$ (b) $\rho(x, t)$, $t = 3$ (c) $\rho(x, t)$, $t = 6$

Figure 2.10: Case #2 (local best only). Evolution of the density $\rho(x, t)$ of the SD-PSO system (2.19) and the MF-PSO limit (2.22) for the one-dimensional Rastrigin function with minimum in $x = 0$.

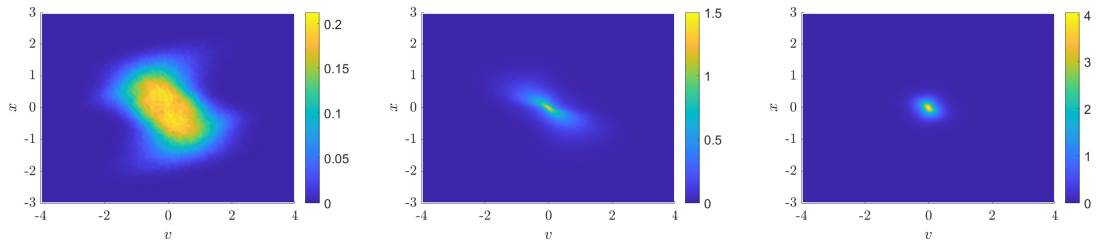

(a) Particle solution, $t = 0.5$ (b) Particle solution, $t = 1$ (c) Particle solution, $t = 3$

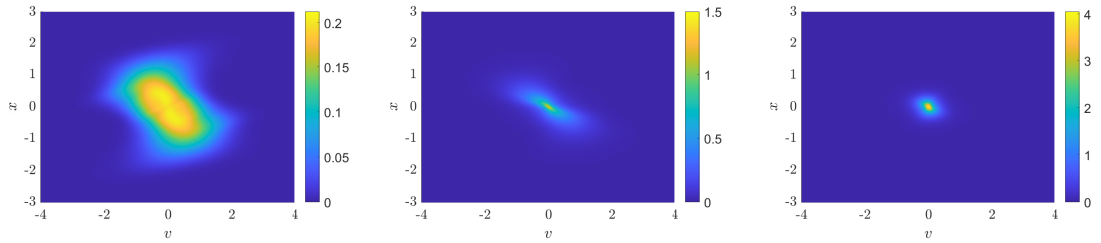

(d) Mean-field solution, $t = 0.5$ (e) Mean-field solution, $t = 1$ (f) Mean-field solution, $t = 3$

Figure 2.11: Case #3 (general case). Optimization of the one-dimensional Ackley function with minimum in $x = 0$. First row: solution of the SD-PSO system (2.19). Second row: solution of the MF-PSO limit (2.22).

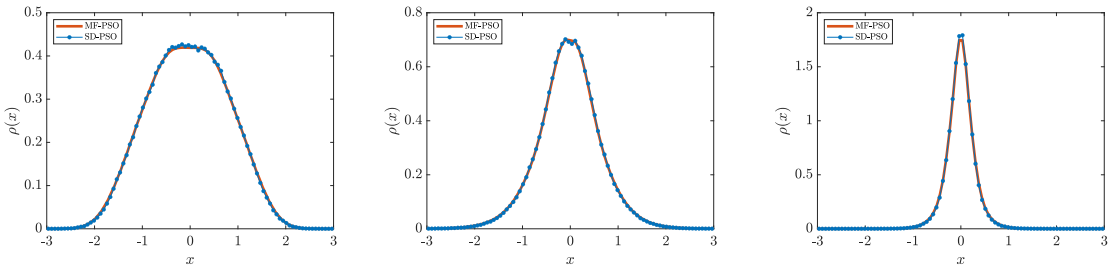

(a) $\rho(x,t)$, $t = 0.5$ (b) $\rho(x,t)$, $t = 1$ (c) $\rho(x,t)$, $t = 3$

Figure 2.12: Case #3 (general case). Evolution of the density $\rho(x,t)$ of the SD-PSO system (2.19) and the MF-PSO limit (2.22) for the one-dimensional Ackley function with minimum in $x = 0$.

2.4.2 Numerical small inertia limit

From the analysis in Section 4, in the limit of small inertia the classical CBO model (2.27) is obtained as hydrodynamic approximation of the mean-field PSO system (2.18). Therefore, starting from the discretization of the stochastic particle model without memory effect (2.33), we decrease the inertial weight $m \to 0$ ($\gamma \to 1$) and compare the particle solution with a direct discretization of the limiting mean-field CBO system (2.27).

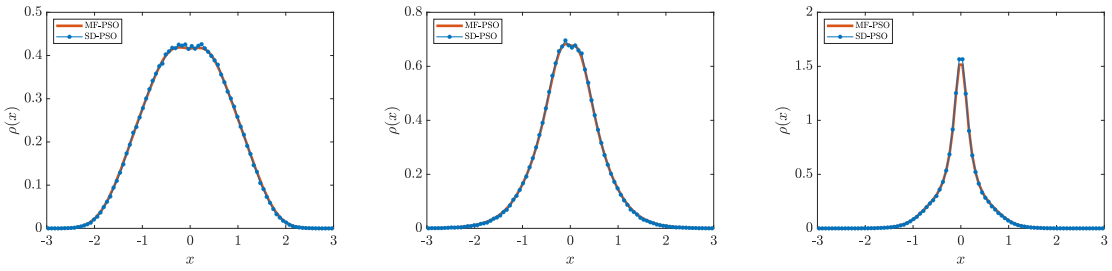

(a) $\rho(x,t)$, $t = 0.5$ (b) $\rho(x,t)$, $t = 1$ (c) $\rho(x,t)$, $t = 3$

Figure 2.14: Case #3 (general case). Evolution of the density $\rho(x,t)$ of the SD-PSO system (2.19) and the MF-PSO limit (2.22) for the one-dimensional Rastrigin function with minimum in $x = 0$.

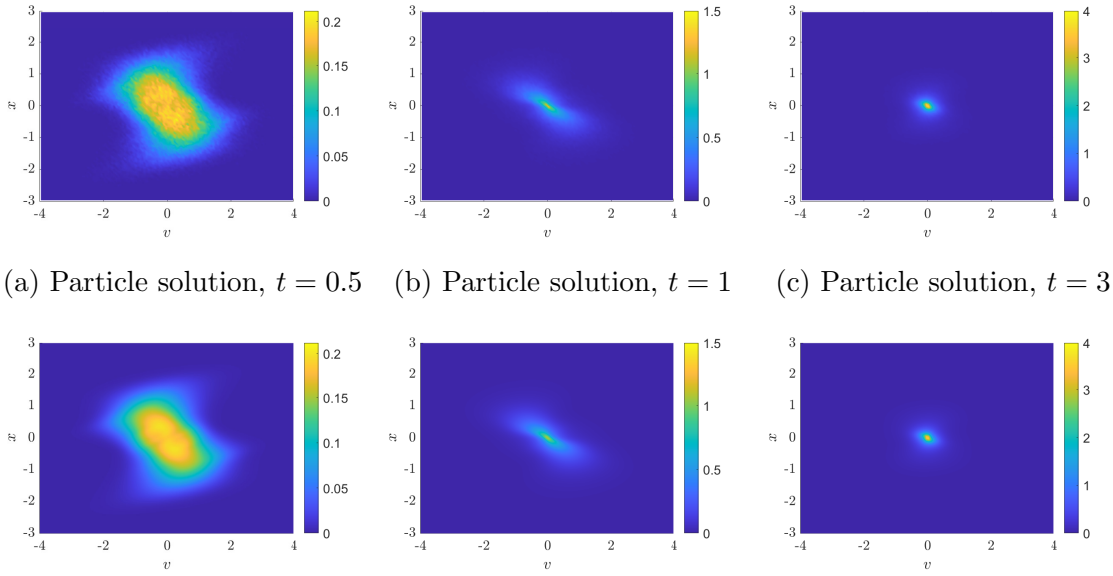

(a) Particle solution, $t = 0.5$ (b) Particle solution, $t = 1$ (c) Particle solution, $t = 3$

(d) Mean-field solution, $t = 0.5$ (e) Mean-field solution, $t = 1$ (f) Mean-field solution, $t = 3$

Figure 2.13: Case #3 (general case). Optimization of the one-dimensional Rastrigin function with minimum in $x = 0$. First row: solution of the SD-PSO system (2.19). Second row: solution of the MF-PSO limit (2.22).

First, let us observe that the semi-implicit discretization scheme (2.33)

$$\begin{aligned} X_i^{n+1} &= X_i^n + \Delta t\, V_i^{n+1}, \\ V_i^{n+1} &= \left(\frac{m}{m+\gamma\,\Delta t}\right) V_i^n + \frac{\lambda\,\Delta t}{m+\gamma\,\Delta t}\,(X_\alpha^n - X_i^n) \\ &+ \frac{\sigma\,\sqrt{\Delta t}}{m+\gamma\,\Delta t} D(X_\alpha^n - X_i^n)\,\vartheta_i^n, \end{aligned} \tag{2.36}$$

satisfies an asymptotic-preserving type property, allowing to pass to the limit $m \to 0$ without any restriction on Δt. In fact, passing to the limit, the second equation in (2.36) gives

$$V_i^{n+1} = \lambda\,(X_\alpha^n - X_i^n) + \frac{\sigma}{\sqrt{\Delta t}} D(X_\alpha^n - X_i^n)\;\vartheta_i^n,$$

which substituted into the first equation of (2.36) corresponds to the Euler-Maruyama scheme applied to the CBO system (2.23)

$$X_i^{n+1} \;=\; X_i^n + \Delta t \lambda\,(X_\alpha^n - X_i^n) + \sqrt{\Delta t}\sigma D(X_\alpha^n - X_i^n)\vartheta_i^n. \tag{2.37}$$

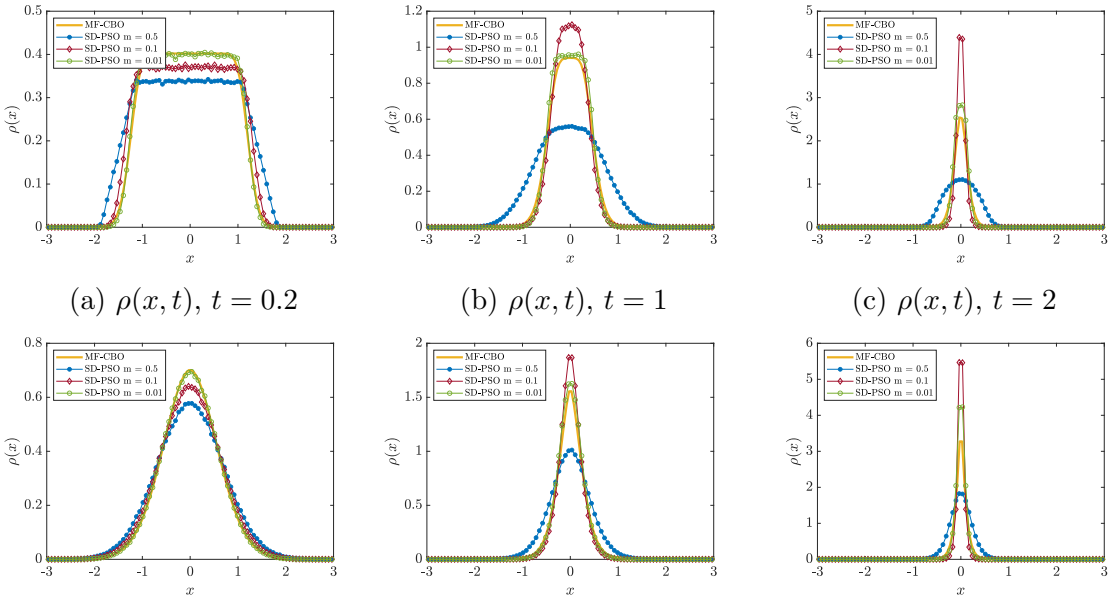

(a) $\rho(x,t)$, $t = 0.2$ (b) $\rho(x,t)$, $t = 1$ (c) $\rho(x,t)$, $t = 2$

(d) $\rho(x,t)$, $t = 0.2$ (e) $\rho(x,t)$, $t = 1$ (f) $\rho(x,t)$, $t = 2$

Figure 2.15: Low inertia limit. Evolution of the density $\rho(x,t)$ of the SD-PSO discretization (2.36), for decreasing inertial weight $m = 0.5, 0.1, 0.01$, and the mean-field CBO model (2.27) for the Ackley function with minimum in $x = 0$. First row: uniform initial data. Second row: Gaussian initial data.

In Figures 2.15 and 2.16 we report the plots of the density that describes the solution of the mean-field CBO model and the stochastic PSO model for different inertial weights ($m = 0.5$, $m = 0.1$ and $m = 0.01$). We considered the minimization problem for the Ackley function with minimum in $x = 0$ and in $x = 1$ with $N = 5 \times 10^5$ particles for the SD-PSO discretization, a grid of 120 points in space for the mean field CBO solver and the same set of parameters (2.35) with two different initial data: a uniform distribution and a Gaussian distribution.

It is clear that in the case of $m = 0.5$ the two densities at the final time $t = 2$ are considerably different and a slower convergence is observed in the SD-PSO system, for

$m = 0.1$ the agreement is higher and the particle solution seems to converge faster to the minimum, finally in the case $m = 0.01$ both densities simultaneously grow towards a Dirac delta centered in the minimum. As expected an initial Gaussian profile, being more concentrated, leads to a faster convergence. For smaller values of m the two solutions becomes indistinguishable and we omitted the results.

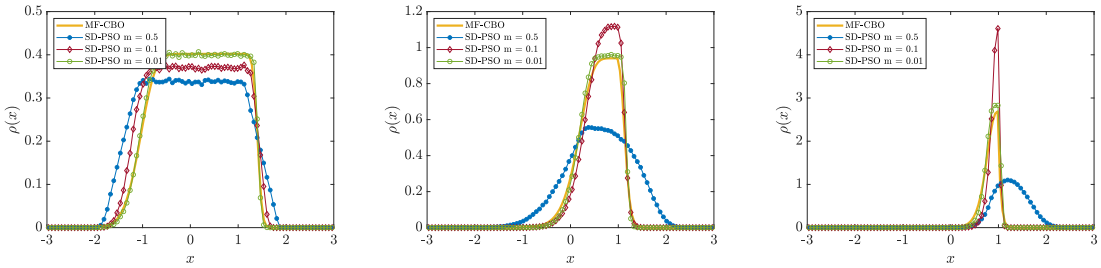

(a) $\rho(x,t)$, $t = 0.2$ (b) $\rho(x,t)$, $t = 1$ (c) $\rho(x,t)$, $t = 2$

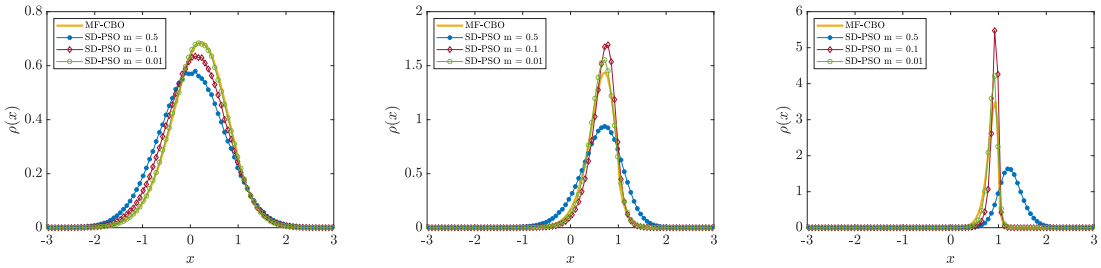

(d) $\rho(x,t)$, $t = 0.2$ (e) $\rho(x,t)$, $t = 1$ (f) $\rho(x,t)$, $t = 2$

Figure 2.16: Low inertia limit. Evolution of the density $\rho(x,t)$ of the SD-PSO discretization (2.36), for decreasing inertial weight $m = 0.5, 0.1, 0.01$, and the mean-field CBO model (2.27) for the Ackley function with minimum in $x = 1$. First row: uniform initial data. Second row: Gaussian initial data.

2.4.3 Comparison on high dimensional test cases

In this section we report the results of several experiments concerning the behavior of the stochastic PSO models, discretized using (2.33) in absence of memory or (2.35) in the general case, in high dimension ($d = 20$) for various prototype test functions (see Appendix A). For the sake of simplicity we will focus our attention mostly to the case of the Ackley function and the Rastrigin function, used also in the previous examples, and report additional results for other global optimization test functions at the end of the Section. These two functions, in fact, although with several local minima presents very different levels of difficulty and have been used as test functions for CBO methods in various other papers [20, 23, 39, 40, 83, 96].

In all tables reported in this section we will use the following terminology:

1. the *success rate*, computed averaging over $n_r = 500$ runs and using as convergence

criterion

$$\|X_\alpha^{n_*} - x_{min}\|_\infty < \delta_{err}, \qquad \text{or} \qquad \|\overline{Y}_\alpha^{n_*} - x_{min}\|_\infty < \delta_{err}$$

where x_{min} is the position of the minimum, n_* the final time, and $\delta_{err} = 0.25$ as in [23, 83].

2. the *error*, calculated as expected value in the L_2 norm over the successful runs

$$\mathbb{E}(\|X_\alpha^{n_*} - x_{min}\|_2), \qquad \text{or} \qquad \mathbb{E}(\|\overline{Y}_\alpha^{n_*} - x_{min}\|_2);$$

3. the *number of iterations*, where for a given tolerance $\delta_{stall} = 10^{-4}$, we stop the iteration if

$$\|X_\alpha^n - X_\alpha^{n-1}\| < \delta_{stall}, \qquad \text{or} \qquad \|\overline{Y}_\alpha^n - X_\alpha^{n-1}\| < \delta_{stall}$$

for $n_{stall} = 250$ consecutive iterations or a maximum number of 10^4 iterations has been reached.

It is important to remark that, while in previous simple one-dimensional validation examples we have chosen a low α value, increasing the dimension, a larger value of $\alpha \gg 1$ provides better performance [83]. On the other hand, a large value of α may generate numerical instabilities given by the definition of X_α^n in (2.15). To avoid this, we used the algorithm presented in [40] which prevents the value of N^α from being close to 0 by substituting, in absence of memory,

$$\frac{\omega_\alpha(X_i^n)}{N^\alpha} = \frac{\exp(-\alpha(\mathcal{F}(X_i^n) - \mathcal{F}(X_*^n)))}{\sum_{i=1}^N \exp(-\alpha(\mathcal{F}(X_i^n) - \mathcal{F}(X_*^n)))}, \tag{2.38}$$

with $X_*^n := \text{argmin}_{X \in \{X_i^n\}_{i=1}^N} \mathcal{F}(X)$. In a similar way, the method extends to the evaluation of $\overline{Y}_\alpha^n$ in the general case including memory.

Let us emphasize that, it is beyond the scopes of the present manuscript to perform an extensive testing of the various methods performances and to discuss the additional practical algorithmic enhancements that can be adopted to increase the success rate, like for example the use of random batch methods [4, 23, 64], particle reduction techniques [40] and parameters adaptivity [86]. In contrast, in the following test cases, we will address the role of the various parameters, of the presence of memory and of the local best when solving high dimensional global optimization problems. We refer also to [95] for additional comparisons. In all simulations we used Gaussian samples $\mathcal{N}(0, 1)$ in the exploration term but in principle it is possible to use another distribution hav-

Rastrigin		Case $\alpha = 5 \times 10$				Case $\alpha = 5 \times 10^4$			
m		σ	$N = 50$	$N = 100$	$N = 200$	σ	$N = 50$	$N = 100$	$N = 200$
0.00	Rate	7.0	100.0%	100.0%	100.0%	9.0	100.0%	100.0%	100.0%
	Error		6.10e-04	3.91e-04	2.52e-04		1.19e-04	1.11e-04	9.68e-05
	n_{iter}		10000.0	10000.0	10000.0		10000.0	10000.0	9912.4
0.01	Rate	6.5	100.0%	100.0%	100.0%	7.0	100.0%	100.0%	100.0%
	Error		8.57e-04	4.94e-04	3.08e-04		9.74e-05	2.01e-05	1.62e-05
	n_{iter}		10000.0	10000.0	10000.0		10000.0	6899.2	2060.1
0.05	Rate	3.5	42.5%	85.0%	92.0%	3.5	37.0%	74.0%	94.0%%
	Error		1.02e-03	7.98e-04	6.40e-04		4.27e-04	1.26e-04	1.14e-04
	n_{iter}		10000.0	10000.0	10000.0		8233.2	7814.0	7326.6
0.10	Rate	2.0	0.7%	2.5%	12.5%	2.0	1.0%	5.5%	29.5%
	Error		3.52e-03	2.24e-03	2.05e-03		2.00e-04	1.28e-04	1.11e-04
	n_{iter}		6818.3	7495.8	8680.9		6155.4	6221.9	6214.3

Table 2.1: SD-PSO without memory and with b.c. for $\lambda = 1$ and $\Delta t = 0.01$.

Ackley		Case $\alpha = 5 \times 10$				Case $\alpha = 5 \times 10^4$			
m		σ	$N = 50$	$N = 100$	$N = 200$	σ	$N = 50$	$N = 100$	$N = 200$
0.00	Rate	7.0	100.0%	100.0%	100.0%	9.0	100.0%	100.0%	100.0%
	Error		3.43e-03	1.90e-03	1.18e-03		8.46e-05	4.20e-05	1.27e-05
	n_{iter}		10000.0	10000.0	10000.0		1364.9	1032.4	869.2
0.01	Rate	6.5	100.0%	100.0%	100.0%	7.0	100.0%	100.0%	100%
	Error		5.03e-03	2.52e-03	1.36e-03		9.49e-05	5.89e-05	2.81e-05
	n_{iter}		10000.0	10000.0	10000.0		2192.9	1886.7	1723.6
0.05	Rate	3.5	100.0%	100.0%	100.0%	3.5	100.0%	100.0%	100.0%
	Error		3.76e-03	2.82e-03	7.74e-03		2.27e-04	1.48e-04	1.03e-04
	n_{iter}		10000.0	9857.2	6031.1		5367.3	4459.4	3928.4
0.10	Rate	2.0	99.5%	100.0%	100.0%	2.0	100.0%	100.0%	100.0%
	Error		2.34e-03	2.28e-03	2.24e-03		8.31e-04	2.76e-04	1.91e-04
	n_{iter}		5914.0	3856.7	2909.1		5480.8	4514.1	3909.4

Table 2.2: SD-PSO without memory and with b.c. for $\lambda = 1$ and $\Delta t = 0.01$.

ing mean 0 and variance 1. We analyzed also the use of a uniform noise $\mathcal{U}(-\sqrt{3}, \sqrt{3})$ similarly to the original discrete PSO dynamic but without noticing significant changes in the results except that smaller values of σ are needed to achieve convergence. In our experiments, additionally, the PSO constraints (2.6) have shown strong limitations in terms of success rates and have not been considered. This has been verified both by direct simulations using traditional PSO parameters in our numerical scheme and by using standard PSO libraries such as the `particleswarm` function of the Matlab Global Optimization Toolbox.

Rastrigin		Case $\alpha = 5 \times 10$				Case $\alpha = 5 \times 10^4$			
m		σ_2	$N = 50$	$N = 100$	$N = 200$	σ_2	$N = 50$	$N = 100$	$N = 200$
0.00	Rate	11.0	18.8%	16.8%	20.0%	11.0	100.0%	100.0%	100.0%
	Error		1.30e-03	5.09e-03	7.31e-03		6.83e-04	4.70e-04	4.69e-04
	n_{iter}		2331.9	1382.5	1289.6		10000.0	9878.2	3290.2
0.01	Rate	9.0	25.4%	25.6%	39.5%	9.0	100.0%	100.0%	100.0%
	Error		4.53e-03	7.44e-03	9.06e-03		8.60e-04	8.56e-04	8.81e-04
	n_{iter}		3536.0	3016.4	3128.9		9939.5	7012.2	5422.1
0.05	Rate	4.5	30.4%	34.8%	44.4%	4.5	100.0%	100.0%	100.0%
	Error		4.51e-03	5.74e-03	9.87e-03		1.15e-03	6.67e-04	6.54e-04
	n_{iter}		4646.0	4277.9	3598.5		9978.0	7657.6	5639.7
0.10	Rate	3.0	8.6%	20.8%	35.2%	3.0	80.8%	96.8%	100.0%
	Error		2.72e-02	1.71e-02	1.31e-02		2.94e-03	8.96e-04	8.24e-04
	n_{iter}		3686.7	4577.5	5361.4		9661.5	8676.5	7331.8

Table 2.3: SD-PSO with memory for $\lambda_1 = \sigma_1 = 0$, $\lambda_2 = 1$, $\Delta t = 0.01$, $\nu = 50$, $\beta = 3 \times 10^3$.

Ackley		Case $\alpha = 5 \times 10$				Case $\alpha = 5 \times 10^4$			
m		σ_2	$N = 50$	$N = 100$	$N = 200$	σ_2	$N = 50$	$N = 100$	$N = 200$
0.00	Rate	11.0	100.0%	100.0%	100.0%	11.0	100.0%	100.0%	100.0%
	Error		2.84e-03	3.96e-03	5.47e-03		1.02e-04	7.66e-05	5.44e-05
	n_{iter}		2260.2	1762.0	1346.5		2457.0	1778.0	1513.1
0.01	Rate	9.0	100.0%	100.0%	100.0%	9.0	100.0%	100.0%	100.0%
	Error		3.34e-03	4.70e-03	6.46e-03		2.34e-03	1.91e-04	1.61e-04
	n_{iter}		3722.2	2809.9	2104.2		6430.4	5447.8	4598.3
0.05	Rate	4.5	100.0%	100.0%	100.0%	4.5	100.0%	100.0%	100.0%
	Error		4.17e-03	6.06e-03	8.24e-03		2.41e-04	1.84e-04	1.48e-04
	n_{iter}		5300.6	4059.0	3113.1		7186.1	5996.0	5074.6
0.10	Rate	3.0	100.0%	100.0%	100.0%	3.0	100.0%	100.0%	100.0%
	Error		6.72e-03	9.58e-03	1.25e-02		3.90e-03	2.64e-03	2.06e-03
	n_{iter}		6411.8	4856.5	3783.5		8590.6	7326.4	6350.2

Table 2.4: SD-PSO with memory for $\lambda_1 = \sigma_1 = 0$, $\lambda_2 = 1$, $\Delta t = 0.01$, $\nu = 50$, $\beta = 3 \times 10^3$.

Effect of the inertial parameter m

Initially we report in Table 2.1 and Table 2.2 the results obtained with the formulation (2.33) that does not exploit the memory of particles. The initial data is a uniform distribution on the whole domain of definition that here is fixed to $[-3, 3]^d$. Since, typically, optimizing the Rastrigin function is far more difficult than the Ackley function due to the presence of multiple local minima from which it is hard to escape and in which the fitness function assumes values close to the global minimum, we explore the space of parameters searching for optimal values of σ and Δt for the Rastrigin function, then we used the same values for the Ackley function. This optimization has

been done roughly through simple variations of a given step size for the parameters. In the numerical examples we consider $\alpha = 5 \times 10$ and $\alpha = 5 \times 10^4$ to emphasize the role of such parameter in improving both the convergence rate as well as the efficiency of the solver.

Rastrigin		Case $\xi = 0$, $\sigma_2 = 11.0$			Case $\xi = 0.25$, $\sigma_2 = 8.5$		
		$N = 50$	$N = 100$	$N = 200$	$N = 50$	$N = 100$	$N = 200$
$x_{min} = 0$	Rate	100.0%	100.0%	100.0%	100.0%	100.0%	100.0%
	Error	7.04e-04	4.58e-04	3.29e-04	9.28e-04	6.11e-04	4.31e-04
	n_{iter}	10000.0	9963.9	4635.1	9978.0	8311.5	5754.1
$x_{min} = 1$	Rate	98.8%	100.0%	100.0%	99.2%	100.0%	100.0%
	Error	7.08e-04	4.60e-04	3.27e-04	9.31e-04	6.74e-04	4.59e-04
	n_{iter}	10000.0	10000.0	4670.0	9987.0	9746.7	7460.1
$x_{min} = 2$	Rate	96.0%	99.1%	100.0%	93.5%	100.0%	100.0%
	Error	6.91e-04	4.52e-04	3.28e-04	8.78e-04	6.74e-04	5.66e-04
	n_{iter}	10000.0	10000.0	5035.5	9980.3	9854.1	8971.9

Table 2.5: SD-PSO with memory ($m = 0$) for λ_1 and σ_1 given by (2.39), $\lambda_2 = 1$, $\Delta t = 0.01$, $\nu = 50$, $\beta = 3 \times 10^3$, $\alpha = 5 \times 10^4$.

Ackley		Case $\xi = 0$, $\sigma_2 = 11.0$			Case $\xi = 0.25$, $\sigma_2 = 8.5$		
		$N = 50$	$N = 100$	$N = 200$	$N = 50$	$N = 100$	$N = 200$
$x_{min} = 0$	Rate	100.0%	100.0%	100.0%	100.0%	100.0%	100.0%
	Error	7.36e-05	5.13e-05	3.26e-05	2.54e-05	1.13e-05	1.07e-05
	n_{iter}	2778.6	2030.0	1623.0	1942.9	1663.8	1442.5
$x_{min} = 1$	Rate	100.0%	100.0%	100.0%	100.0%	100.0%	100.0%
	Error	7.31e-05	5.14e-05	3.26e-05	2.58e-05	1.12e-05	1.02e-05
	n_{iter}	5298.5	3640.6	2575.9	2465.3	1948.5	1632.5
$x_{min} = 2$	Rate	100.0%	100.0%	100.0%	100.0%	100.0%	100.0%
	Error	7.30e-05	5.07e-05	3.22e-05	2.64e-05	1.09e-05	1.01e-05
	n_{iter}	7819.8	5771.3	4235.9	3126.8	2286.0	1803.8

Table 2.6: SD-PSO with memory ($m = 0$) for λ_1 and σ_1 given by (2.39), $\lambda_2 = 1$, $\Delta t = 0.01$, $\nu = 50$, $\beta = 3 \times 10^3$, $\alpha = 5 \times 10^4$.

The structure of the tables is the same: the results are given for two different choices of α and for different numbers of particles N. Since we are using a different solver we computed a different optimal value of σ for the Rastrigin function which is then used also for the Ackley function. The other two important parameters to be set are β and ν, chosen respectively equal to 3×10^3 and $1/(2\Delta t) = 50$ so that the memory dynamics

is close enough to the classical one of discrete PSO methods. In this case, thanks to the memory effect there is no need to bound the computational domain since particle tend to converge to the global minimum without spreading in the whole space. Introducing the boundary conditions, the situation improves but not significantly, and we omit the corresponding results. Finally, from Table 2.3 and Table 2.4 it is clear that, within the memory formulation, the choice of $\alpha \gg 1$ is essential to achieve good performances and therefore, the use of the algorithm described in (2.38) is fundamental in the practical implementation of the method.

Introduction of local best dynamics

Next we have considered the formulation (2.35) introducing the dynamics that lead the particles to move towards their local historical minimum. To reduce the number of free parameters we made the following assumption between the parameter defining the local best and the global best

$$\lambda_1 = \xi \cdot \lambda_2, \qquad \sigma_1 = \xi \cdot \sigma_2 \tag{2.39}$$

with $\xi \in [0, 1]$ so that the local best is always weighted less than the global best. In this test we keep the inertial value $m = 0$ and $\lambda_1 = 1$, so that we are solving the generalized stochastic differential CBO model with memory (2.28). For each value of ξ reported, we have computed an optimal σ_2 achieving the maximum rate of success. We chose $\beta = 3 \times 10^3$, $\Delta t = 0.01$ and $\nu = 0.5/\Delta t = 50$ as in the previous case and consider $\alpha = 5 \times 10^4$ in evaluating the global best.

First, in Tables 2.5 and 2.6 we report the behavior of the particle optimizer on the Ackley and Rastrigin functions for different positions of the minimum $x_{min} = 0$, $x_{min} = 1$ and $x_{min} = 2$. In this test we need to use the boundary conditions in order to achieve a high success rate when the minimum is close to the boundary of the domain. Since for large values of ξ we must decrease σ_2 to avoid a reduction of the convergence rate we expect that the total number of iterations may decrease. This is the case of the Ackley function in Table 2.6 where a considerable speed-up is obtained thanks to the local best when the minimum is close to the boundary.

Finally, in Table 2.7 we report the results obtained by solving simultaneously a set of different optimization functions considered in their standard domains (see Appendix A). Here, instead of trying to find an optimal set of parameters for each function we use the same parameters for all functions. Even if further investigations are necessary in terms of identifying optimal set of parameters, through the previous simplifications assumptions we reduced our analysis to a minimal choice of parameters which seems

the more relevant for the success of the algorithm.

Thus, we let most parameters fixed as in previous test case, namely $\alpha = 5 \times 10^4$, $\beta = 3 \times 10^3$, $\nu = 0.5/\Delta t$ since these essentially define the modeling process of the local best and global best. Additionally we keep $m = 0$, $\Delta t = 0.01$, and for a given value of $\xi = 0$ (absence of local best) and $\xi = 0.25$ (local best weighted 1/4 of global best) estimate the value for σ_2 in order to maximize the average convergence rate among all functions. Again this has been done roughly with simple variations of step 0.5 for σ_2 in the simulations.

The results confirm the potential of the method in identifying correctly the global minima for different test functions. Overall, with the exception of the Rastrigin function for which the local best produces a reduction in the convergence rate using this set of parameters, the importance of the local best is evident. In particular, the presence of the local best yields a significant reduction in the number of iterations for the Salomon function and an increase in the convergence rate for the XSY random function.

		Case $\xi = 0$, $\sigma_2 = 8.0$			Case $\xi = 0.25$, $\sigma_2 = 6.5$		
		$N = 50$	$N = 100$	$N = 200$	$N = 50$	$N = 100$	$N = 200$
Ackley	Rate	100.0%	100.0%	100.0%	100.0%	100.0%	100.0%
	Error	7.74e-05	6.12e-05	5.22e-05	2.08e-04	1.98e-04	1.65e-04
	n_{iter}	1325.0	1114.8	924.9	1263.2	992.3	902.4
Rastrigin	Rate	31.4%	65.7%	95.6%	5.3%	10.5%	27.9%
	Error	5.59e-04	7.70e-04	9.68e-04	1.46e-03	9.73e-04	1.06e-03
	n_{iter}	1404.7	1107.8	954.1	4390.0	4756.2	4643.6
Griewalk	Rate	100.0%	100.0%	100.0%	100.0%	100.0%	100.0%
	Error	9.12e-02	7.55e-02	5.78e-02	8.22e-02	5.34e-02	4.12e-02
	n_{iter}	10000.0	10000.0	10000.0	10000.0	10000.0	9978.4
Schwefel	Rate	99.6%	100.0%	100.0%	100.0%	100.0%	100.0%
	Error	1.16e-05	1.22e-05	1.39e-05	2.69e-05	2.80e-05	2.85e-05
	n_{iter}	1211.2	1044.1	987.3	1127.9	964.8	849.7
Salomon	Rate	96.7%	98.3%	100.0%	100.0%	100.0%	100.0%
	Error	9.26e-02	8.73e-02	8.02e-02	8.22e-02	6.12e-02	5.23e-02
	n_{iter}	9443.0	8176.2	7443.3	6476.0	3009.7	1923.2
XSY random	Rate	35.5%	59.5%	94.2%	75.1%	94.2%	100.0%
	Error	1.12e-01	9.81e-02	8.82e-02	1.06e-01	9.79e-02	8.57e-02
	n_{iter}	10000.0	10000.0	10000.0	10000.0	10000.0	10000.0

Table 2.7: SD-PSO with memory ($m = 0$) for λ_1 and σ_1 given by (2.39), $\lambda_2 = 1$, $\Delta t = 0.01$, $\nu = 50$, $\beta = 3 \times 10^3$, $\alpha = 5 \times 10^4$.

2.5 Concluding remarks

In this chapter, with the aim of providing a contribution to the construction of a general mathematical theory that will allow the rigorous analysis of optimization methods based on particle swarms (PSO), starting from the original discrete formulation, we derived, by approximating in an appropriate way the memory dynamics, the corresponding systems of SDEs. In the large particle limit, using a regularized version of these systems we obtain a mean-field PDE of Vlasov-Fokker-Planck type describing the PSO dynamic. The new mean-field formalism, for small values of the inertia parameter, permits to compute as hydrodynamic approximation a generalization of consensus-based optimization models (CBO) with local best, thus highlighting the relationships between these two classes of metaheuristic optimization methods.

These results are numerically validated through several examples that compare the mean-field and the particle dynamics. The methods are then tested against some prototype high dimensional global optimization functions with the goal of understanding the effects of the various parameters and the main differences between the novel stochastic differential models and standard CBO systems, namely the presence of memory effects together with the local best. The numerical results confirmed the ability of the local best to improve the performance of the methods in terms of speed of convergence and rate of success. It is worth noting that the SD-PSO models here introduced, thanks to the increased independence of the search parameters, allow better performances of the classic PSO methods (which represent a particular case included in the choices of possible optimization parameters).

Chapter 3

Theoretical analysis: mean-field convergence and small inertia limit

In this chapter we report a rigorous mathematical treatment of the formalism introduced in Chapter 2 which permitted to generalize PSO methods to continuum second-order dynamics and to derive CBO methods as the corresponding first-order low inertia limit. We analyze separately the case without and with memory effects by justifying first the mean-field limit and subsequently, the zero inertia limit for the mean-field system. A general result of convergence to the global minimum in the absence of memory effects and without local best is illustrated in the final part.

3.1 Mean-field limit of particle swarm optimization

In this section we use the two modified versions of the canonical stochastic differential PSO system for which we can formally compute its mean-field limit. We first consider the case in absence of memory effects (2.14) and then we extend the results to the general case (2.19). Throughout this section, our theoretical analysis assumes the cost function $\mathcal{F}$ satisfies the following

Assumption 1. *For the given cost function $\mathcal{F} : \mathbb{R}^d \to \mathbb{R}$, it holds that:*

(1) There exists some constant $L > 0$ such $|\mathcal{F}(x) - \mathcal{F}(y)| \leq L(|x| + |y|)|x - y|$ for all $x, y \in \mathbb{R}^d$;

(2) $\mathcal{F}$ is bounded from below with $-\infty < \underline{\mathcal{F}} := \inf \mathcal{F}$ and there exists some constant $C_u > 0$ such that

$$\mathcal{F}(x) - \underline{\mathcal{F}} \leq C_u(1 + |x|^2) \text{ for all } x \in \mathbb{R}^d ;$$

(3) $\mathcal{F}$ *has quadratic growth at infinity. Namely, there exist constants* C_l, $M > 0$ *such that*

$$\mathcal{F}(x) - \underline{\mathcal{F}} \geq C_l|x|^2 \text{ for all } |x| \geq M\,.$$

3.1.1 Theoretical analysis on PSO dynamics without memory effects

Let us consider a PSO approach where the dynamic is instantaneous without memory of the local best positions and the global best has been regularized as in [83]. The corresponding second order system of SDEs describing the *regularized SD-PSO dynamics* takes the form

$$\begin{aligned} dX_t^{i,N} &= V_t^{i,N}dt, \\ mdV_t^{i,N} &= -\gamma V_t^{i,N}dt + \lambda(X^\alpha(\rho_t^N) - X_t^{i,N})dt \\ &\quad + \sigma D(X^\alpha(\rho_t^N) - X_t^{i,N})dB_t^i\,, \end{aligned} \tag{3.1}$$

that we rewrite from (2.14) adding the superscript N with we aim of underlining the dependence on the number of particles in the system. We emphasize that the stochastic particle system above has locally Lipschitz coefficients, thus it admits strong solutions and pathwise uniqueness holds up to any finite time $T > 0$, see [25, 35]. As the particle number $N \to \infty$, one expects to derive the *mean-field PSO description without local best* characterized by the following nonlinear *Vlasov-Fokker-Planck equation* (2.18) which represents the mean-field PSO (MF-PSO) model without local best and should be accompanied by initial (and boundary) data. We refer to [12, 21, 48, 61, 93] and the references therein, for more details and rigorous results about mean-field models of Vlasov-Fokker-Planck type. Note, however, that the presence of $X^\alpha(\rho)$ makes the Vlasov-Fokker-Planck equation nonlinear and nonlocal. This is nonstandard in the literature and raises several analytical and numerical questions (see [20, 40]).

Following [60] we provide a rigorous justification of the mean-field limit of PSO model (2.14) towards its mean-field PDE (2.18) through a compactness argument. More precisely, we first prove that the sequence of empirical measures $\{f^N\}_{N\geq 2}$ ($f^N = \frac{1}{N}\sum_{i=1}^N \delta_{(X^{i,N},V^{i,N})}$ are $\mathcal{P}(\mathcal{C}([0,T];\mathbb{R}^d)\times\mathcal{C}([0,T];\mathbb{R}^d))$-valued random variables) is tight. Prokhorov's theorem indicates that there exists a subsequence of $\{f^N\}_{N\geq 2}$ converging in law to a random measure f. Then, to identify the limit, we verify that the limit measure f is a weak solution to the mean-field PSO equation (2.18) almost surely, while the uniqueness of the weak solution to PDE (2.18) yields that f is actually deterministic. Our main result can be described in the following way:

Theorem 3.1. *Let $\mathcal{F}$ satisfy Assumption 1 and $f_0 \in \mathcal{P}_4(\mathbb{R}^{2d})$. For any $N \geq 2$, we assume that $\{(X_t^{i,N}, V_t^{i,N})_{t\in[0,T]}\}_{i=1}^N$ is the unique solution to the SD-PSO system (2.14) with $f_0^{\otimes N}$-distributed initial data $\{X_0^{i,N}, V_0^{i,N}\}_{i=1}^N$. Then the limit for $N \to \infty$ (denoted by f) of the sequence of the empirical measure $f^N = \frac{1}{N}\sum_{i=1}^N \delta_{(X^{i,N},V^{i,N})}$ exists. Moreover, f is the unique weak solution to the MF-PSO equation (2.18).*

To obtain the above theorem, let us first prove the following lemma on a uniform moment estimate for the particle system (2.14).

Lemma 3.2. *Let $\mathcal{F}$ satisfy Assumption 1 and $f_0 \in \mathcal{P}_4(\mathbb{R}^{2d})$. For any $N \geq 2$, assume that $\{(X_t^{i,N}, V_t^{i,N})_{t\in[0,T]}\}_{i=1}^N$ is the unique solution to the SD-PSO system (2.14) with $f_0^{\otimes N}$-distributed initial data $\{(X_0^{i,N}, V_0^{i,N})\}_{i=1}^N$. Then there exists a constant $K > 0$ independent of N such that*

$$\begin{aligned}\sup_{i=1,\cdots,N}\left\{\sup_{t\in[0,T]}\mathbb{E}\left[|X_t^{i,N}|^2+|X_t^{i,N}|^4+|V_t^{i,N}|^2+|V_t^{i,N}|^4\right]\right\}\\ +\sup_{t\in[0,T]}\mathbb{E}\left[|X^\alpha(\rho_t^N)|^2+|X^\alpha(\rho_t^N)|^4\right]\leq K\,.\end{aligned} \tag{3.2}$$

The proof follows similar arguments as in [20, Lemma 3.4].

Let Ω be a generic space, we treat $(X^{i,N}, V^{i,N}) : \Omega \mapsto \mathcal{C}([0,T];\mathbb{R}^d)\times\mathcal{C}([0,T];\mathbb{R}^d)$. Then $f^N = \sum_{i=1}^N \delta_{(X^{i,N},V^{i,N})} : \Omega \mapsto \mathcal{P}(\mathcal{C}([0,T];\mathbb{R}^d)\times\mathcal{C}([0,T];\mathbb{R}^d))$ is a random measure. Let us denote $\mathcal{L}(f^N) := \mathrm{Law}(f^N) \in \mathcal{P}(\mathcal{P}(\mathcal{C}([0,T];\mathbb{R}^d)\times\mathcal{C}([0,T];\mathbb{R}^d)))$. We can prove that $\{\mathcal{L}(f^N)\}_{N\geq 2}$ is tight, or we say $\{f^N\}_{N\geq 2}$ is tight, which can be done by verifying the Aldous criteria [10] as presented below:

Lemma 3.3. *Let $\{X^n\}_{n\in\mathbb{N}}$ be a sequence of random variables defined on a probability space $(\Omega,\mathcal{F},\mathbb{P})$ and valued in $\mathcal{C}([0,T];\mathbb{R}^d)$. The sequence of probability distributions $\{\mu_{X^n}\}_{n\in\mathbb{N}}$ of $\{X^n\}_{n\in\mathbb{N}}$ is tight on $\mathcal{C}([0,T];\mathbb{R}^d)$ if the following two conditions hold.*

(Con1) For all $t \in [0,T]$, the set of distributions of X_t^n, denoted by $\{\mu_{X_t^n}\}_{n\in\mathbb{N}}$, is tight as a sequence of probability measures on $\mathbb{R}^d$.

(Con2) For all $\varepsilon > 0$, $\eta > 0$, there exists $\delta_0 > 0$ and $n_0 \in \mathbb{N}$ such that for all $n \geq n_0$ and for all discrete-valued $\sigma(X_s^n; s \in [0,T])$-stopping times β with $0 \leq \beta + \delta_0 \leq T$, it holds that

$$\sup_{\delta\in[0,\delta_0]}\mathbb{P}\left(|X_{\beta+\delta}^n - X_\beta^n| \geq \eta\right) \leq \varepsilon\,. \tag{3.3}$$

We can then prove:

Theorem 3.4. *Let $\mathcal{F}$ satisfy Assumption 1 and $f_0 \in \mathcal{P}_4(\mathbb{R}^{2d})$. For any $N \geq 2$, we assume that $\{(X_t^{i,N}, V_t^{i,N})_{t\in[0,T]}\}_{i=1}^N$ is the unique solution to the SD-PSO system (2.14)*

with $f_0^{\otimes N}$-distributed initial data $\{X_0^{i,N}, V_0^{i,N}\}_{i=1}^N$. Then the sequence $\{\mathcal{L}(f^N)\}_{N\geq 2}$ is tight in $\mathcal{P}(\mathcal{P}(\mathcal{C}([0,T];\mathbb{R}^d)\times\mathcal{C}([0,T];\mathbb{R}^d)))$.

Proof. According to Proposition 2.2 (ii) in [93, Proposition 2.2 (ii)], we only need to prove that the law $\{\mathcal{L}((X^{1,N},V^{1,N}))\}_{N\geq 2}$ is tight in $\mathcal{P}(\mathcal{C}([0,T];\mathbb{R}^d)\times\mathcal{C}([0,T];\mathbb{R}^d))$ because of the exchangeability of the particle system. It is sufficient to justify conditions $(Con1)$ and $(Con2)$ in Lemma 3.3.

• *Step 1: Checking* $(Con1)$. For any $\varepsilon>0$, there exists a compact subset $U_\varepsilon := \{(x,v):\ |x|^2+|v|^2\leq \frac{K}{\varepsilon}\}$ such that by Markov's inequality

$$\begin{aligned}\mathcal{L}((X_t^{1,N},V_t^{1,N}))\ ((U_\varepsilon)^c) &= \mathbb{P}\left(|X_t^{1,N}|^2+|V_t^{1,N}|^2>\frac{K}{\varepsilon}\right)\\ &\leq \frac{\varepsilon\mathbb{E}[|X_t^{1,N}|^2+|V_t^{1,N}|^2]}{K}\leq\varepsilon,\quad \forall\ N\geq 2\,,\end{aligned}$$

where we have used Lemma 3.2 in the last inequality. This means that for each $t\in[0,T]$, the sequence $\{\mathcal{L}((X_t^{1,N},V_t^{1,N}))\}_{N\geq 2}$ is tight, which verifies condition $(Con1)$ in Lemma 3.3.

• *Step 2: Checking* $(Con2)$. Let β be a $\sigma((X_s^{1,N},V_s^{1,N});s\in[0,T])$-stopping time with discrete values such that $\beta+\delta_0\leq T$. We have

$$\mathbb{E}[|X_{\beta+\delta}^{1,N}-X_\beta^{1,N}|^2]\leq\delta\int_0^T\mathbb{E}[|V_s^{1,N}|^2]ds\leq C\delta\,, \tag{3.4}$$

where $C>0$ is independent of N by (3.2). Furthermore,

$$\begin{aligned}V_{\beta+\delta}^{1,N}-V_\beta^{1,N} = &-\frac{\gamma}{m}\int_\beta^{\beta+\delta}V_s^{1,N}ds+\frac{\lambda}{m}\int_\beta^{\beta+\delta}(X^\alpha(\rho_s^N)-X_s^{1,N})ds\\ &+\frac{\sigma}{m}\int_\beta^{\beta+\delta}D(X^\alpha(\rho_s^N)-X_s^{1,N})dB_s^1\,.\end{aligned}$$

Notice that

$$\begin{aligned}\mathbb{E}\left[\left|\int_\beta^{\beta+\delta}(X^\alpha(\rho_s^N)-X_s^{1,N})ds\right|^2\right]&\leq\delta\int_0^T\mathbb{E}\left[|X^\alpha(\rho_s^N)-X_s^{1,N}|^2\right]ds\\ \leq 2\delta T\left(\sup_{t\in[0,T]}\mathbb{E}\left[|X_t^{1,N}|^2\right]+\sup_{t\in[0,T]}\mathbb{E}\left[|X^\alpha(\rho_t^N)|^2\right]\right)&\leq 2TK\delta\,,\end{aligned} \tag{3.5}$$

where we have used Lemma 3.2 in the last inequality. Similarly we have

$$\mathbb{E}\left[\left|\int_\beta^{\beta+\delta}V_s^{1,N}ds\right|^2\right]\leq TK\delta\,. \tag{3.6}$$

Further we apply Itô's isometry

$$\begin{aligned}\mathbb{E}\left[\left|\int_\beta^{\beta+\delta} D(X^\alpha(\rho_s^N)-X_s^{1,N})dB_s^1\right|^2\right] &= \mathbb{E}\left[\int_\beta^{\beta+\delta}|X^\alpha(\rho_s^N)-X_s^{1,N}|^2 ds\right]\\ &\le \delta^{\frac12}\mathbb{E}\left[\left(\int_0^T |X^\alpha(\rho_s^N)-X_s^{1,N}|^4 ds\right)^{\frac12}\right]\\ &\le \delta^{\frac12}\left(\int_0^T \mathbb{E}[|X^\alpha(\rho_s^N)-X_s^{1,N}|^4]ds\right)^{\frac12} \le \delta^{\frac12}T^{\frac12}(8K)^{\frac12}\,. \end{aligned} \tag{3.7}$$

Combining estimates (3.5)–(3.7) one has

$$\mathbb{E}[|V_{\beta+\delta}^{1,N}-V_\beta^{1,N}|^2] \le C(\gamma.\lambda,m,\sigma,T,K)\left(\delta^{\frac12}+\delta\right)\,. \tag{3.8}$$

Hence, for any $\varepsilon>0$, $\eta>0$, there exists some $\delta_0>0$ such that for all $N\ge 2$ it holds that

$$\begin{aligned}&\sup_{\delta\in[0,\delta_0]}\mathbb{P}\left(|X_{\beta+\delta}^{1,N}-X_\beta^{1,N}|^2+|V_{\beta+\delta}^{1,N}-V_\beta^{1,N}|^2\ge\eta\right)\\ &\qquad\le \sup_{\delta\in[0,\delta_0]}\frac{\mathbb{E}\left[|X_{\beta+\delta}^{1,N}-X_\beta^{1,N}|^2+|V_{\beta+\delta}^{1,N}-V_\beta^{1,N}|^2\right]}{\eta}\le\varepsilon\,.\end{aligned} \tag{3.9}$$

Hence $(Con2)$ is verified. □

For any $\varphi\in\mathcal{C}_c^2(\mathbb{R}^d\times\mathbb{R}^d)$, define a functional on $\mathcal{P}(\mathcal{C}([0,T];\mathbb{R}^d)\times\mathcal{C}([0,T];\mathbb{R}^d))$ as follows

$$\begin{aligned}F_\varphi(f) &:= \langle\varphi(\mathbf{x}_t,\mathbf{v}_t),f(d\mathbf{x},d\mathbf{v})\rangle-\langle\varphi(\mathbf{x}_0,\mathbf{v}_0),f(d\mathbf{x},d\mathbf{v})\rangle+\int_0^t\langle\mathbf{v}_s\cdot\nabla_x\varphi,f(d\mathbf{x},d\mathbf{v})\rangle ds\\ &\quad-\frac{\gamma}{m}\int_0^t\langle\mathbf{v}_s\cdot\nabla_v\varphi,f(d\mathbf{x},d\mathbf{v})\rangle ds+\frac{\lambda}{m}\int_0^t\langle(\mathbf{x}_s-X^\alpha(\rho_s))\cdot\nabla_v\varphi,f(d\mathbf{x},d\mathbf{v})\rangle ds\\ &\quad-\frac{\sigma^2}{2m^2}\int_0^t\sum_{k=1}^d\langle(\mathbf{x}_s-X^\alpha(\rho_s))_k^2\frac{\partial^2\varphi}{\partial v_k^2},f(d\mathbf{x},d\mathbf{v})\rangle ds\\ &= \langle\varphi(x,v),f_t(dx,dv)\rangle-\langle\varphi(x,v),f_0(dx,dv)\rangle+\int_0^t\langle v\cdot\nabla_x\varphi,f_s(dx,dv)\rangle ds\\ &\quad-\frac{\gamma}{m}\int_0^t\langle v\cdot\nabla_v\varphi,f_s(dx,dv)\rangle ds+\frac{\lambda}{m}\int_0^t\langle(x-X^\alpha(\rho_s))\cdot\nabla_v\varphi,f_s(dx,dv)\rangle ds\\ &\quad-\frac{\sigma^2}{2m^2}\int_0^t\sum_{k=1}^d\langle(x-X^\alpha(\rho_s))_k^2\frac{\partial^2\varphi}{\partial v_k^2},f_s(dx,dv)\rangle ds\,,\end{aligned}$$

for all $f\in\mathcal{P}(\mathcal{C}([0,T];\mathbb{R}^d)\times\mathcal{C}([0,T];\mathbb{R}^d))$ and $\mathbf{x},\mathbf{v}\in\mathcal{C}([0,T];\mathbb{R}^d)$, where $\rho_t(x)=\int_{\mathbb{R}^d}f_t(x,dv)$.

Then we have the following estimate by the reasoning in [60, Proposition 3.2].

Lemma 3.5. *Let $\mathcal{F}$ satisfy Assumption 1 and $f_0 \in \mathcal{P}_4(\mathbb{R}^{2d})$. For any $N \geq 2$, assume that $\{(X_t^{i,N}, V_t^{i,N})_{t\in[0,T]}\}_{i=1}^N$ is the unique solution to the SD-PSO system (2.14) with $f_0^{\otimes N}$-distributed initial data $\{(X_0^{i,N}, V_0^{i,N})\}_{i=1}^N$. There exists a constant $C > 0$ depending only on $\sigma, \gamma, \lambda, m, K, T$, and $\|\nabla\varphi\|_\infty$ such that*

$$\mathbb{E}[|F_\varphi(f^N)|^2] \leq \frac{C}{N}, \tag{3.10}$$

where $f^N = \frac{1}{N}\sum_{i=1}^N \delta_{(X^{i,N},V^{i,N})}$ is the empirical measure.

By Skorokhod's lemma (see [10, Theorem 6.7 on page 70]), using Theorem 3.4 we may find a common probability space $(\Omega, \mathcal{F}, \mathbb{P})$ on which the processes $\{f^N\}_{N\in\mathbb{N}}$ converge to some process f as a random variable valued in $\mathcal{P}(\mathcal{C}([0,T];\mathbb{R}^d) \times \mathcal{C}([0,T];\mathbb{R}^d))$ almost surely. In particular, we have that for all $t \in [0,T]$ and $\varphi \in C_b(\mathbb{R}^d \times \mathbb{R}^d)$,

$$\lim_{N\to\infty} |\langle\varphi, f_t^N - f_t\rangle| + \left|X^\alpha(\rho_t^N) - X^\alpha(\rho_t)\right| = 0, \quad \text{a.s.} \tag{3.11}$$

Indeed, according to Assumption 1, one has $xe^{-\alpha\mathcal{F}(x)}, e^{-\alpha\mathcal{F}(x)} \in \mathcal{C}_b(\mathbb{R}^d)$, which gives

$$\lim_{N\to\infty} X^\alpha(\rho_t^N) = \lim_{N\to\infty} \frac{\langle xe^{-\alpha\mathcal{F}(x)}, \rho_t^N(dx)\rangle}{\langle e^{-\alpha\mathcal{F}(x)}, \rho_t^N(dx)\rangle} = \frac{\langle xe^{-\alpha\mathcal{F}(x)}, \rho_t(dx)\rangle}{\langle e^{-\alpha\mathcal{F}(x)}, \rho_t(dx)\rangle} = X^\alpha(\rho_t) \quad \text{a.s.}$$

Lemma 3.6. *[20, Lemma 3.3] Let $\mathcal{F}$ satisfy Assumption 1 and $\mu \in \mathcal{P}_2(\mathbb{R}^d)$. Then it holds that*

$$|X^\alpha(\mu)|^2 \leq b_1 + b_2 \int_{\mathbb{R}^d} |x|^2 \mu(dx), \tag{3.12}$$

where b_1 and b_2 depends only on M, C_u, and C_l.

For each $A > 0$, it follows from (3.11) that

$$\begin{aligned}
&\mathbb{E}\left[\iint_{\mathbb{R}^{2d}} ((|x|^4 + |v|^4) \wedge A) f_t(dx, dv)\right] \\
&= \mathbb{E}\left[\lim_{N\to\infty} \iint_{\mathbb{R}^{2d}} ((|x|^4 + |v|^4) \wedge A) f_t^N(dx, dv)\right] \\
&\leq \lim_{N\to\infty} \frac{\sum_{i=1}^N \mathbb{E}[|X_t^{i,N}|^4 + |V_t^{i,N}|^4]}{N} \leq K,
\end{aligned}$$

where we have used Lemma 3.2. Letting $A \to \infty$, we have

$$\sup_{t\in[0,T]} \mathbb{E}\left[\iint_{\mathbb{R}^{2d}} (|x|^4 + |v|^4) f_t(dx, dv)\right] \leq K. \tag{3.13}$$

Then Lemma 3.6 implies that

$$\mathbb{E}[|X^\alpha(\rho_t)|^4] < \infty\,, \tag{3.14}$$

for all $t \in [0,T]$. Furthermore, it holds that

$$\lim_{N\to\infty} \mathbb{E}\left[\left|\langle \varphi, f_t^N - f_t\rangle\right|^2 + |X^\alpha(\rho_t^N) - X^\alpha(\rho_t)|^2\right] = 0, \tag{3.15}$$

which follows directly from the pointwise convergences of $\langle \varphi, f_t^N - f_t\rangle$ and $X^\alpha(\rho_t^N) - X^\alpha(\rho_t)$, and the uniform estimate (3.2) in Lemma 3.2 and (3.14).

We can now prove the main result in Theorem 3.1:

Proof. **(Theorem 3.1)** Suppose the $\mathcal{P}(\mathcal{C}([0,T];\mathbb{R}^d) \times \mathcal{C}([0,T];\mathbb{R}^d))$-valued random variable f_t is the limit of a subsequence of the empirical measure $f^N = \frac{1}{N}\sum_{i=1}^N \delta_{(X^{i,N},V^{i,N})}$. Without loss of generality, we denote the subsequence again by itself. We may continue to work on the above common probability space $(\Omega, \mathcal{F}, \mathbb{P})$ by Skorokhod's lemma where the convergence is holding almost surely (see (3.11) for instance). We may first check that f_t is a.s. continuous in time. Indeed for any $\varphi \in \mathcal{C}_b(\mathbb{R}^{2d})$ and $t_n \to t$ we may apply dominated convergence theorem

$$\begin{aligned}&\iint_{\mathcal{C}([0,T];\mathbb{R}^d)\times\mathcal{C}([0,T];\mathbb{R}^d)} \varphi(\mathbf{x}_{t_n}, \mathbf{v}_{t_n}) f(d\mathbf{x}, d\mathbf{v})\\ &\quad\to \iint_{\mathcal{C}([0,T];\mathbb{R}^d)\times\mathcal{C}([0,T];\mathbb{R}^d)} \varphi(\mathbf{x}_t, \mathbf{v}_t) f(d\mathbf{x}, d\mathbf{v}) \quad \text{a.s.},\end{aligned}$$

which gives

$$\iint_{\mathbb{R}^{2d}} \varphi(x,v) f_{t_n}(dx,dv) \to \iint_{\mathbb{R}^{2d}} \varphi(x,v) f_t(dx,dv) \quad \text{a.s.}$$

For $\varphi \in \mathcal{C}_c^2(\mathbb{R}^{2d})$, using the convergence result in (3.15) one has

$$\lim_{N\to\infty} \mathbb{E}\left[|(\langle \varphi, f_t^N\rangle - \langle \varphi, f_0^N\rangle) - (\langle \varphi, f_t\rangle - \langle \varphi, f_0\rangle)|\right] = 0\,. \tag{3.16}$$

Further we notice that

$$\begin{aligned}
&\left|\int_0^t \langle (x - X^\alpha(\rho_s^N)) \cdot \nabla_v \varphi, f_s^N \rangle ds - \int_0^t \langle (x - X^\alpha(\rho_s)) \cdot \nabla_v \varphi, f_s \rangle ds \right| \\
&\quad \leq \int_0^t \left| \langle (x - X^\alpha(\rho_s^N)) \cdot \nabla_v \varphi, f_s^N - f_s \rangle \right| ds \\
&\qquad + \int_0^t \left| \langle (X^\alpha(\rho_s) - X^\alpha(\rho_s^N)) \cdot \nabla_v \varphi, f_s \rangle \right| ds \\
&\quad =: \int_0^t |I_1^N(s)| ds + \int_0^t |I_2^N(s)| ds \,.
\end{aligned}$$

One computes

$$\begin{aligned}
&\mathbb{E}[|I_1^N(s)|] \\
&\quad \leq \mathbb{E}[|\langle x \cdot \nabla_v \varphi, f_s^N - f_s \rangle|] + \mathbb{E}[|X^\alpha(\rho_s^N) \cdot \langle \nabla_v \varphi, f_s^N - f_s \rangle|] \\
&\quad \leq \mathbb{E}[|\langle x \cdot \nabla_v \varphi, f_s^N - f_s \rangle|] + K^{\frac{1}{2}} (\mathbb{E}[|\langle \nabla_v \varphi, f_s^N - f_s \rangle|^2])^{\frac{1}{2}} \,,
\end{aligned}$$

where we have used Lemma 3.2 in the second inequality. Since φ has a compact support, applying (3.15) leads to

$$\lim_{N \to \infty} \mathbb{E}\left[|I_1^N(s)|\right] = 0 \,. \tag{3.17}$$

Moreover, the uniform boundedness of $\mathbb{E}\left[|I_1^N(s)|\right]$ follows directly from (3.13), (3.14), and the estimates in Lemma 3.2, which by the dominated convergence theorem implies

$$\lim_{N \to \infty} \int_0^t \mathbb{E}[|I_1^N(s)|] ds = 0 \,. \tag{3.18}$$

As for I_2^N, we know that

$$\left| \langle (X^\alpha(\rho_s) - X^\alpha(\rho_s^N)) \cdot \nabla_v \varphi, f_s \rangle \right| \leq \|\nabla_v \varphi\|_\infty \left| X^\alpha(\rho_s) - X^\alpha(\rho_s^N) \right| . \tag{3.19}$$

Hence by (3.15) it yields that

$$\lim_{N \to \infty} \mathbb{E}[|I_2^N(s)|] = 0 \,. \tag{3.20}$$

Again by the dominated convergence theorem, we have

$$\lim_{N \to \infty} \int_0^t \mathbb{E}[|I_2^N(s)|] ds = 0 \,. \tag{3.21}$$

This combined with (3.18) leads to

$$\lim_{N\to\infty} \mathbb{E}\left[\left|\int_0^t \langle (x - X^\alpha(\rho_s^N)) \cdot \nabla_v \varphi, f_s^N\rangle ds \right.\right. \\ \left.\left. - \int_0^t \langle (x - X^\alpha(\rho_s)) \cdot \nabla_v \varphi, f_s\rangle ds \right|\right] = 0\,. \tag{3.22}$$

Similarly we split the error

$$\begin{aligned} &\left|\int_0^t \langle (x - X^\alpha(\rho_s^N))_k^2 \frac{\partial^2}{\partial {v_k}^2}\varphi, f_s^N\rangle ds - \int_0^t \langle (x - X^\alpha(\rho_s))_k^2 \frac{\partial^2}{\partial {v_k}^2}\varphi, f_s\rangle ds\right| \\ &\quad \le \left|\int_0^t \langle (x - X^\alpha(\rho_s^N))_k^2 \frac{\partial^2}{\partial {v_k}^2}\varphi, f_s^N - f_s\rangle ds\right| \\ &\qquad + \left|\int_0^t \langle ((x - X^\alpha(\rho_s^N))_k^2 - (x - X^\alpha(\rho_s))_k^2) \frac{\partial^2}{\partial {v_k}^2}\varphi, f_s\rangle ds\right| \\ &\quad =: \int_0^t |I_3^N(s)| ds + \int_0^t |I_4^N(s)| ds\,. \end{aligned}$$

Following the same argument as for I_1^N and I_2^N, one has

$$\lim_{N\to\infty} \int_0^t \mathbb{E}[|I_3^N(s)|] ds = 0 \text{ and } \lim_{N\to\infty} \int_0^t \mathbb{E}[|I_4^N(s)|] ds = 0\,. \tag{3.23}$$

This implies that

$$\lim_{N\to\infty} \mathbb{E}\left[\left| \int_0^t \sum_{k=1}^d \langle (x - X^\alpha(\rho_s^N))_k^2 \frac{\partial^2}{\partial {v_k}^2}\varphi(x), f_s^N\rangle ds \right.\right. \\ \left.\left. - \int_0^t \sum_{k=1}^d \langle (x - X^\alpha(\rho_s))_k^2 \frac{\partial^2}{\partial {v_k}^2}\varphi(x), f_s\rangle ds \right|\right] = 0\,. \tag{3.24}$$

Moreover, we have

$$\lim_{N\to\infty} \mathbb{E}\left[\left|\int_0^t \langle v \cdot \nabla_x \varphi, f_s^N\rangle ds - \int_0^t \langle v \cdot \nabla_x \varphi, f_s\rangle ds\right|\right] = 0 \tag{3.25}$$

and

$$\lim_{N\to\infty} \mathbb{E}\left[\left|\int_0^t \langle v \cdot \nabla_v \varphi, f_s^N\rangle ds - \int_0^t \langle v \cdot \nabla_v \varphi, f_s\rangle ds\right|\right] = 0\,. \tag{3.26}$$

Collecting estimates (3.16), (3.22), (3.24), (3.25) and (3.26) we have

$$\lim_{N\to\infty} \mathbb{E}[|F_\varphi(f^N) - F_\varphi(f)|] = 0\,. \tag{3.27}$$

Then we have

$$\begin{aligned}\mathbb{E}[|F_\varphi(f)|] &\leq \mathbb{E}[|F_\varphi(f^N) - F_\varphi(f)|] + \mathbb{E}[|F_\varphi(f^N)|] \\ &\leq \mathbb{E}[|F_\varphi(f^N) - F_\varphi(f)|] + \frac{C}{\sqrt{N}} \to 0 \quad \text{as } N \to \infty\,,\end{aligned}$$

where we have used Lemma 3.5 in the last inequality. This implies that

$$F_\varphi(f) = 0 \quad \text{a.s.} \tag{3.28}$$

In other words, it holds that

$$\begin{aligned}&\langle \varphi(x,v), f_t(dx,dv)\rangle - \langle \varphi(x,v), f_0(dx,dv)\rangle + \int_0^t \langle v\cdot\nabla_x\varphi, f_s(dx,dv)\rangle ds \\ &- \frac{\gamma}{m}\int_0^t \langle v\cdot\nabla_v\varphi, f_s(dx,dv)\rangle ds + \frac{\lambda}{m}\int_0^t \langle (x - X^\alpha(\rho_s))\cdot\nabla_v\varphi, f_s(dx,dv)\rangle ds \\ &- \frac{\sigma^2}{2m^2}\int_0^t \sum_{k=1}^d \langle (x - X^\alpha(\rho_s))_k^2 \frac{\partial^2\varphi}{\partial v_k^2}, f_s(dx,dv)\rangle ds = 0\,,\end{aligned}$$

for any $\varphi \in \mathcal{C}_c^2(\mathbb{R}^{2d})$.

Until now we have proved that f a.s. is a weak solution to PDE (2.18). Finally combining the uniqueness of weak solution to (2.18) (see for example in [12]) and the arbitrariness of the subsequence of $\{f^N\}_{N\geq 2}$, the (deterministic) weak solution f to PDE (2.18) must be the limit of the whole sequence $\{f^N\}_{N\geq 2}$. We completed the proof. □

3.1.2 Theoretical analysis on PSO dynamic with memory and local best

In this part, we consider the second order system of SDEs corresponding to the *regularized SD-PSO method with local best* (2.19) that we rewrite with the superscript N as follow:

$$
\begin{aligned}
dX_t^{i,N} &= V_t^{i,N} dt, \\
dY_t^{i,N} &= \nu \left(X_t^{i,N} - Y_t^{i,N} \right) S^\beta(X_t^{i,N}, Y_t^{i,N}) dt, \\
m dV_t^{i,N} &= -\gamma V_t^{i,N} dt + \lambda_1 \left(Y_t^{i,N} - X_t^{i,N} \right) dt \\
&\quad + \lambda_2 \left(Y^\alpha(\overline{\rho}_t^N) - X_t^{i,N} \right) dt \\
&\quad + \sigma_1 D(Y_t^{i,N} - X_t^{i,N}) dB_t^{1,i} \\
&\quad + \sigma_2 D(Y^\alpha(\overline{\rho}_t^N) - X_t^{i,N}) dB_t^{2,i},
\end{aligned}
$$

and where, we introduced the *regularized global best* (2.20). Furthermore, we remark that in the right hand side of (2.19) we have replaced the $\mathrm{sgn}(x)$ function with a *sigmoid*; thanks to these regularizations, also the stochastic particle system (2.19) has locally Lipschitz coefficients and therefore it admits strong solutions and pathwise uniqueness holds for any finite time $T > 0$.

In order to derive a mean-field description of system, we can follow the same arguments as in previous part. The only difference is that we have an additional variable Y, which can be treated easily because of the regularity of the function S^β. Namely we can prove the tightness of the empirical measures $\{f^N\}_{N\geq 2}$ by verifying the Aldous criteria (Lemma 3.3). Then there exists a subsequence of $\{f^N\}_{N\geq 2}$ converging in law to a deterministic measure $f \in \mathcal{P}(\mathcal{C}([0,T];\mathbb{R}^d) \times \mathcal{C}([0,T];\mathbb{R}^d) \times \mathcal{C}([0,T];\mathbb{R}^d))$, which is the unique weak solution to the following *mean-field PSO system with local best* characterized by the nonlinear Vlasov-Fokker-Planck equation (2.22). This can be summarized in the following theorem

Theorem 3.7. *Let $\mathcal{F}$ satisfy Assumption 1 and $f_0 \in \mathcal{P}_4(\mathbb{R}^{3d})$. For any $N \geq 2$, we assume that $\{(X_t^{i,N}, Y_t^{i,N}, V_t^{i,N})_{t\in[0,T]}\}_{i=1}^N$ is the unique solution to the SD-PSO system (2.19) with $f_0^{\otimes N}$-distributed initial data $\{X_0^{i,N}, Y_0^{i,N}, V_0^{i,N}\}_{i=1}^N$. Then the limit for $N \to \infty$ (denoted by f) of the sequence of the empirical measure $f^N = \frac{1}{N}\sum_{i=1}^N \delta_{(X^{i,N},Y^{i,N},V^{i,N})}$ exists. Moreover, f is the unique weak solution to MF-PSO equation (2.22).*

3.2 Zero-inertia limit and consensus-based optimization

In this section we consider the asymptotic behavior of the previous Vlasov-Fokker-Planck equations modelling the PSO dynamic in the small inertia limit, i.e. $m \to 0$. We will derive the corresponding macroscopic equations which permit to recover and

generalize the recently introduced consensus-based optimization (CBO) methods [23]. We refer to [26, 34] for a theoretical background concerning the related problem of the overdamped limit of nonlinear Vlasov-Fokker-Planck systems.

3.2.1 The case without memory effects

Let us first consider the simplified setting in absence of local best. Now we write down the so called McKean-Vlasov process [76] underlying PSO equation (2.18), which is of the form[1]

$$
\begin{aligned}
d\overline{X}_t^m &= \overline{V}_t^m dt\,, && \text{(3.29a)}\\
d\overline{V}_t^m &= -\frac{\gamma}{m}\overline{V}_t^m dt + \frac{\lambda}{m}(X^\alpha(\rho_t^m) - \overline{X}_t^m)dt \\
&\quad + \frac{\sigma}{m} D(X^\alpha(\rho_t^m) - \overline{X}_t^m)dB_t\,, && \text{(3.29b)}
\end{aligned}
$$

where

$$
X^\alpha(\rho_t^m) = \frac{\int_{\mathbb{R}^d} x\omega_\alpha^{\mathcal{E}}(x)\rho^m(t,dx)}{\int_{\mathbb{R}^d}\omega_\alpha^{\mathcal{E}}(x)\rho^m(t,dx)}, \quad \rho^m(t,x) = \int_{\mathbb{R}^d} f^m(t,x,dv)\,, \tag{3.30}
$$

and the initial data $(\overline{X}_0, \overline{V}_0)$ is the same as in (2.14). Here $f^m(t,x,v)$ is the distribution of $(\overline{X}_t^m, \overline{V}_t^m)$ at time t , which makes the set of equations (3.29) nonlinear. A direct application of the Itô-Doeblin formula yields that the law $f_t^m := f^m(t,\cdot,\cdot)$ at time t is a weak solution to (2.18).

To illustrate the limiting procedure, let us observe that for $m \to 0^+$ from the equation (3.29b) we formally have

$$
\overline{V}_t^0 dt = \lambda\left(X^\alpha(\rho_t^0) - \overline{X}_t^0\right)dt + \sigma D(X^\alpha(\rho_t^0) - \overline{X}_t^0)dB_t,
$$

where we used the fact that $\gamma = 1 - m \to 1$. Substituting the above identity into the equation (3.29a) and omitting the superscripts gives the first order CBO system [23]

$$
d\overline{X}_t = \lambda(X^\alpha(\rho_t) - \overline{X}_t)dt + \sigma D(X^\alpha(\rho_t) - \overline{X}_t)dB_t\,. \tag{3.31}
$$

Therefore, the CBO models based on a multiplicative noise can be understood as reduced order approximations of SD-PSO dynamics.

Now, we present a rigorous derivation of the zero-inertia limit [27]. More precisely we prove that as $m \to 0^+$, the processes $\{\overline{X}^m\}$ satisfying the SDEs (3.29) converge weakly to the solution $\overline{X}$ to the SDE (3.31) in the continuous path space $\mathcal{C}([0,T];\mathbb{R}^d)$,

[1] We used the superscript m to emphasize its dependence on the inertia coefficient m.

and a convergence rate is obtained. The main theorem can be stated as below:

Theorem 3.8. *Let Assumption 1 hold and $(X_t^m, V_t^m)_{t\in[0,T]}$ satisfy the system (3.29). Then as $m \to 0^+$, the sequence of stochastic processes $\{\overline{X}^m\}_{0<m\leq\frac{1}{2}}$ converges weakly to $\overline{X}$, which is the unique solution to the following SDE:*

$$\begin{aligned}\overline{X}_t = \overline{X}_0 + \lambda \int_0^t (X^\alpha(\rho_s) - \overline{X}_s)ds \\ + \sigma \int_0^t D(X^\alpha(\rho_s) - \overline{X}_s)dB_s\,.\end{aligned} \tag{3.32}$$

Moreover it holds that

$$\sup_{t\in[0,T]} \mathbb{E}[|\overline{X}_t^m - \overline{X}_t|^2] \leq C\,m\,, \tag{3.33}$$

where the constant C depends only on $\mathbb{E}[|\overline{X}_0|^4]$, $\mathbb{E}[|\overline{V}_0|^4]$, M, C_u, C_l, λ, σ, d, and T.

Remark 1. *It follows from the definition of Wasserstein distance that*

$$\sup_{t\in[0,T]} W_2^2(\rho_t^m, \rho_t) \leq \sup_{t\in[0,T]} \mathbb{E}[|\overline{X}_t^m - \overline{X}_t|^2] \leq C\,m\,, \tag{3.34}$$

which in a way is consistent with the result obtained in [26, Theorem 1.3], where the authors obtained a quantified overdamped limit (with the same rate m) of the singular Vlasov-Poisson-Fokker-Planck system to the aggregation-diffusion equation.

The following theorem gives the well-posedness of the mean-field PSO dynamic (3.29) whose proof is analogous to [57, Theorem 2.3] or [20, Theorem 3.1], and thus omitted.

Theorem 3.9. *Let Assumption 1 hold. If $(\overline{X}_0^m, \overline{V}_0^m) = (\overline{X}_0, \overline{V}_0)$ is distributed according to f_0 with $f_0 \in \mathcal{P}_4(\mathbb{R}^{2d})$, then for each $T > 0$and $m \in (0, 1]$, the nonlinear SDE (3.29) admits a unique strong solution up to time T with the initial data $(\overline{X}_0^m, \overline{V}_0^m)$ and it holds further that*

$$\sup_{t\in[0,T]} \mathbb{E}\left[|\overline{X}_t^m|^4 + |\overline{V}_t^m|^4\right] \leq e^{CT} \cdot \mathbb{E}\left[|\overline{X}_0|^4 + |\overline{V}_0|^4\right]\,, \tag{3.35}$$

where C depends only on λ, m, σ, M, C_u, and C_l.

Solving (3.29b) for $\overline{V}_t^m$ gives

$$\begin{aligned}\overline{V}_t^m = e^{-\frac{\gamma}{m}t}\overline{V}_0 + \frac{\lambda}{m}\int_0^t e^{-\frac{\gamma}{m}(t-s)}(X^\alpha(\rho_s^m) - \overline{X}_s^m)ds \\ + \frac{\sigma}{m}\int_0^t e^{-\frac{\gamma}{m}(t-s)}D(X^\alpha(\rho_s^m) - \overline{X}_s^m)dB_s\,,\end{aligned}$$

which implies that

$$\begin{aligned}\overline{X}_t^m = \overline{X}_0 + \int_0^t \overline{V}_\tau d\tau = \overline{X}_0 + \int_0^t e^{-\frac{\gamma}{m}\tau}\overline{V}_0 d\tau \\ + \frac{\lambda}{m}\int_0^t\int_0^\tau e^{-\frac{\gamma}{m}(\tau-s)}(X^\alpha(\rho_s^m) - \overline{X}_s^m)dsd\tau \\ + \frac{\sigma}{m}\int_0^t\int_0^\tau e^{-\frac{\gamma}{m}(\tau-s)}D(X^\alpha(\rho_s^m) - \overline{X}_s^m)dB_s d\tau\,.\end{aligned} \tag{3.36}$$

Then $\overline{X}_t^m$ has the law ρ_t^m for each $t \geq 0$.

Each continuous stochastic process $\overline{X}^m$ may be seen as a $\mathcal{C}([0,T];\mathbb{R}^d)$-valued random function and it induces a probability measure (or law, denoted by ρ^m) on $\mathcal{C}([0,T];\mathbb{R}^d)$. We shall use the weak convergence in the space of probability measures on $\mathcal{C}([0,T];\mathbb{R}^d)$. In what follows, we write $\overline{X}^m \rightharpoonup \overline{X}$ or $\rho^m \rightharpoonup \rho$ with ρ being the law of $\overline{X}$, if $\{\rho^m\}_{m>0}$, as a sequence of probability measures, converges weakly to ρ, i.e., for each bounded continuous functional Φ on $\mathcal{C}([0,T];\mathbb{R}^d)$, there holds $\lim_{m\to 0^+}\mathbb{E}\left[\Phi(\overline{X}^m)\right] = \mathbb{E}\left[\Phi(\overline{X})\right]$. The weak convergence $\overline{X}^m \rightharpoonup \overline{X}$ is stronger than and actually implies the convergence of $\{\rho_t^m\}_{m>0}$ to ρ_t with ρ_t being the law of $\overline{X}_t$ for each $t \geq 0$, while the converse need not hold. Moreover, due to the separability and completeness of the space $\mathcal{C}([0,T];\mathbb{R}^d)$, Prohorov's theorem implies that the relative compactness is equivalent to the tightness; see [10] for more details.

Theorem 3.10. *Let Assumption 1 hold and $(X_t^m, V_t^m)_{t\in[0,T]}$ satisfy the system (3.29). For each countable subsequence $\{m_k\}_{k\in\mathbb{N}} \subset [0, \frac{1}{2}]$ with $\lim_{k\to\infty} m_k = 0$, the sequence of probability distributions $\{\rho^{m_k}\}_{k\in\mathbb{N}}$ of $\{\overline{X}^{m_k}\}_{k\in\mathbb{N}}$ is tight.*

Proof. By Lemma 3.3, it is sufficient to justify conditions $(Con1)$ and $(Con2)$ in Aldous tightness criteria .

- *Step 1: Checking* $(Con1)$. First, for $0 < m \leq \frac{1}{2}$, recalling (3.36), we have by

Fubini's theorem (see [30, Theorem 4.33] for the stochastic version)

$$\begin{aligned}
\overline{X}_t^m &= \overline{X}_0 + \int_0^t e^{-\frac{\gamma}{m}\tau}\overline{V}_0 d\tau + \frac{\lambda}{m}\int_0^t\int_0^\tau e^{-\frac{\gamma}{m}(\tau-s)}(X^\alpha(\rho_s^m) - \overline{X}_s^m)dsd\tau \\
&\quad + \frac{\sigma}{m}\int_0^t\int_0^\tau e^{-\frac{\gamma}{m}(\tau-s)}D(X^\alpha(\rho_s^m) - \overline{X}_s^m)dB_s d\tau \\
&= \overline{X}_0 + \int_0^t e^{-\frac{\gamma}{m}\tau}\overline{V}_0 d\tau + \frac{\lambda}{m}\int_0^t\int_s^t e^{-\frac{\gamma}{m}(\tau-s)}d\tau(X^\alpha(\rho_s^m) - \overline{X}_s^m)ds \\
&\quad + \frac{\sigma}{m}\int_0^t\int_s^t e^{-\frac{\gamma}{m}(\tau-s)}d\tau D(X^\alpha(\rho_s^m) - \overline{X}_s^m)dB_s \\
&= \overline{X}_0 + \frac{m}{\gamma}(1-e^{-\frac{\gamma}{m}t})\overline{V}_0 + \frac{\lambda}{\gamma}\int_0^t(1-e^{-\frac{\gamma}{m}(t-s)})(X^\alpha(\rho_s^m) - \overline{X}_s^m)ds \\
&\quad + \frac{\sigma}{\gamma}\int_0^t(1-e^{-\frac{\gamma}{m}(t-s)})D(X^\alpha(\rho_s^m) - \overline{X}_s^m)dB_s\,.
\end{aligned} \tag{3.37}$$

Note here the assumption on $0 < m \le \frac{1}{2}$ ensures that $\gamma = 1 - m \in [\frac{1}{2}, 1)$, so $\frac{1}{\gamma}$ is well defined. It follows from Hölder's inequality that

$$\begin{aligned}
|\overline{X}_t^m|^4 &\le 64|\overline{X}_0|^4 + \frac{64m^4}{\gamma^4}|\overline{V}_0|^4 + \frac{64\lambda^4 t^3}{\gamma^4}\int_0^t |X^\alpha(\rho_s^m) - \overline{X}_s^m|^4 ds \\
&\quad + \frac{64\sigma^4}{\gamma^4}\left|\int_0^t (1-e^{-\frac{\gamma}{m}(t-s)})D(X^\alpha(\rho_s^m) - \overline{X}_s^m)dB_s\right|^4,
\end{aligned} \tag{3.38}$$

where we have used the fact that for any sequence $\{a_i\}_{i=1}^n \ge 0$ and $p \ge 2$, there holds

$$\left(\sum_{i=1}^n a_i\right)^p \le n^{p-1}\sum_{i=1}^n a_i^p\,.$$

Using the moment inequality for stochastic integrals as in [74, Theorem 7.1] yields that

$$\begin{aligned}
&\mathbb{E}\left[\left|\int_0^t (1-e^{-\frac{\gamma}{m}(t-s)})D(X^\alpha(\rho_s^m) - \overline{X}_s^m)dB_s\right|^4\right] \\
&\le d^3\mathbb{E}\left[\sum_{k=1}^d \left|\int_0^t (1-e^{-\frac{\gamma}{m}(t-s)})(X^\alpha(\rho_s^m) - \overline{X}_s^m)_k dB_s^k e_k\right|^4\right] \\
&\le 36d^3 t\int_0^t \mathbb{E}\left[\sum_{k=1}^d |(X^\alpha(\rho_s^m) - \overline{X}_s^m)_k|^4\right] ds \\
&\le 36d^3 t\int_0^t \mathbb{E}\left[|X^\alpha(\rho_s^m) - \overline{X}_s^m|^4\right] ds\,.
\end{aligned}$$

Thus,

$$\mathbb{E}[|\overline{X}_t^m|^4] \leq 64\mathbb{E}[|\overline{X}_0|^4] + \frac{64m^4}{\gamma^4}\mathbb{E}[|\overline{V}_0|^4] + \frac{64(\lambda^4 t^3 + 36d^3 t\sigma^4)}{\gamma^4}\int_0^t \mathbb{E}[|X^\alpha(\rho_s^m) - \overline{X}_s^m|^4]ds\,.$$

Notice that

$$\begin{aligned}\mathbb{E}[|X^\alpha(\rho_t^m) - \overline{X}_t^m|^4] &\leq 8|X^\alpha(\rho_t^m)|^4 + 8\mathbb{E}[|\overline{X}_t^m|^4] \\ &\leq 8(b_1 + b_2\mathbb{E}[|\overline{X}_t^m|^2])^2 + 8\mathbb{E}[|\overline{X}_t^m|^4] \\ &\leq c_1 + c_2\mathbb{E}[|\overline{X}_t^m|^4]\,,\end{aligned} \tag{3.39}$$

where we have used Lemma 3.6 in the second inequality, and c_1, c_2 depend only on C_u, M and C_l. Thus we have

$$\mathbb{E}[|\overline{X}_t^m|^4] \leq 64\mathbb{E}[|\overline{X}_0|^4] + \frac{64m^4}{\gamma^4}\mathbb{E}[|\overline{V}_0|^4] + c_3 + \frac{64c_2(\lambda^4 t^3 + 36d^3 t\sigma^4)}{\gamma^4}\int_0^t \mathbb{E}[|\overline{X}_s^m|^4]ds\,.$$

Using Gronwall's inequality leads to

$$\begin{aligned}\mathbb{E}[|\overline{X}_t^m|^4] \leq \Big(64\mathbb{E}[|\overline{X}_0|^4] + \frac{64m^4}{\gamma^4}\mathbb{E}[|\overline{V}_0|^4] + c_3\Big)\cdot \\ \cdot \exp\Big(\frac{64c_2(\lambda^4 T^3 + 36d^3 T\sigma^4)}{\gamma^4}T\Big)\,,\end{aligned} \tag{3.40}$$

for all $t \in [0, T]$. Recalling $0 \leq m \leq \frac{1}{2}$ and $\frac{1}{\gamma} = \frac{1}{1-m} \leq 2$, from estimate (3.40) we obtain the boundedness:

$$\mathbb{E}[|\overline{X}_t^m|^4] \leq C(\mathbb{E}[|\overline{X}_0|^4], \mathbb{E}[|\overline{V}_0|^4], M, C_u, C_l, \lambda, d, \sigma, T)\,. \tag{3.41}$$

This yields that

$$\begin{aligned}&\sup_{m\in(0,1]}\sup_{t\in[0,T]}\mathbb{E}[|\overline{X}_t^m|^4] \\ &\quad\leq C(\mathbb{E}[|\overline{X}_0|^4], \mathbb{E}[|\overline{V}_0|^4], M, C_u, C_l, \lambda, \sigma, d, T) =: C_1\end{aligned} \tag{3.42}$$

where the constant $C_1 > 0$ is independent of m. Therefore, for any $\varepsilon > 0$, there exists a compact subset $K_\varepsilon := \{x : |x|^4 \leq \frac{C_1}{\varepsilon}\}$ such that by Markov's inequality

$$\rho_t^m((K_\varepsilon)^c) = \mathcal{P}(|X_t^m|^4 > \frac{C_1}{\varepsilon}) \leq \frac{\varepsilon\mathbb{E}[|X_t^m|^4]}{C_1} \leq \varepsilon, \quad \forall\ 0 < m \leq 1\,. \tag{3.43}$$

This means that for each $t \in [0,T]$, each countable subset of $\{\rho_t^m\}_{0<m\leq 1}$ is tight, which verifies condition $(Con1)$ in Lemma 3.3.

• *Step 2: Checking* $(Con2)$. Let β be a $\sigma(X_s^m; s \in [0,T])$-stopping time with discrete values such that $\beta + \delta_0 \leq T$. Without any loss of generality, we may assume that the concerned countable subsequence $\{m_k\}_{k\in\mathbb{N}} \subset [0,1]$ satisfies $m_k \leq \frac{1}{2}$ for all $k \in \mathbb{N}$; thus, we may just consider the case of $0 < m \leq \frac{1}{2}$ which indicates $\frac{1}{2} \leq \gamma < 1$. Recall (3.36) and compute

$$\begin{aligned}
\overline{X}^m_{\beta+\delta} - \overline{X}^m_{\beta} &= \int_\beta^{\beta+\delta} \overline{V}_\tau d\tau = \int_\beta^{\beta+\delta} e^{-\frac{\gamma}{m}\tau}\overline{V}_0 d\tau \\
&\quad + \frac{\lambda}{m}\int_\beta^{\beta+\delta}\int_0^\tau e^{-\frac{\gamma}{m}(\tau-s)}(X^\alpha(\rho_s^m) - \overline{X}^m_s) ds d\tau \\
&\quad + \frac{\sigma}{m}\int_\beta^{\beta+\delta}\int_0^\tau e^{-\frac{\gamma}{m}(\tau-s)} D(X^\alpha(\rho_s^m) - \overline{X}^m_s) dB_s d\tau \\
&= \int_\beta^{\beta+\delta} e^{-\frac{\gamma}{m}\tau}\overline{V}_0 d\tau \\
&\quad + \frac{\lambda}{m}\int_0^{\beta}\int_\beta^{\beta+\delta} e^{-\frac{\gamma}{m}(\tau-s)} d\tau (X^\alpha(\rho_s^m) - \overline{X}^m_s) ds \\
&\quad + \frac{\lambda}{m}\int_\beta^{\beta+\delta}\int_s^{\beta+\delta} e^{-\frac{\gamma}{m}(\tau-s)} d\tau (X^\alpha(\rho_s^m) - \overline{X}^m_s) ds \\
&\quad + \frac{\sigma}{m}\int_0^{\beta}\int_\beta^{\beta+\delta} e^{-\frac{\gamma}{m}(\tau-s)} d\tau D(X^\alpha(\rho_s^m) - \overline{X}^m_s) dB_s \\
&\quad + \frac{\sigma}{m}\int_\beta^{\beta+\delta}\int_s^{\beta+\delta} e^{-\frac{\gamma}{m}(\tau-s)} d\tau D(X^\alpha(\rho_s^m) - \overline{X}^m_s) dB_s .
\end{aligned}$$

Then it yields

$$\begin{aligned}
\overline{X}^m_{\beta+\delta} - \overline{X}^m_{\beta} &= \frac{m}{\gamma}(e^{-\frac{\gamma}{m}\beta} - e^{-\frac{\gamma}{m}(\beta+\delta)})\overline{V}_0 \\
&\quad + \frac{\lambda}{\gamma}\int_0^\beta (e^{-\frac{\gamma}{m}(\beta-s)} - e^{-\frac{\gamma}{m}(\beta+\delta-s)})(X^\alpha(\rho_s^m) - \overline{X}^m_s) ds \\
&\quad + \frac{\lambda}{\gamma}\int_\beta^{\beta+\delta} (1 - e^{-\frac{\gamma}{m}(\beta+\delta-s)})(X^\alpha(\rho_s^m) - \overline{X}^m_s) ds \\
&\quad + \frac{\sigma}{\gamma}\int_0^\beta (e^{-\frac{\gamma}{m}(\beta-s)} - e^{-\frac{\gamma}{m}(\beta+\delta-s)}) D(X^\alpha(\rho_s^m) - \overline{X}^m_s) dB_s \\
&\quad + \frac{\sigma}{\gamma}\int_\beta^{\beta+\delta} (1 - e^{-\frac{\gamma}{m}(\beta+\delta-s)}) D(X^\alpha(\rho_s^m) - \overline{X}^m_s) dB_s .
\end{aligned} \tag{3.44}$$

Note that there holds $|e^{-x} - e^{-y}| \leq |x-y| \wedge 1$ for all $x, y \in [0,\infty)$. Basic computations

further indicate that for each $q \geq 1$ and $\tau \in [0, T]$,

$$\begin{aligned}\int_0^\tau \left| e^{-\frac{\gamma(\tau-s)}{m}} - e^{-\frac{\gamma(\tau+\delta-s)}{m}} \right|^q ds &\leq \int_0^\tau \left(e^{-\frac{\gamma(\tau-s)}{m}} - e^{-\frac{\gamma(\tau+\delta-s)}{m}} \right) ds \\ &= \frac{m}{\gamma}\left(1 - e^{-\frac{\gamma\delta}{m}}\right) - \frac{m}{\gamma}\left(e^{-\frac{\gamma\tau}{m}} - e^{-\frac{\gamma(\tau+\delta)}{m}}\right) \\ &\leq \frac{m}{\gamma} \cdot \frac{\gamma\delta}{m} = \delta,\end{aligned}$$

and in particular,

$$\int_\beta^{\beta+\delta} \left(1 - e^{-\frac{\gamma(\beta+\delta-s)}{m}}\right)^q ds \leq \int_\beta^{\beta+\delta} 1\, ds = \delta.$$

Then, it is obvious that

$$\mathbb{E}\left[\left|\frac{m}{\gamma}(e^{-\frac{\gamma}{m}\beta} - e^{-\frac{\gamma}{m}(\beta+\delta)})\overline{V}_0\right|^2\right] \leq \frac{m^2}{\gamma^2} \cdot \frac{\gamma^2\delta^2}{m^2} \left(\mathbb{E}[|\overline{V}_0|^4]\right)^{\frac{1}{2}} \leq \delta^2 \left(\mathbb{E}[|\overline{V}_0|^4]\right)^{\frac{1}{2}}.$$

Next, it follows that

$$\begin{aligned}&\mathbb{E}\left[\left|\int_0^\beta (e^{-\frac{\gamma}{m}(\beta-s)} - e^{-\frac{\gamma}{m}(\beta+\delta-s)})(X^\alpha(\rho_s^m) - \overline{X}_s^m) ds\right|^2\right] \\ &\leq\ \mathbb{E}\left[\int_0^\beta |e^{-\frac{\gamma}{m}(\beta-s)} - e^{-\frac{\gamma}{m}(\beta+\delta-s)}|^2 ds \cdot \int_0^\beta |X^\alpha(\rho_s^m) - \overline{X}_s^m|^2 ds\right] \\ &\leq\ \delta \cdot T \sup_{s\in[0,T]} \left(\mathbb{E}\left[|X^\alpha(\rho_s^m) - \overline{X}_s^m|^4\right]\right)^{1/2},\end{aligned}$$

and analogously,

$$\begin{aligned}&\mathbb{E}\left[\left|\int_\beta^{\beta+\delta} (1 - e^{-\frac{\gamma}{m}(\beta+\delta-s)})(X^\alpha(\rho_s^m) - \overline{X}_s^m) ds\right|^2\right] \\ &\leq\ \mathbb{E}\left[\int_\beta^{\beta+\delta} \left(1 - e^{-\frac{\gamma(\beta+\delta-s)}{m}}\right)^2 ds \cdot \int_\beta^{\beta+\delta} |X^\alpha(\rho_s^m) - \overline{X}_s^m|^2 ds\right] \\ &\leq\ \delta \cdot \mathbb{E}\left[\int_\beta^{\beta+\delta} |X^\alpha(\rho_s^m) - \overline{X}_s^m|^2 ds\right] \\ &\leq\ \delta \cdot T \sup_{s\in[0,T]} \left(\mathbb{E}\left[|X^\alpha(\rho_s^m) - \overline{X}_s^m|^4\right]\right)^{1/2}.\end{aligned}$$

Further, applying Itô's isometry gives

$$\begin{aligned}
&\mathbb{E}\left[\left|\int_0^\beta (e^{-\frac{\gamma}{m}(\beta-s)} - e^{-\frac{\gamma}{m}(\beta+\delta-s)}) D(X^\alpha(\rho_s^m) - \overline{X}_s^m) dB_s\right|^2\right] \\
&\leq\ d\mathbb{E}\left[\int_0^\beta |e^{-\frac{\gamma}{m}(\beta-s)} - e^{-\frac{\gamma}{m}(\beta+\delta-s)}|^2 |X^\alpha(\rho_s^m) - \overline{X}_s^m|^2 ds\right] \\
&\leq\ d\left(\mathbb{E}\left[\int_0^\beta |e^{-\frac{\gamma}{m}(\beta-s)} - e^{-\frac{\gamma}{m}(\beta+\delta-s)}|^4 ds\right]\right)^{1/2} \cdot \\
&\quad \cdot \left(\mathbb{E}\left[\int_0^\beta |X^\alpha(\rho_s^m) - \overline{X}_s^m|^4 ds\right]\right)^{1/2} \\
&\leq\ d\delta^{1/2}\left(T \sup_{s\in[0,T]} \mathbb{E}\left[|X^\alpha(\rho_s^m) - \overline{X}_s^m|^4\right]\right)^{1/2},
\end{aligned}$$

and analogously,

$$\begin{aligned}
&\mathbb{E}\left[\left|\int_\beta^{\beta+\delta} (1 - e^{-\frac{\gamma}{m}(\beta+\delta-s)}) D(X^\alpha(\rho_s^m) - \overline{X}_s^m) dB_s\right|^2\right] \\
&\leq\ d\delta^{1/2}\left(T \sup_{s\in[0,T]} \mathbb{E}\left[|X^\alpha(\rho_s^m) - \overline{X}_s^m|^4\right]\right)^{1/2}.
\end{aligned}$$

Therefore, summing up the above estimates and recalling $0 < m \leq m_0 = \frac{1}{2}$, $\frac{1}{\gamma} \leq 2$, and the relations (3.39) and (3.42), we arrive at

$$\begin{aligned}
&\mathbb{E}[|\overline{X}_{\beta+\delta}^m - \overline{X}_\beta^m|^2] \\
&\leq\ \frac{5}{\gamma^2}\delta^2(\mathbb{E}[|\overline{V}_0|^4])^{\frac{1}{2}} + \frac{10}{\gamma^2}\left(\lambda^2\delta T + \sigma^2 d\,(\delta T)^{1/2}\right) \sup_{s\in[0,T]} \left(\mathbb{E}\left[|X^\alpha(\rho_s^m) - \overline{X}_s^m|^4\right]\right)^{1/2} \\
&\leq\ C\left(\mathbb{E}[|\overline{X}_0|^4], \mathbb{E}[|\overline{V}_0|^4], M, C_u, C_l, \lambda, \sigma, d, T\right)\left(\delta^{\frac{1}{2}} + \delta + \delta^2\right).
\end{aligned}$$

Hence, for any $\varepsilon > 0$, $\eta > 0$, there exists some $\delta_0 > 0$ such that for all $0 < m \leq \frac{1}{2}$ it holds that

$$\sup_{\delta\in[0,\delta_0]} \mathcal{P}(|\overline{X}_{\beta+\delta}^m - \overline{X}_\beta^m|^2 \geq \eta) \leq \sup_{\delta\in[0,\delta_0]} \frac{\mathbb{E}[|\overline{X}_{\beta+\delta}^m - \overline{X}_\beta^m|^2]}{\eta} \leq \varepsilon. \tag{3.45}$$

This justifies condition $Con2$ in Lemma 3.3. □

Next we shall identify the limit process, before which we recall a lemma on the stability estimate of the nonlinear term $X^\alpha(\rho)$.

Lemma 3.11. *[20, Lemma 3.2] Assume that $\rho, \widehat{\rho} \in \mathcal{P}_4(\mathbb{R}^d)$. Then the following stabil-*

ity estimate holds

$$|X^\alpha(\rho) - X^\alpha(\widehat{\rho})| \le C W_2(\rho, \widehat{\rho})\,, \tag{3.46}$$

where W_2 is the 2-Wasserstein distance, and C depends only on α, L, $\int_{\mathbb{R}^d} |x|^4 \rho(dx)$, and $\int_{\mathbb{R}^d} |x|^4 \widehat{\rho}(dx)$.

Finally let us prove Theorem 3.8:

Proof. **(Theorem 3.8)** By Theorem 3.10, each subsequence $\{\overline{X}^{m_k}\}_{k\in\mathbb{N}}$ with $m_0 \le 1/2$ and m_k converging to 0 as $k \to \infty$ admits a subsequence (denoted w.l.o.g. by itself) that converges weakly. By Skorokhod's lemma (see [10, Theorem 6.7 on page 70]) and the existence and uniqueness of strong solution to SDE (3.29), we may find a common probability space $(\Omega, \mathcal{F}, \mathcal{P})$ on which the joint processes $\{(\overline{X}^{m_k}, B)\}_{k\in\mathbb{N}}$ converge to some process $(\widehat{X}, B)$ as random variables valued in $\mathcal{C}([0,T];\mathbb{R}^{2d})$ almost surely. Here B is an identical d-dimensional Wiener process on $(\Omega, \mathcal{F}, \mathcal{P})$. In particular, we have

$$\mathbb{P}\left(\lim_{k\to\infty} \sup_{t\in[0,T]} |\overline{X}_t^{m_k} - \widehat{X}_t| = 0\right) = 1\,. \tag{3.47}$$

We shall verify that the limit $\widehat{X}$ is indeed the unique solution $\overline{X}$ to SDE (3.32).

Recalling the existence and uniqueness of the strong solution $\overline{X}^{m_k}$ to SDE (3.37) in Theorem 3.9, we have

$$\begin{aligned}\overline{X}_t^{m_k} = \overline{X}_0 + \frac{m_k}{\gamma}(1 - e^{-\frac{\gamma}{m_k}t})\overline{V}_0 + \frac{\lambda}{\gamma}\int_0^t (1 - e^{-\frac{\gamma}{m_k}(t-s)})(X^\alpha(\rho_s^{m_k}) - \overline{X}_s^{m_k})ds \\ + \frac{\sigma}{\gamma}\int_0^t (1 - e^{-\frac{\gamma}{m_k}(t-s)}) D(X^\alpha(\rho_s^{m_k}) - \overline{X}_s^{m_k}) dB_s\,.\end{aligned} \tag{3.48}$$

By the estimates in (3.42) and Fatou's lemma there exists a constant C_2 being independent of m_k such that

$$\begin{aligned}&\sup_{k\in\mathbb{N}} \sup_{t\in[0,T]} \mathbb{E}\left[|\overline{X}_t^{m_k}|^4\right] + \sup_{t\in[0,T]} \mathbb{E}\left[\left|\widehat{X}_t\right|^4\right] \\ &\qquad \le C_2 := C(\mathbb{E}[|\overline{X}_0|^4], \mathbb{E}[|\overline{V}_0|^4], C_{\alpha,\mathcal{F}}, \lambda, \sigma, d, T) < \infty.\end{aligned} \tag{3.49}$$

As a straightforward consequence of the above boundedness, it holds that

$$\sup_{k\in\mathbb{N}, t\in[0,T]} \mathcal{P}(|\overline{X}_t^{m_k} - \widehat{X}_t| > A) \le \frac{2^4 C_2}{A^4}, \quad \forall\, A > 0. \tag{3.50}$$

Thus, the dominated convergence theorem gives that for each $A > 0$,

$$\begin{aligned}
&\lim_{k\to\infty} \mathbb{E}\left[\int_0^T |\overline{X}_t^{m_k} - \widehat{X}_t|^2 \, dt\right] \\
&\le \limsup_{k\to\infty} \Bigg(\mathbb{E}\left[\int_0^T |\overline{X}_t^{m_k} - \widehat{X}_t|^2 \wedge A^2 \, dt\right] \\
&\quad + \mathbb{E}\left[\int_0^T |\overline{X}_t^{m_k} - \widehat{X}_t|^2 1_{\{|\overline{X}_t^{m_k} - \widehat{X}_t| > A\}} \, dt\right] \Bigg) \\
&\le \limsup_{k\to\infty} \mathbb{E}\left[\int_0^T |\overline{X}_t^{m_k} - \widehat{X}_t|^2 \wedge A^2 \, dt\right] \\
&\quad + T \cdot \sup_{k\in\mathbb{N}} \sup_{t\in[0,T]} \left(\mathbb{E}\left[|\overline{X}_t^{m_k} - \widehat{X}_t|^4\right]\right)^{1/2} \left|\mathcal{P}(|\overline{X}_t^{m_k} - \widehat{X}_t| > A)\right|^{1/2} \\
&\le \limsup_{k\to\infty} \mathbb{E}\left[\int_0^T |\overline{X}_t^{m_k} - \widehat{X}_t|^2 \wedge A^2 \, dt\right] + \frac{2^4 C_2 T}{A^2} \\
&= \frac{2^4 C_2 T}{A^2},
\end{aligned}$$

which by the arbitrariness of $A > 0$ indicates that

$$\lim_{k\to\infty} \mathbb{E}\left[\int_0^T |\overline{X}_t^{m_k} - \widehat{X}_t|^2 \, dt\right] = 0. \tag{3.51}$$

Letting $\rho(t, dx)$ be the probability distribution of $\widehat{X}_t$ for $t \in [0, T]$, Lemma 3.6 gives

$$|X^\alpha(\rho_t)| \le (b_1 + b_2 \mathbb{E}[|\widehat{X}_t|^2])^{\frac{1}{2}} \le (b_1 + b_2 C_2^{\frac{1}{2}})^{\frac{1}{2}} =: C_3,$$

and thus

$$\sup_{k\in\mathbb{N}} \sup_{t\in[0,T]} |X^\alpha(\rho_t^{m_k})| \le C_3, \quad \text{and} \quad \sup_{t\in[0,T]} |X^\alpha(\rho_t)| \le C_3\,. \tag{3.52}$$

Then we compare the SDEs (3.32) and (3.48) term by term. By Lemma 3.11, we have

$$|X^\alpha(\rho_t^{m_k}) - X^\alpha(\rho_t)|^2 \le C W_2^2(\rho_t^{m_k}, \rho_t) \le C\mathbb{E}[|\overline{X}_t^{m_k} - \widehat{X}_t|^2],$$

and thus by using the fact that $\gamma = 1 - m_k$, one has

$$\begin{aligned}
&\mathbb{E}\Big[\Big|\frac{\lambda}{\gamma}\int_0^t (1-e^{-\frac{\gamma}{m_k}(t-s)})(X^\alpha(\rho_s^{m_k}) - \overline{X}_s^{m_k})ds - \lambda\int_0^t (X^\alpha(\rho_s) - \widehat{X}_s)ds\Big|^2\Big] \\
&\quad\le 2\mathbb{E}\Big[\Big|\frac{\lambda}{1-m_k}\int_0^t (1-e^{-\frac{1-m_k}{m_k}(t-s)})\cdot(X^\alpha(\rho_s^{m_k}) - X^\alpha(\rho_s) + \widehat{X}_s - \overline{X}_s^{m_k})ds\Big|^2\Big] \\
&\qquad + 2\mathbb{E}\left[\left|\lambda\int_0^t \left(\frac{1-e^{-\frac{1-m_k}{m_k}(t-s)}}{1-m_k} - 1\right)(X^\alpha(\rho_s) - \widehat{X}_s)ds\right|^2\right] \\
&\quad\le C\mathbb{E}\left[\int_0^t \left|\widehat{X}_s - \overline{X}_s^{m_k}\right|^2 ds\right] + C\lambda^2\int_0^t \left|\frac{1-e^{-\frac{1-m_k}{m_k}(t-s)}}{1-m_k} - 1\right|^2 ds \\
&\qquad\cdot\mathbb{E}\left[\int_0^T \left|X^\alpha(\rho_s) - \widehat{X}_s\right|^2 ds\right] \\
&\quad\le C\mathbb{E}\left[\int_0^t \left|\widehat{X}_s - \overline{X}_s^{m_k}\right|^2 ds\right] + C\int_0^t \left|\frac{1-e^{-\frac{1-m_k}{m_k}(t-s)} - (1-m_k)}{1-m_k}\right|^2 ds \\
&\quad\le C\mathbb{E}\left[\int_0^t \left|\widehat{X}_s - \overline{X}_s^{m_k}\right|^2 ds\right] + C\int_0^t \left(|m_k|^2 + e^{-\frac{2(1-m_k)}{m_k}(t-s)}\right) ds \\
&\quad\le C\mathbb{E}\left[\int_0^t \left|\widehat{X}_s - \overline{X}_s^{m_k}\right|^2 ds\right] + C\left(t\,|m_k|^2 + \frac{m_k}{2(1-m_k)}\right),
\end{aligned} \tag{3.53}$$

where the constants Cs are independent of k. For the stochastic integrals, it holds analogously that

$$\begin{aligned}
&\mathbb{E}\left[\left|\frac{\sigma}{\gamma}\int_0^t (1-e^{-\frac{\gamma}{m_k}(t-s)})D(X^\alpha(\rho_s^{m_k}) - \overline{X}_s^{m_k})dB_s\right.\right. \\
&\qquad\left.\left. - \sigma\int_0^t D(X^\alpha(\rho_s) - \widehat{X}_s)dB_s\right|^2\right] \\
&\quad\le d\sigma^2\sum_{n=1}^d \mathbb{E}\Big[\Big|\frac{1}{\gamma}\int_0^t (1-e^{-\frac{\gamma}{m_k}(t-s)})(X^\alpha(\rho_s^{m_k}) - \overline{X}_s^{m_k})_n dB_s^n e_n \\
&\qquad - \int_0^t (X^\alpha(\rho_s) - \widehat{X}_s)_n dB_s^n e_n\Big|^2\Big] \\
&\quad= d\sigma^2\sum_{n=1}^d \mathbb{E}\Big[\int_0^t \Big|\frac{1-e^{-\frac{\gamma}{m_k}(t-s)}}{\gamma}(X^\alpha(\rho_s^{m_k}) - \overline{X}_s^{m_k})_n \\
&\qquad - (X^\alpha(\rho_s) - \widehat{X}_s)_n\Big|^2 ds\Big].
\end{aligned} \tag{3.54}$$

Thus we have

$$
\begin{aligned}
&\mathbb{E}\Big[\Big|\frac{\sigma}{\gamma}\int_0^t(1-e^{-\frac{\gamma}{m_k}(t-s)})D(X^\alpha(\rho_s^{m_k})-\overline{X}_s^{m_k})dB_s \\
&\quad-\sigma\int_0^t D(X^\alpha(\rho_s)-\widehat{X}_s)dB_s\Big|^2\Big] \\
&\le 2d\sigma^2\sum_{n=1}^d\mathbb{E}\Big[\int_0^t\Big|\frac{1-e^{-\frac{\gamma}{m_k}(t-s)}}{\gamma}\cdot \\
&\quad\Big((X^\alpha(\rho_s^{m_k})-\overline{X}_s^{m_k})_n-(X^\alpha(\rho_s)-\widehat{X}_s)_n\Big)\Big|^2 ds\Big] \\
&\quad+2d\sigma^2\sum_{n=1}^d\mathbb{E}\left[\int_0^t\left|\left(\frac{1-e^{-\frac{\gamma}{m_k}(t-s)}}{\gamma}-1\right)(X^\alpha(\rho_s)-\widehat{X}_s)_n\right|^2 ds\right] \\
&\le C\mathbb{E}\left[\int_0^t\left|\overline{X}_s^{m_k}-\widehat{X}_s\right|^2 ds\right] \\
&\quad+2d\sigma^2\sup_{s\in[0,t]}\mathbb{E}\left[\left|(X^\alpha(\rho_s)-\widehat{X}_s)\right|^2\right]\cdot\int_0^t\left|\left(\frac{1-e^{-\frac{\gamma}{m_k}(t-s)}}{\gamma}-1\right)\right|^2 ds \\
&\le C\mathbb{E}\left[\int_0^t\left|\widehat{X}_s-\overline{X}_s^{m_k}\right|^2 ds\right]+C\left(t\left|m_k\right|^2+\frac{m_k}{2(1-m_k)}\right).
\end{aligned}
\tag{3.55}
$$

In addition, it is obvious that

$$
\left|\frac{m_k}{\gamma}(1-e^{-\frac{\gamma}{m_k}t})\overline{V}_0\right|\le Cm_k\left|\overline{V}_0\right|. \tag{3.56}
$$

Combining the estimates (3.53)-(3.56), letting k tend to infinity on both sides of (3.48) and recalling $\frac{1}{2}\ge m_k\to 0^+$ and the relation (3.51), we have

$$
\widehat{X}_t=\overline{X}_0+\lambda\int_0^t(X^\alpha(\rho_s)-\widehat{X}_s)ds+\sigma\int_0^t D(X^\alpha(\rho_s)-\widehat{X}_s)dB_s.
$$

Therefore, the limit $\widehat{X}$ turns out to be a solution to SDE (3.32). Meanwhile, in view of the continuity of $X^\alpha(\rho)$ in Lemma 3.11, we can easily show that (3.32) admits a unique (strong) solution as in Theorem 3.9 by using Leray-Schauder fixed point theorem as in [20, Theorem 3.1]. Thus, we must have $\widehat{X}=\overline{X}$ that is the unique strong solution to SDE (3.32) with $\sup_{t\in[0,T]}\mathbb{E}\left[|\overline{X}_t|^4\right]\le C_2$. Further, due to the arbitrariness of the subsequence $\{\overline{X}^{m_k}\}_{k\in\mathbb{N}}$, we conclude that as $m\to 0^+$, the sequence of stochastic processes $\{\overline{X}^m\}_{0<m\le\frac{1}{2}}$ converge weakly to the unique solution $\overline{X}$ to SDE (3.32).

Finally, to measure the distance between $\overline{X}^m$ and the limit $\widehat{X}=\overline{X}$, we may have similar calculations to (3.53)-(3.56), subtract both sides of SDEs (3.32) from those of

(3.48), and arrive at

$$\mathbb{E}[|\overline{X}_t^m - \overline{X}_t|^2] \leq C \int_0^t \mathbb{E}[|\overline{X}_s^m - \overline{X}_s|^2] ds + C\, m, \quad t \in [0,T].$$

By Gronwall's inequality it implies that

$$\sup_{t\in[0,T]} \mathbb{E}[|\overline{X}_t^m - \overline{X}_t|^2] \leq Cm, \tag{3.57}$$

where C depends only on $\mathbb{E}[|\overline{X}_0|^4], \mathbb{E}[|\overline{V}_0|^4], C_u, M, C_l, \lambda, \sigma, d$, and T. This completes the proof. □

3.2.2 The general case with memory

Next, we consider the same small inertia scaling in the general case with dependence from the local best. Again, we first write down the nonlinear McKean-Vlasov process corresponding to the SD-PSO system (2.19), which is of the form

$$\begin{aligned}
d\overline{X}_t^m &= \overline{V}_t^m dt, && \text{(3.58a)}\\
d\overline{Y}_t^m &= \nu \left(\overline{X}_t^m - \overline{Y}_t^m\right) S^\beta \left(\overline{X}_t^m, \overline{Y}_t^m\right) dt, && \text{(3.58b)}\\
d\overline{V}_t^m &= -\frac{\gamma}{m}\overline{V}_t^m dt + \frac{\lambda_1}{m}\left(\overline{Y}_t^m - \overline{X}_t^m\right) dt \\
&\quad + \frac{\lambda_2}{m}\left(Y^\alpha(\overline{\rho}_t^m) - \overline{X}_t^m\right) dt + \frac{\sigma_1}{m} D\left(\overline{Y}_t^m - \overline{X}_t^m\right) dB_t^1 && \text{(3.58c)}\\
&\quad + \frac{\sigma_2}{m} D\left(Y^\alpha(\overline{\rho}_t^m) - \overline{X}_t^m\right) dB_t^2,
\end{aligned}$$

where B^1 and B^2 are two mutually independent d-dimensional Wiener processes, and similarly to the previous section, we introduce the following regularization of the global best position

$$Y^\alpha(\overline{\rho}_t^m) = \frac{\int_{\mathbb{R}^d} y\omega_\alpha(y)\overline{\rho}^m(t,dy)}{\int_{\mathbb{R}^d} \omega_\alpha(y)\overline{\rho}^m(t,dy)}, \qquad \overline{\rho}^m(t,y) = \iint_{\mathbb{R}^d\times\mathbb{R}^d} f^m(t,dx,y,dv)\,.$$

As $m \to 0^+$ we formally get from (3.58c)

$$\begin{aligned}
\overline{V}_t^0 dt = \lambda_1 \left(\overline{Y}_t^0 - \overline{X}_t^0\right) dt + \lambda_2 \left(Y^\alpha(\overline{\rho}_t^0) - \overline{X}_t^0\right) dt \\
+ \sigma_1 D(\overline{Y}_t^0 - \overline{X}_t^0) dB_t^1 + \sigma_2 D(Y^\alpha(\overline{\rho}_t^0) - \overline{X}_t^0) dB_t^2,
\end{aligned}$$

which inserted into (3.58a) and omitting the superscripts corresponds to a novel *CBO system with local best*

$$\begin{aligned} d\overline{X}_t &= \lambda_1(\overline{Y}_t - \overline{X}_t)dt + \lambda_2(Y^\alpha(\overline{\rho}_t) - \overline{X}_t)dt \\ &\quad + \sigma_1 D(\overline{Y}_t - \overline{X}_t)dB_t^1 + \sigma_2 D(Y^\alpha(\overline{\rho}_t) - \overline{X}_t)dB_t^2, \\ d\overline{Y}_t &= \nu\left(\overline{X}_t - \overline{Y}_t\right) S^\beta\left(\overline{X}_t, \overline{Y}_t\right) dt\,. \end{aligned} \tag{3.59}$$

In contrast with the model recently introduced in [96] the above first order CBO method avoids backward time integration through the use of an additional differential equation. We refer to [14] for further details on the above CBO system.

Since the proof of the zero-inertia limit for the PSO dynamics with memory effects follows similar arguments as developed in the previous section and no essential innovation is needed to be explained, we only recall the main results here.

Let us solve (3.58c) to obtain

$$\begin{aligned} \overline{X}_t^m &= \overline{X}_0 + \frac{m}{\gamma}(1 - e^{-\frac{\gamma}{m}t})\overline{V}_0 + \frac{\lambda_1}{\gamma}\int_0^t (1 - e^{-\frac{\gamma}{m}(t-s)})(\overline{Y}_s^m - \overline{X}_s^m)ds \\ &\quad + \frac{\sigma_1}{\gamma}\int_0^t (1 - e^{-\frac{\gamma}{m}(t-s)})D(\overline{Y}_s^m - \overline{X}_s^m)dB_s^1 \\ &\quad + \frac{\lambda_2}{\gamma}\int_0^t (1 - e^{-\frac{\gamma}{m}(t-s)})(Y^\alpha(\overline{\rho}_s^m) - \overline{X}_s^m)ds \\ &\quad + \frac{\sigma_2}{\gamma}\int_0^t (1 - e^{-\frac{\gamma}{m}(t-s)})D(Y^\alpha(\overline{\rho}_s^m) - \overline{X}_s^m)dB_s^2 \end{aligned} \tag{3.60}$$

and

$$\overline{Y}_t^m = \overline{Y}_0 + \nu\int_0^t \left(\overline{X}_s^m - \overline{Y}_s^m\right) S^\beta\left(\overline{X}_s^m, \overline{Y}_s^m\right) ds\,. \tag{3.61}$$

Similar to Theorem 3.10 one can prove the following result of tightness.

Theorem 3.12. *Let Assumption 1 hold and $(\overline{X}_t^m, \overline{Y}_t^m, \overline{V}_t^m)_{t\in[0,T]}$ satisfy the system (3.58a)–(3.58c). For each countable subsequence $\{m_k\}_{k\in\mathbb{N}} \subset [0, \frac{1}{2}]$ with $\lim_{k\to\infty} m_k = 0$, the sequence of probability distributions $\{\rho^{m_k}\}_{k\in\mathbb{N}}$ of $\{(\overline{X}^{m_k}, \overline{Y}^{m_k})\}_{k\in\mathbb{N}}$ is tight.*

Then following the lines of the proof in Theorem 3.8, one can obtain

Theorem 3.13. *Let Assumption 1 hold and $(\overline{X}_t^m, \overline{Y}_t^m)_{t\in[0,T]}$ satisfy the system (3.60)–(3.61). Then as $m \to 0^+$, the sequence of stochastic processes $\{(\overline{X}^m, \overline{Y}^m)\}_{0<m\leq\frac{1}{2}}$ con-*

verge weakly to $(\overline{X}, \overline{Y})$ *which is the unique solution to the following coupled SDE:*

$$\begin{aligned}
\overline{X}_t &= \overline{X}_0 + \lambda_1 \int_0^t (\overline{Y}_s - \overline{X}_s) ds + \sigma_1 \int_0^t D(\overline{Y}_s - \overline{X}_s) dB_s^1 \\
&\quad + \lambda_2 \int_0^t (Y^\alpha(\overline{\rho}_s) - \overline{X}_s) ds + \sigma_2 \int_0^t D(Y^\alpha(\overline{\rho}_s) - \overline{X}_s) dB_s^2, \\
\overline{Y}_t &= \overline{Y}_0 + \nu \int_0^t \left(\overline{X}_s - \overline{Y}_s\right) S^\beta\left(\overline{X}_s, \overline{Y}_s\right) ds \,.
\end{aligned}$$

Moreover it holds that

$$\sup_{t\in[0,T]} \mathbb{E}\left[\left|\overline{X}_t^m - \overline{X}_t\right|^2 + \left|\overline{Y}_t^m - \overline{Y}_t\right|^2\right] \leq C\, m \,, \tag{3.62}$$

where the constant C *depends only on* $\mathbb{E}[|\overline{X}_0|^4]$, $\mathbb{E}[|\overline{Y}_0|^4]$, $\mathbb{E}[|\overline{V}_0|^4]$, λ_1, σ_2, λ_2, σ_2, d, β, T, C_u, M, C_l, *and* ν.

3.3 Convergence to the global minimum

In this section we present some results on the global convergence of the PSO model (2.14) without memory effects. The extension to the case with memory effects is not strightforward and is actually under study. Here we will follow the presentation in [60], we refer to [9, 20, 23, 40, 41] for similar results for CBO and related models. A different approach to the global convergence of CBO has been presented recently in [42].

Let $(\overline{X}_t, \overline{V}_t)_{t\geq 0}$ be the solution to the nonlinear SDE (3.29) (dropping the superscript m), and consider the quantity

$$\mathcal{H}(t) := (\frac{\gamma}{2m})^2 |\overline{X}_t - \mathbb{E}[\overline{X}_t]|^2 + |\overline{V}_t|^2 + \frac{\gamma}{2m}(\overline{X}_t - \mathbb{E}[\overline{X}_t]) \cdot \overline{V}_t,$$

then it holds that

$$\begin{aligned}
\mathcal{H}(t) &\geq \frac{1}{2}(\frac{\gamma}{2m})^2 |\overline{X}_t - \mathbb{E}[\overline{X}_t]|^2 + \frac{1}{2}|\overline{V}_t|^2 \\
\mathcal{H}(t) &\leq \frac{3}{2}(\frac{\gamma}{2m})^2 |\overline{X}_t - \mathbb{E}[\overline{X}_t]|^2 + \frac{3}{2}|\overline{V}_t|^2 \\
&\leq \frac{3}{2}((\frac{\gamma}{2m})^2 + 1)(|\overline{X}_t - \mathbb{E}[\overline{X}_t]|^2 + |\overline{V}_t|^2) \,.
\end{aligned} \tag{3.63}$$

The goal is then to obtain the decay property of $\mathcal{H}(t)$.

In the following we shall use the notation

$$\delta\overline{X}_t := \overline{X}_t - \mathbb{E}[\overline{X}_t] \,, \tag{3.64}$$

then $\mathbb{E}[|\delta\overline{X}_t|^2]$ is the variance of X_t. Now we can derive an evolution inequality of the quantity $\mathbb{E}[\mathcal{H}(t)]$.

Theorem 3.14. *Under the Assumption 1, let $(\overline{X}_t, \overline{V}_t)_{t\geq 0}$ be the solution to the non-linear SDE (3.29). Then $\mathbb{E}[\mathcal{H}(t)]$ satisfies*

$$\begin{aligned}\frac{d}{dt}\mathbb{E}[\mathcal{H}(t)] \leq &-\frac{\gamma}{m}\mathbb{E}[|\overline{V}_t|^2] \\ &-\left(\frac{\lambda\gamma}{2m^2} - (\frac{2\lambda^2}{\gamma m} + \frac{\sigma^2}{m^2})\frac{2e^{-\alpha\underline{\mathcal{F}}}}{\mathbb{E}[e^{-\alpha\mathcal{F}(\overline{X}_t)}]}\right)\mathbb{E}[|\delta\overline{X}_t|^2]\,. \end{aligned} \tag{3.65}$$

Proof. First the integration by parts formula gives

$$\frac{d}{dt}\mathbb{E}[|\delta\overline{X}_t|^2] = 2\mathbb{E}[\delta\overline{X}_t \cdot \overline{V}_t]\,, \tag{3.66}$$

where we have used the fact that $\mathbb{E}[\delta\overline{X}_t \cdot \mathbb{E}[V_t]] = 0$. Applying Itô-Doeblin formula and taking zero-value of the stochastic integrals, we have for any $\varepsilon > 0$,

$$\begin{aligned}\frac{d}{dt}\mathbb{E}[|\overline{V}_t|^2] =& -2\frac{\gamma}{m}\mathbb{E}[|\overline{V}_t|^2] + 2\frac{\lambda}{m}\mathbb{E}[\overline{V}_t \cdot (X^\alpha(\rho_t) - \overline{X}_t)] \\ &+ \frac{\sigma^2}{m^2}\mathbb{E}[|X^\alpha(\rho_t) - \overline{X}_t|^2] \\ \leq& -(\frac{2\gamma}{m} - \frac{\lambda}{\varepsilon m})\mathbb{E}[|\overline{V}_t|^2] + (\frac{\varepsilon\lambda}{m} + \frac{\sigma^2}{m^2})\mathbb{E}[|X^\alpha(\rho_t) - \overline{X}_t|^2]\,. \end{aligned} \tag{3.67}$$

Further by Itô-Doeblin formula, it holds that

$$\begin{aligned}&\frac{d}{dt}\mathbb{E}[\delta\overline{X}_t \cdot \overline{V}_t] \\ &\quad= \mathbb{E}[|\overline{V}_t|^2] - (\mathbb{E}[\overline{V}_t])^2 - \frac{\gamma}{m}\mathbb{E}[\delta\overline{X}_t \cdot \overline{V}_t] + \frac{\lambda}{m}\mathbb{E}[\delta\overline{X}_t \cdot (X^\alpha(\rho_t) - \overline{X}_t)] \\ &\quad\leq \mathbb{E}[|\overline{V}_t|^2] - \frac{\gamma}{2m}\frac{d}{dt}\mathbb{E}[|\delta\overline{X}_t|^2] - \frac{\lambda}{m}\mathbb{E}[|\delta\overline{X}_t|^2] + \frac{\lambda}{m}\mathbb{E}[\delta\overline{X}_t \cdot (X^\alpha(\rho_t) - \mathbb{E}[\overline{X}_t])] \\ &\quad= \mathbb{E}[|\overline{V}_t|^2] - \frac{\gamma}{2m}\frac{d}{dt}\mathbb{E}[|\delta\overline{X}_t|^2] - \frac{\lambda}{m}\mathbb{E}[|\delta\overline{X}_t|^2]\,. \end{aligned} \tag{3.68}$$

where we have used (3.66) and the fact that $\mathbb{E}[\delta\overline{X}_t \cdot (X^\alpha(\rho_t) - \mathbb{E}[\overline{X}_t])] = 0$. Thus, we have

$$\begin{aligned}(\frac{\gamma}{2m})^2\frac{d}{dt}\mathbb{E}[|\delta\overline{X}_t|^2] + \frac{\gamma}{2m}\frac{d}{dt}\mathbb{E}[\delta\overline{X}_t \cdot \overline{V}_t] \\ \leq \frac{\gamma}{2m}\mathbb{E}[|\overline{V}_t|^2] - \frac{\lambda\gamma}{2m^2}\mathbb{E}[|\delta\overline{X}_t|^2]\,. \end{aligned} \tag{3.69}$$

Collecting estimates (3.67) and (3.69) yields that

$$\frac{d}{dt}\mathbb{E}[\mathcal{H}(t)] \leq -\left(\frac{2\gamma}{m} - \frac{\lambda}{\varepsilon m} - \frac{\gamma}{2m}\right)\mathbb{E}[|\overline{V}_t|^2] - \frac{\lambda\gamma}{2m^2}\mathbb{E}[|\delta\overline{X}_t|^2] + (\frac{\varepsilon\lambda}{m} + \frac{\sigma^2}{m^2})\mathbb{E}[|X^\alpha(\rho_t) - \overline{X}_t|^2]\,. \tag{3.70}$$

To estimate the term $\mathbb{E}[|\overline{X}_t - X^\alpha(\rho_t)|^2]$, we apply Jensen's inequality to obtain

$$\begin{aligned}\mathbb{E}[|\overline{X}_t - X^\alpha(\rho_t)|^2] &\leq \frac{\iint |x-y|^2\omega_\alpha^{\mathcal{F}}(y)\rho_t(dy)\rho_t(dx)}{\int \omega_\alpha^{\mathcal{F}}(y)\rho_t(dy)} \\ &\leq 2e^{-\alpha\underline{\mathcal{F}}}\frac{\mathbb{E}[|\delta\overline{X}_t|^2]}{\mathbb{E}[e^{-\alpha\mathcal{F}(\overline{X}_t)}]}\,.\end{aligned} \tag{3.71}$$

Hence, by choosing $\varepsilon = \frac{2\lambda}{\gamma}$ we obtain

$$\begin{aligned}\frac{d}{dt}\mathbb{E}[\mathcal{H}(t)] \leq &-\frac{\gamma}{m}\mathbb{E}[|\overline{V}_t|^2] \\ &-\left(\frac{\lambda\gamma}{2m^2} - (\frac{2\lambda^2}{\gamma m} + \frac{\sigma^2}{m^2})\frac{2e^{-\alpha\underline{\mathcal{F}}}}{\mathbb{E}[e^{-\alpha\mathcal{F}(\overline{X}_t)}]}\right)\mathbb{E}[|\delta\overline{X}_t|^2],\end{aligned} \tag{3.72}$$

which completes the proof. □

Next we study the evolution of the quantity $\mathbb{E}[e^{-\alpha\mathcal{F}(\overline{X}_t)}]$, and we need an additional assumption on the cost function $\mathcal{F}$ that

A1: $\mathcal{F} \in C^2(\mathbb{R}^d)$ with $\|\nabla^2\mathcal{F}\|_\infty \leq c_{\mathcal{F}}$ for some constant $c_{\mathcal{F}} > 0$.

Lemma 3.15. *Under the Assumption 1 and* ***A1****, let $(\overline{X}_t, \overline{V}_t)_{t\geq 0}$ be the solution to the nonlinear SDE (3.29). Then it holds that*

$$\begin{aligned}\frac{d^2}{dt^2}(\mathbb{E}[e^{-\alpha\mathcal{F}(\overline{X}_t)}])^2 \geq &-\frac{\gamma}{m}\frac{d}{dt}(\mathbb{E}[e^{-\alpha\mathcal{F}(\overline{X}_t)}])^2 \\ &-4(\alpha + \frac{\alpha\lambda}{m}2(\frac{2m}{\gamma})^2)c_{\mathcal{F}}e^{-2\alpha\underline{\mathcal{F}}}\mathbb{E}[\mathcal{H}(t)]\,.\end{aligned} \tag{3.73}$$

Proof. First, applying Itô-Doeblin formula and taking zero-value of the stochastic in-

tegrals, we have

$$\begin{aligned}
\frac{d}{dt}\mathbb{E}[e^{-\alpha\mathcal{F}(\overline{X}_t)}] &= -\alpha\mathbb{E}[e^{-\alpha\mathcal{F}(\overline{X}_t)}\nabla\mathcal{F}(\overline{X}_t)\cdot\overline{V}_t] \\
&= -\alpha\mathbb{E}[\int_0^t d\langle e^{-\alpha\mathcal{F}(\overline{X}_s)}\nabla\mathcal{F}(\overline{X}_s),\overline{V}_s\rangle] + \alpha\mathbb{E}[e^{-\alpha\mathcal{F}(\overline{X}_0)}\langle\nabla\mathcal{F}(\overline{X}_0),\overline{V}_0\rangle] \\
&= \alpha\mathbb{E}[e^{-\alpha\mathcal{F}(\overline{X}_0)}\langle\nabla\mathcal{F}(\overline{X}_0),\overline{V}_0\rangle] - \alpha\mathbb{E}[\int_0^t\langle e^{-\alpha\mathcal{F}(\overline{X}_s)}\overline{V}_s\nabla^2\mathcal{F}(\overline{X}_s),\overline{V}_s\rangle ds] \\
&\quad + \alpha^2\mathbb{E}[\int_0^t e^{-\alpha\mathcal{F}(\overline{X}_s)}|\langle\nabla\mathcal{F}(\overline{X}_s),\overline{V}_s\rangle|^2 ds] \\
&\quad - \alpha\mathbb{E}[\int_0^t e^{-\alpha\mathcal{F}(\overline{X}_s)}\langle\nabla\mathcal{F}(\overline{X}_s),-\frac{\gamma}{m}\overline{V}_s\rangle ds] \\
&\quad - \alpha\mathbb{E}[\int_0^t e^{-\alpha\mathcal{F}(\overline{X}_s)}\langle\nabla\mathcal{F}(\overline{X}_s),\frac{\lambda}{m}(X^\alpha(\rho_s)-\overline{X}_s)\rangle ds]\,.
\end{aligned}$$

Further, differentiating both sides with respect to t gives

$$\begin{aligned}
\frac{d^2}{dt^2}\mathbb{E}[e^{-\alpha\mathcal{F}(\overline{X}_t)}] &= -\alpha\mathbb{E}[\langle e^{-\alpha\mathcal{F}(\overline{X}_t)}\overline{V}_t\nabla^2\mathcal{F}(\overline{X}_t),\overline{V}_t\rangle] \\
&\quad + \alpha^2\mathbb{E}[e^{-\alpha\mathcal{F}(\overline{X}_t)}|\langle\nabla\mathcal{F}(\overline{X}_t),\overline{V}_t\rangle|^2] \\
&\quad - \alpha\mathbb{E}[e^{-\alpha\mathcal{F}(\overline{X}_t)}\langle\nabla\mathcal{F}(\overline{X}_t),-\frac{\gamma}{m}\overline{V}_t\rangle] \\
&\quad - \alpha\mathbb{E}[e^{-\alpha\mathcal{F}(\overline{X}_t)}\langle\nabla\mathcal{F}(\overline{X}_t),\frac{\lambda}{m}(X^\alpha(\rho_t)-\overline{X}_t)\rangle] \\
&\geq -\frac{\gamma}{m}\frac{d}{dt}\mathbb{E}[e^{-\alpha\mathcal{F}(\overline{X}_t)}] - \alpha\mathbb{E}[\langle e^{-\alpha\mathcal{F}(\overline{X}_t)}\overline{V}_t\nabla^2\mathcal{F}(\overline{X}_t),\overline{V}_t\rangle] \\
&\quad - \alpha\mathbb{E}[e^{-\alpha\mathcal{F}(\overline{X}_t)}\langle\nabla\mathcal{F}(\overline{X}_t),\frac{\lambda}{m}(X^\alpha(\rho_t)-\overline{X}_t)\rangle] \\
&=: -\frac{\gamma}{m}\frac{d}{dt}\mathbb{E}[e^{-\alpha\mathcal{F}(\overline{X}_t)}] + I_1 + I_2\,,
\end{aligned} \tag{3.74}$$

where one has used the fact that

$$-\frac{\gamma}{m}\frac{d}{dt}\mathbb{E}[e^{-\alpha\mathcal{F}(\overline{X}_t)}] = \frac{\alpha\gamma}{m}\mathbb{E}[e^{-\alpha\mathcal{F}(\overline{X}_t)}\langle\nabla\mathcal{F}(\overline{X}_t),\overline{V}_t\rangle]\,. \tag{3.75}$$

According to assumption ***A1***, one can show that

$$I_1 \geq -\alpha\mathbb{E}[e^{-\alpha\mathcal{F}(\overline{X}_t)}\|\nabla^2\mathcal{F}(\overline{X}_t)\|_\infty|\overline{V}_t|^2] \geq -\alpha c_{\mathcal{F}}e^{-\alpha\underline{\mathcal{F}}}\mathbb{E}[|\overline{V}_t|^2]. \tag{3.76}$$

We further notice that

$$\begin{aligned}
&\left|\mathbb{E}[e^{-\alpha\mathcal{F}(\overline{X}_t)}\langle\nabla\mathcal{F}(\overline{X}_t),(X^\alpha(\rho_t)-\overline{X}_t)\rangle]\right| \\
&\quad=\left|\mathbb{E}[e^{-\alpha\mathcal{F}(\overline{X}_t)}\langle\nabla\mathcal{F}(\overline{X}_t)-\nabla\mathcal{F}(X^\alpha(\rho_t)),(\overline{X}_t-X^\alpha(\rho_t))\rangle]\right| \\
&\quad\le e^{-\alpha\underline{\mathcal{F}}}c_{\mathcal{F}}\mathbb{E}[|\overline{X}_t-X^\alpha(\rho_t)|^2]\,,
\end{aligned}\tag{3.77}$$

where we have used the fact that $\mathbb{E}[e^{-\alpha\mathcal{F}(\overline{X}_t)}\langle\nabla\mathcal{F}(X^\alpha(\rho_t)),(\overline{X}_t-X^\alpha(\rho_t))\rangle]=0$. Furthermore since $\mathbb{E}[|\overline{X}_t-X^\alpha(\rho_t)|^2]\le 2e^{-\alpha\underline{\mathcal{F}}}\frac{\mathbb{E}[|\delta\overline{X}_t|^2]}{\mathbb{E}[e^{-\alpha\mathcal{F}(\overline{X}_t)}]}$, one has

$$\begin{aligned}
I_2&\ge-\frac{\alpha\lambda}{m}e^{-\alpha\underline{\mathcal{F}}}c_{\mathcal{F}}\mathbb{E}[|\overline{X}_t-X^\alpha(\rho_t)|^2] \\
&\ge-\frac{\alpha\lambda}{m}2e^{-2\alpha\underline{\mathcal{F}}}c_{\mathcal{F}}\frac{\mathbb{E}[|\delta\overline{X}_t|^2]}{\mathbb{E}[e^{-\alpha\mathcal{F}(\overline{X}_t)}]}\,.
\end{aligned}\tag{3.78}$$

This combining with (3.76) leads to

$$\begin{aligned}
\frac{d^2}{dt^2}\mathbb{E}[e^{-\alpha\mathcal{F}(\overline{X}_t)}]\ge&-\frac{\gamma}{m}\frac{d}{dt}\mathbb{E}[e^{-\alpha\mathcal{F}(\overline{X}_t)}]-\alpha c_{\mathcal{F}}e^{-\alpha\underline{\mathcal{F}}}\mathbb{E}[|\overline{V}_t|^2] \\
&-\frac{\alpha\lambda}{m}c_{\mathcal{F}}2e^{-2\alpha\underline{\mathcal{F}}}\frac{\mathbb{E}[|\delta\overline{X}_t|^2]}{\mathbb{E}[e^{-\alpha\mathcal{F}(\overline{X}_t)}]}\,.
\end{aligned}\tag{3.79}$$

Using this, one can obtain

$$\begin{aligned}
&\frac{d}{dt}\left(\frac{1}{2}\frac{d}{dt}(\mathbb{E}[e^{-\alpha\mathcal{F}(\overline{X}_t)}])^2\right)=\frac{d}{dt}\left(\mathbb{E}[e^{-\alpha\mathcal{F}(\overline{X}_t)}]\frac{d}{dt}(\mathbb{E}[e^{-\alpha\mathcal{F}(\overline{X}_t)}])\right) \\
&\quad=\left(\frac{d}{dt}(\mathbb{E}[e^{-\alpha\mathcal{F}(\overline{X}_t)}])\right)^2+\mathbb{E}[e^{-\alpha\mathcal{F}(\overline{X}_t)}]\frac{d^2}{dt^2}\mathbb{E}[e^{-\alpha\mathcal{F}(\overline{X}_t)}] \\
&\quad\ge-\frac{\gamma}{2m}\frac{d}{dt}(\mathbb{E}[e^{-\alpha\mathcal{F}(\overline{X}_t)}])^2-\alpha c_{\mathcal{F}}e^{-2\alpha\underline{\mathcal{F}}}\mathbb{E}[|\overline{V}_t|^2] \\
&\qquad-\frac{\alpha\lambda}{m}2e^{-2\alpha\underline{\mathcal{F}}}c_{\mathcal{F}}\mathbb{E}[|\delta\overline{X}_t|^2] \\
&\quad\ge-\frac{\gamma}{2m}\frac{d}{dt}(\mathbb{E}[e^{-\alpha\mathcal{F}(\overline{X}_t)}])^2 \\
&\qquad-\left(2\alpha+2\frac{\alpha\lambda}{m}2(\frac{2m}{\gamma})^2\right)c_{\mathcal{F}}e^{-2\alpha\underline{\mathcal{F}}}\mathbb{E}[\mathcal{H}(t)]\,,
\end{aligned}\tag{3.80}$$

where we have used (3.63) in the last inequality. This completes the proof. □

Our main theorem on global convergence can be described in the following way:

Theorem 3.16. *Under the Assumption 1 and **A1**, let $(\overline{X}_t,\overline{V}_t)_{t\ge0}$ be the solution to*

the nonlinear SDE (3.29). *Further we assume that the initial data* $\overline{X}_0$ *and* $\overline{V}_0$ *satisfy*

$$\mu := \frac{\lambda\gamma}{2m^2} - (\frac{2\lambda^2}{\gamma m} + \frac{\sigma^2}{m^2})\frac{4e^{-\alpha\underline{\mathcal{F}}}}{\mathbb{E}[e^{-\alpha\mathcal{F}(\overline{X}_0)}]} > 0, \tag{3.81}$$

and

$$\begin{aligned} &2\alpha\frac{\gamma}{m}\mathbb{E}[e^{-\alpha\mathcal{F}(\overline{X}_0)}]\left(\mathbb{E}[e^{-\alpha\mathcal{F}(\overline{X}_0)}\nabla\mathcal{F}(\overline{X}_0)\cdot\overline{V}_0]\right)_+ \\ &\quad + 4(\alpha + \frac{\alpha\lambda}{m}2(\frac{2m}{\gamma})^2)c_{\mathcal{F}}e^{-2\alpha\underline{\mathcal{F}}}\frac{\mathbb{E}[\mathcal{H}(0)]}{\chi(\frac{\gamma}{m}-\chi)} < \frac{3}{4}(\mathbb{E}[e^{-\alpha\mathcal{F}(\overline{X}_0)}])^2\,, \end{aligned} \tag{3.82}$$

where we denote $x_+ = \max\{x, 0\}$, $\forall\, x \in \mathbb{R}$, *and*

$$\chi = \frac{\min\{\mu, \frac{\gamma}{m}\}}{\frac{3}{2}((\frac{\gamma}{2m})^2 + 1)}.$$

Then $\mathbb{E}[|\overline{X}_t - \mathbb{E}[\overline{X}_t]|^2] \to 0, \mathbb{E}[|\overline{V}_t|^2] \to 0$ *exponentially fast as* $t \to \infty$, *and there exists some* $\widetilde{x}$ *depending on* α *such that* $\mathbb{E}[\overline{X}_t] \to \widetilde{x}$ *and* $X^\alpha(\rho_t) \to \widetilde{x}$ *exponentially fast as* $t \to \infty$. *Moreover it holds that*

$$\mathcal{F}(\widetilde{x}) - \underline{\mathcal{F}} \le \frac{1}{\alpha}\log(2) - \frac{1}{\alpha}\log(\mathbb{E}[e^{-\alpha\mathcal{F}(\overline{X}_0)}]) - \underline{\mathcal{F}} \to 0 \text{ as } \alpha \to \infty\,. \tag{3.83}$$

Remark 2. *If we additionally assume the inverse continuity of* $\mathcal{F}$ *holds, namely for any* $x \in \mathbb{R}^d$ *there exists a minimizer* x^* *of* $\mathcal{F}$ *(which may depend on* x*) such that it holds*

$$|x - x^*| \le C_0|\mathcal{F}(x) - \underline{\mathcal{F}}|^\ell\,,$$

where ℓ, C_0 *are some positive constants, then one can conclude that* $\widetilde{x} \to x^*$ *as* $\alpha \to \infty$.

Proof. Define

$$T := \inf\left\{t \ge 0 :\ \mathbb{E}[e^{-\alpha\mathcal{F}(\overline{X}_t)}] < \frac{1}{2}\mathbb{E}[e^{-\alpha\mathcal{F}(\overline{X}_0)}]\right\} \text{ with } \inf\emptyset = \infty\,. \tag{3.84}$$

Obviously, $T > 0$. Assume that $T < \infty$, then for $t \in [0, T]$, one can deduce that

$$\begin{aligned} &\frac{\lambda\gamma}{2m^2} - (\frac{2\lambda^2}{\gamma m} + \frac{\sigma^2}{m^2})\frac{2e^{-\alpha\underline{\mathcal{F}}}}{\mathbb{E}[e^{-\alpha\mathcal{F}(\overline{X}_t)}]} \\ \ge\ &\frac{\lambda\gamma}{2m^2} - (\frac{2\lambda^2}{\gamma m} + \frac{\sigma^2}{m^2})\frac{4e^{-\alpha\underline{\mathcal{F}}}}{\mathbb{E}[e^{-\alpha\mathcal{F}(\overline{X}_0)}]} = \mu > 0\,. \end{aligned} \tag{3.85}$$

Consequently by (3.72) we have

$$\begin{aligned}\frac{d}{dt}\mathbb{E}[\mathcal{H}(t)] &\leq -\frac{\gamma}{m}\mathbb{E}[|\overline{V}_t|^2] - \mu\mathbb{E}[|\delta\overline{X}_t|^2] \\ &\leq -\min\{\mu, \frac{\gamma}{m}\}(\mathbb{E}[|\delta\overline{X}_t|^2] + \mathbb{E}[|\overline{V}_t|^2]) \\ &\leq -\frac{\min\{\mu, \frac{\gamma}{m}\}}{\frac{3}{2}((\frac{\gamma}{2m})^2+1)}\mathbb{E}[\mathcal{H}(t)]\,, \end{aligned} \tag{3.86}$$

where we have used the estimate (3.63). This implies that

$$\mathbb{E}[\mathcal{H}(t)] \leq \mathbb{E}[\mathcal{H}(0)]\exp\left(-\frac{\min\{\mu, \frac{\gamma}{m}\}}{\frac{3}{2}((\frac{\gamma}{2m})^2+1)}t\right) = \mathbb{E}[\mathcal{H}(0)]\exp(-\chi t)\,. \tag{3.87}$$

One further notice that

$$\chi \leq \frac{\frac{\gamma}{m}}{\frac{3}{2}((\frac{\gamma}{2m})^2+1)} < \frac{\gamma}{m}\,.$$

Set $\mathcal{Y}(t) := (\mathbb{E}[e^{-\alpha\mathcal{F}(\overline{X}_t)}])^2$. Then we have

$$\mathcal{Y}'(0) = -2\alpha\mathbb{E}[e^{-\alpha\mathcal{F}(\overline{X}_0)}]\mathbb{E}[e^{-\alpha\mathcal{F}(\overline{X}_0)}\nabla\mathcal{F}(\overline{X}_0)\cdot\overline{V}_0]. \tag{3.88}$$

By Gronwall's inequality, it follows from Lemma 3.15 that

$$\begin{aligned}\frac{d}{dt}\mathcal{Y}(t) &\geq \mathcal{Y}'(0)\exp(-\frac{\gamma}{m}t) \\ &\quad - 4\left(\alpha + \frac{\alpha\lambda}{m}2(\frac{2m}{\gamma})^2\right)c_{\mathcal{F}}e^{-2\alpha\underline{\mathcal{F}}}\exp(-\frac{\gamma}{m}t)\int_0^t\exp(\frac{\gamma}{m}s)\mathbb{E}[\mathcal{H}(s)]ds \\ &\geq \mathcal{Y}'(0)\exp(-\frac{\gamma}{m}t) \\ &\quad - 4\left(\alpha + \frac{\alpha\lambda}{m}2(\frac{2m}{\gamma})^2\right)c_{\mathcal{F}}e^{-2\alpha\underline{\mathcal{F}}}\mathbb{E}[\mathcal{H}(0)]\exp(-\frac{\gamma}{m}t)\int_0^t\exp((\frac{\gamma}{m}-\chi)s)ds \\ &\geq \mathcal{Y}'(0)\exp(-\frac{\gamma}{m}t) \\ &\quad - 4\left(\alpha + \frac{\alpha\lambda}{m}2(\frac{2m}{\gamma})^2\right)c_{\mathcal{F}}e^{-2\alpha\underline{\mathcal{F}}}\frac{\mathbb{E}[\mathcal{H}(0)]}{\frac{\gamma}{m}-\chi}\exp(-\chi t)\,,\end{aligned}$$

which implies that

$$\begin{aligned}\mathcal{Y}(t) &\geq \mathcal{Y}(0) - \frac{m}{\gamma}(-\mathcal{Y}'(0))_+ \\ &\quad - 4\left(\alpha + \frac{\alpha\lambda}{m}2(\frac{2m}{\gamma})^2\right)c_{\mathcal{F}}e^{-2\alpha\underline{\mathcal{F}}}\frac{\mathbb{E}[\mathcal{H}(0)]}{\chi(\frac{\gamma}{m}-\chi)}\,.\end{aligned}$$

By assumption (3.82), this means that

$$\begin{aligned}
&(\mathbb{E}[e^{-\alpha\mathcal{F}(\overline{X}_t)}])^2 \\
&\quad\geq (\mathbb{E}[e^{-\alpha\mathcal{F}(\overline{X}_0)}])^2 - 2\alpha\frac{\gamma}{m}\mathbb{E}[e^{-\alpha\mathcal{F}(\overline{X}_0)}]\left(\mathbb{E}[e^{-\alpha\mathcal{F}(\overline{X}_0)}\nabla\mathcal{F}(\overline{X}_0)\cdot\overline{V}_0]\right)_+ \\
&\qquad - 4\left(\alpha+\frac{\alpha\lambda}{m}2(\frac{2m}{\gamma})^2\right)c_{\mathcal{F}}e^{-2\alpha\underline{\mathcal{F}}}\frac{\mathbb{E}[\mathcal{H}(0)]}{\chi(\frac{\gamma}{m}-\chi)} \\
&\quad\geq \frac{1}{4}(\mathbb{E}[e^{-\alpha\mathcal{F}(\overline{X}_0)}])^2\,.
\end{aligned}$$

This means that there exists $\delta>0$ such that $\mathbb{E}[e^{-\alpha\mathcal{F}(\overline{X}_t)}]\geq\frac{1}{2}\mathbb{E}[e^{-\alpha\mathcal{F}(\overline{X}_0)}]$ in $[T,T+\delta)$ as well. This then contradicts with the definition of T. Hence $T=\infty$. Consequently it holds that

$$\mathbb{E}[\mathcal{H}(t)]\leq\mathbb{E}[\mathcal{H}(0)]\exp(-\chi t)\text{ and }\mathbb{E}[e^{-\alpha\mathcal{F}(\overline{X}_t)}]\geq\frac{1}{2}\mathbb{E}[e^{-\alpha\mathcal{F}(\overline{X}_0)}],\tag{3.89}$$

for all $t\geq 0$. Recalling the fact (3.71) this infers that

$$\begin{aligned}
\mathbb{E}[|\overline{X}_t-X^\alpha(\rho_t)|^2]&\leq 2e^{-\alpha\underline{\mathcal{F}}}\frac{\mathbb{E}[|\delta\overline{X}_t|^2]}{\mathbb{E}[e^{-\alpha\mathcal{F}(\overline{X}_t)}]} \\
&\leq 4e^{-\alpha\underline{\mathcal{F}}}(\frac{2m}{\gamma})^2\frac{2\mathbb{E}[\mathcal{H}(0)]}{\mathbb{E}[e^{-\alpha\mathcal{F}(\overline{X}_0)}]}\exp(-\chi t).
\end{aligned}\tag{3.90}$$

Additionally, one has

$$\begin{aligned}
\mathbb{E}[|\overline{X}_t-\mathbb{E}[\overline{X}_t]|^2]&\leq 2(\frac{2m}{\gamma})^2\mathbb{E}[\mathcal{H}(t)] \\
&\leq C\exp(-\chi t)\mathbb{E}[|\overline{V}_t|^2] \\
&\leq 2\mathbb{E}[\mathcal{H}(t)]\leq C\exp(-\chi t)\,.
\end{aligned}\tag{3.91}$$

Moreover we have

$$|\frac{d}{dt}\mathbb{E}[\overline{X}_t]|\leq\mathbb{E}[|\overline{V}_t|]\leq C\exp(-\frac{1}{2}\chi t)\to 0\text{ as }t\to\infty\,.\tag{3.92}$$

This means that $\mathbb{E}[\overline{X}_t]\to\widetilde{x}$ for some $\widetilde{x}$ depending on α, then it follows from (3.91) that $\overline{X}_t\to\widetilde{x}$ in mean square. Thus we have $X^\alpha(\rho_t)\to\widetilde{x}$ according to (3.90). Furthermore, by (3.89) one as $\frac{1}{2}\mathbb{E}[e^{-\alpha\mathcal{F}(\overline{X}_0)}]\leq\mathbb{E}[e^{-\alpha\mathcal{F}(\overline{X}_t)}]\to e^{-\alpha\mathcal{F}(\widetilde{x})}$. Therefore we conclude that

$$\mathcal{F}(\widetilde{x})\leq\frac{1}{\alpha}\log(2)-\frac{1}{\alpha}\log\left(\mathbb{E}[e^{-\alpha\mathcal{F}(\overline{X}_0)}]\right).\tag{3.93}$$

By the Laplace principle (2.16), one has

$$0 \leq \mathcal{F}(\widetilde{x}) - \underline{\mathcal{F}} \leq \frac{1}{\alpha}\log(2) - \frac{1}{\alpha}\log(\mathbb{E}[e^{-\alpha\mathcal{F}(\overline{X}_0)}]) - \underline{\mathcal{F}} \to 0 \text{ as } \alpha \to \infty\,. \tag{3.94}$$

This completes the proof. □

3.4 Concluding remarks

This chapter, based on some recent results [27, 49, 50, 57, 60] representing important step towards the construction of a general mathematical theory for swarm based methods, is devoted to the rigorous analysis of the formal derivations introduced in Chapter 2. In the mean-field limit, starting from the regularized second-order SDEs describing the PSO dynamics, we derive rigorously the corresponding mean-field Vlasov-Fokker-Planck type equation. The behaviour of the system for small values of the inertia parameter is rigorously justified, showing how in this limit the MF-PSO dynamics converges to a generalization of CBO models containing memory and the local best. A convergence result in the mean-field limit to the global minimum was then proved for a large class of objective functions in the case where the dynamics are governed only by the global best.

Chapter 4

Consensus based optimization with memory and random selection

In this chapter we focus on a particular subclass of the methods derived in Chapter 2 and subsequently analyzed in Chapter 3, namely consensus-based optimization that use memory effects and only the global best. In such methods, the consensus point is computed taking into account the past positions of all particles. We also discuss some improvements that lead to an increased efficiency while preserving the performances of the original algorithm. In particular, we show how using a random selection strategy to discard particles during the calculation improves overall performance. Several benchmark problems are proposed to validate and test the algorithm and its acceleration techniques. A theoretical analysis allows us to recover convergence guarantees under weak assumptions of the objective function even in presence of the random selection. This is done by first approximating the evolution of the particles with a continuous dynamic over time and then considering the mean-field limit of that dynamic. Note that in this chapter some notations are slightly changed from those used in Chapters 1 and 2.

4.1 Consensus-based optimization with memory effects

We introduce the consensus-based optimization algorithm with memory effects (CBO-ME) to solve problems of the form (1.1), highlighting similarities and differences between classical CBO methods and PSO algorithms. Note that a different discrete-level notation is adopted here in CBO-ME to make the comparison with the classical PSO method more immediate. Since the latter does not exploit an explicitly time-dependent

dynamics, we set $\Delta t = 1$ instead of $\lambda = 1$ as was usually done for the sake of comparison with previous results from the CBO community.

4.1.1 Particles update rule

At each iteration step k and for every particle $i = 1, \dots, N$, we store its position x_i^k and its best position found so far $y_i^k, \mathcal{F}(y_i^k) = \min_{h \le k} \mathcal{F}(x_i^h)$. The best positions are used to compute a consensus point

$$\overline{y}^{\alpha,k} = \sum_{i=1}^{N} \omega_i^k \, y_i^k \quad \text{with} \quad \omega_i^k = \frac{e^{-\alpha \mathcal{F}(y_i^k)}}{\sum_{j=1}^{N} e^{-\alpha \mathcal{F}(y_j^k)}} \tag{4.1}$$

which approximates the global best solution $\overline{y}^{\infty,k}$ among all particles and all times for $\alpha > 1$. Indeed, thanks to the choice of the weights ω_i^k, we have that

$$\overline{y}^{\alpha,k} \quad \longrightarrow \quad \overline{y}^{\infty,k} := \operatorname{argmin}\{\mathcal{F}(y_1^k), \dots, \mathcal{F}(y_N^k)\}$$

as $\alpha \to \infty$, provided that there is only one global best position among $\{y_1^k, \dots, y_N^k\}$. Such approximation was first introduced for CBO methods [83] as it leads to more amenable theoretical analysis, but it also allows for more flexibility. Indeed, relatively small values of α can be used at the beginning of the computation to promote exploration. Large values of α, on the other hand, lead to better exploitation of the computed solutions and to higher accuracy. We note that the weights used in (4.1) correspond in statistical mechanics to the Boltzmann-Gibbs distribution associated with the energy $\mathcal{F}$. In this context, α plays the role of the inverse of the system temperature T and the limit $\alpha \to \infty$ corresponds to $T \to 0$.

Once the consensus point $\overline{y}^{\alpha,k}$ is computed, the particle positions are then updated according to the law

$$x_i^{k+1} = x_i^k + \lambda \left(\overline{y}^{\alpha,k} - x_i^k\right) + \sigma \left(\overline{y}^{\alpha,k} - x_i^k\right) \otimes \vartheta_i^k \tag{4.2}$$

with $\vartheta_i^k \in \mathbb{R}^d$ randomly sampled from the normal distribution ($\vartheta_i^k \sim \mathcal{N}(0, \mathbf{I}_d)$) and where $\otimes$ is the component-wise product.

The update rule is characterized by a deterministic component of strength $\lambda \in (0, 1)$ promoting concentration around the consensus point $\overline{y}^{\alpha,k}$ and a stochastic component of strength $\sigma > 0$ promoting exploration of the search space. As the latter depends on the difference $(\overline{y}^{\alpha,k} - x_i^k)$, the random behavior is stronger for particles which are far from the consensus point, whereas it is weaker for those that are close to it. Also, such exploration resembles an anisotropic diffusive behavior in which every coordinate

direction is explored at a different rate. This approach was first proposed in [23] in the context of CBO methods and has been proved to suffer less from the curse of dimensionality with the respect to the originally proposed isotropic diffusion given by $\sigma\|\overline{y}^{\alpha,k} - x_i^k\|_2 \vartheta_i^k$ with ϑ_i^k being again a normally distributed d-dimensional vector [23].

4.1.2 Random selection strategy

When the particle system concentrates around the consensus point, showing a mostly exploitative behavior, we employ a particle selection strategy. Discarding particles introduces additional stochasticity to the system, while reducing the computational cost. Following the approach suggested in [40], we check the evolution of the system variance to decide how many particles to (eventually) discard.

For a given set of particles $\mathbf{z} = \{z_i\}_{i\in J}$, the system variance is given by

$$\mathrm{var}(\mathbf{z}) := \frac{1}{|J|}\sum_{j\in J} \|z_j - \mathrm{m}(\mathbf{z})\|_2^2 \quad \text{with} \quad \mathrm{m}(\mathbf{z}) := \frac{1}{|J|}\sum_{i\in J} z_i\,, \tag{4.3}$$

where $|J|$ indicates the cardinality of J, that is, the number of particles in this context.

Let $I_k \subseteq \{1,\dots,N\}$ be the set of active particles at step k and $N_k = |I_k|$. To decide how many particles to select, we compare the variance of the particle system before the position update (4.2), $\mathbf{x}^k = \{x_i^k\}_{i\in I_k}$ and after it, $\widetilde{\mathbf{x}}^{k+1} = \{x_i^{k+1}\}_{i\in I_k}$. Then, the number N_{k+1} of particles we select for the next iteration is given by

$$\begin{aligned} \widetilde{N}_{k+1} &= \left\lfloor N_k \left(1 + \mu\, \frac{\mathrm{var}(\widetilde{\mathbf{x}}^{k+1}) - \mathrm{var}(\mathbf{x}^{k+1})}{\mathrm{var}(\mathbf{x}^{k+1})}\right)\right\rfloor \\ N_{k+1} &= \min\left\{ \max\left\{\widetilde{N}_{k+1}, N_{\min}\right\}, N_k\right\} \end{aligned} \tag{4.4}$$

with $\lfloor z \rfloor$ being the integer part of a number z and $N_{\min} \in \mathbb{N}$ the smallest amount of particles we allow to have. If $N_{k+1} < N_k$, a subset $I_{k+1} \subset I_k, |I_{k+1}| = N_{k+1}$, of particles is randomly selected to continue the computation. The parameter $\mu \in [0,1]$ regulates the mechanism: for $\mu = 0$ there is no particle discarding, while for $\mu = 1$ the maximum number of particles is discarded if the variance is decreasing. As we will see in Section 4.3, this random selection mechanism reduces the computational time without affecting the algorithm performance. We will also theoretically analyze this aspect in Section 4.4.3, where we show that convergence properties are preserved.

As stopping criterion, we keep a counter n on how many times $\|\overline{y}^{\alpha,k+1} - \overline{y}^{\alpha,k}\|_2$ is smaller than a certain tolerance $\delta_{\text{stall}} > 0$. If this happens for more than a given n_{stall} number of times in a row, we assume the particle system has found a solution and stop the computation. A maximum number of iteration $k_{\max}$ representing the computational

budget is also given. The proposed CBO-ME is summarized in Algorithm 1.

Remark 3. *In the meta-heuristic literature, particles are usually discarded depending on their objective value, in a way that particles with high objective value are more likely to be discarded [71, 91]. The proposed strategy does not add a further heuristic strategy but simply cut down the algorithm complexity. Also, convergence properties are in this way expected to be preserved. We note that, on the other hand, there is no straightforward way to both generate particles and preserve the particle system distribution at the same time.*

Algorithm 1: Consensus-Based Optimization with Memory Effects (CBO-ME)

Input: $\mathcal{F}, N_0, N_{\min}, k_{\max}, \lambda, \sigma, \alpha, n_{\text{stall}}$ and δ_{stall};
Inizialize N_0 particle positions $x_0^i, i = 1, \dots, N$;
$y_i^0 \leftarrow x_i^0$ for all $i = 1, \dots, N_0$;
Compute $\overline{y}^{\alpha,0}$ according to (4.1);
$k \leftarrow 0$, $n \leftarrow 0$;
while $k < k_{\max}$ and $n < n_{\text{stall}}$ **do**
  for $i = 1$ **to** N_k **do**
    $\vartheta_i^k \sim \mathcal{N}(0, \mathbf{I}_d)$;
    Compute x_i^{k+1} according to (4.2);
    if $\mathcal{F}(x_i^{k+1}) < \mathcal{F}(y_i^k)$ **then**
      $y_i^{k+1} \leftarrow x_i^{k+1}$;
    else
      $y_i^{k+1} \leftarrow y_i^k$;
    end
  end
  Compute $\overline{y}^{\alpha,k+1}$ according to (4.1);
  if $\|\overline{y}^{\alpha,k+1} - \overline{y}^{\alpha,k}\|_2 < \delta_{\text{stall}}$ **then**
    $n \leftarrow n + 1$;
  else
    $n \leftarrow 0$;
  end
  Compute N_{k+1} according to (4.4);
  if $N_{k+1} < N_k$ **then**
    Randomly discard $N_{k+1} - N_k$ particles;
  $k \leftarrow k + 1$;
end
return $\overline{y}^{\alpha,k}, \mathbf{F}(\overline{y}^{\alpha,k})$

4.1.3 Comparison with CBO and PSO

What distinguishes CBO-ME from plain CBO, see e.g [23, 83], is clearly the introduction of the best positions $\{y_i^k\}_{i=1}^N$ and the fact that the consensus point is calculated among them and not just among the particle positions $\{x_i^k\}_{i=1}^N$ at that given time k. Indeed, the classical CBO update rule without memory effects (and with anisotropic diffusion and projection step) is given by

$$x_i^{k+1} = x_i^k + \lambda \left(\overline{x}^{\alpha,k} - x_i^k\right) + \sigma \left(\overline{x}^{\alpha,k} - x_i^k\right) \otimes \vartheta_i^k \tag{4.5}$$

where $\overline{x}^{\alpha,k}$ is defined consistently with (4.1) (by substituting y_i^k with x_i^k). As we will see in the numerical tests, the use of memory effects improves the algorithm performance.

Since alignment towards personal bests y_i^k and towards the global best $\overline{y}^{\infty,k}$ are also the fundamental building blocks of PSO algorithms, we highlight now the main differences and similarities between PSO and CBO-ME. For completeness, we recall the canonical PSO method, see e.g. [86], using the notation of (4.2) for easier comparison

$$\begin{cases} x_i^{k+1} &= x_i^k + v_i^{k+1} \\ v_i^{k+1} &= w v_i^k + C_1 \left(y_i^k - x_i^k\right) \otimes \widehat{\vartheta}_{i,1}^k + C_2 \left(\overline{y}^{\infty,k} - x_i^k\right) \otimes \widehat{\vartheta}_{i,2}^k \end{cases} \tag{4.6}$$

where v_i^k are the particles velocities, $w, C_1, C_2 > 0$ are the algorithm parameters and $\vartheta_{i,1}^k, \vartheta_{i,2}^k$ are uniformly sampled from $[0,1]^d$, $(\widehat{\vartheta}_{i,1}^k, \widehat{\vartheta}_{i,2}^k) \sim \mathrm{Unif}([0,1]^d)$. Several variants and improvements have been proposed starting from the above dynamics, but a complete review is beyond the scope of this paper and we refer to the recent survey [99] for more references.

We are interested in highlighting the main differences between (4.2) and (4.6) regarding the stochastic components: in CBO-ME deterministic and stochastic steps are de-coupled and tuned by two different parameters (λ and σ), while in PSO they are coupled. Indeed, in (4.6), deterministic and stochastic components are both controlled by the same parameter: C_1 in the case of personal best dynamics and C_2 for the global best one. By splitting the term $C_2 \left(\overline{y}^{\infty,k} - x_i^k\right) \widehat{\vartheta}_{i,2}^k$ into a deterministic step and a zero-mean term we obtain

$$C_2 \left(\overline{y}^{\infty,k} - x_i^k\right) \otimes \widehat{\vartheta}_{i,2}^k = \frac{C_2}{2} \left(\overline{y}^{\infty,k} - x_i^k\right) + \frac{C_2}{2} \left(\overline{y}^{\infty,k} - x_i^k\right) \otimes \vartheta_{i,2}^k \tag{4.7}$$

with $\vartheta_{i,2}^k = 2\widehat{\vartheta}_{i,2}^k - 1$, $\vartheta_{i,2}^k \sim \mathrm{Unif}([-1,1]^d)$. Suggested in [50], such rewriting highlights how increasing the alignment strength towards the global best (by increasing C_2) necessary increases the stochasticity of the system as well. In (4.2) and (4.5), on the other hand, one is allowed to tune the exploration and exploitation behaviors separately, by

either changing parameter λ or σ.

Clearly, CBO-ME also differs from PSO due to its first-order dynamics. Having the aim of resembling birds flocking, the first PSO algorithm [67] was proposed as a second-order dynamics. The inertia weight w, introduced later in [90], became an essential parameter to prevent early convergence of the swarm and to increase the global exploration behavior, especially at the beginning of the computation, see e.g.[79, 90] and reviews [56, 86, 99] for more references. We note that several other strategies have proposed to improve PSO exploration behavior, see, for example, [104]. As already mentioned, in CBO methods convergence and exploration are de-coupled and can be tuned separately. Therefore, to keep the algorithm more amenable to theoretical analysis, we consider a simpler first-order dynamics. We note that a CBO dynamics with inertia mechanism was proposed in [24].

Similarly, we found the contribution given by the personal best alignment non-essential and difficult to tune. Thus, the lack of alignment towards personal best in (4.2). Replacing alignment towards personal best with Gaussian noise was also suggested in [101] where authors proposed the Accelerated PSO (APSO) algorithm. Further studied in [45, 102], APSO also allows to de-couple the stochastic component from the deterministic one and the noise is heuristically tuned to decrease during the computation as in Simulated Annealing [68]. In CBO methods, the noise strength automatically adapts as it depends on the distance from the consensus point, which is also different for every particle. For completeness, we note that many other variants of PSO have been proposed to include different explorative behaviors, see e.g. Chaotic PSO [73].

4.2 Numerical results

Having discussed the fundamental features of the CBO dynamics with memory effects, we now validate Algorithm 1 and compare its performance with plain CBO and PSO. We will test the methods against several benchmark optimization problems and analyze the impact of the random selection technique on the convergence speed. We also employ Algorithm 1 to solve problems arising from applications, such as image segmentation and training of Machine Learning architectures for function approximation and image classification.

4.3 Tests on benchmark problems

Having discussed the fundamental features of the CBO dynamics with memory effects, we now validate Algorithm 1 and compare its performance with plain CBO and PSO algorithms. We will test the methods against several problems presented and analyze the impact of the random selection technique on the convergence speed.

We test the proposed algorithm against different optimization problems, by considering 8 benchmark objective functions, see e.g. [63], which we report in Appendix (A1) for completeness. The search space dimension is set to $d = 20$ and the location of the global best x^* is known.

As in plain CBO methods, we expect the most important parameters to be λ and σ, governing the balance between the exploitative behavior and the explorative one. In particular, we are interested in the algorithm performance as we change the ratio between λ and σ. Therefore, in the first experiment we fix $\lambda = 0.01$, while considering different values of σ. The parameter α is adapted during the computation: starting form $\alpha_0 = 10$, it increases according to the law

$$\alpha = \alpha_0 \cdot k \cdot \log_2(k)\,. \tag{4.8}$$

Fig. 4.1 shows the accuracy and the objective value reached for $\sigma \in [0, 2]$ after $k_{\max} = 10^4$ algorithm iterations with $N = 200$ particles, and without random selection. The optimal value for σ is clearly problem-dependent, but we note that the optimal values for the problems considered all fall within a relative small range (underlined in gray in Fig. 4.1).

From Fig. 4.1 we infer that a good value for all benchmark problems considered is given by $\sigma = 0.8$. Using this value, we now compare CBO-ME, with plain CBO and the standard PSO (with and without alignment towards personal best) for different population sizes $N = 50, 100, 200$. We keep the random selection mechanism off by setting $\mu = 0$ and use the same previously chosen parameters when memory effects are used. For plain CBO, without memory effects, we set $\sigma = 0.71 \approx \sqrt{2}/2$. Concerning PSO, we use the solver provided by the MATLAB Global Optimization Toolbox (`particleswarm`), changing the maximum number of iterations and the stall condition to the one used for CBO methods, to make the results comparable. The remaining parameters are kept as described in the relative documentation [82]. We set $k_{\max} = 10^4$, $\delta_{\text{stall}} = 10^{-4}$ and consider a run successful when either

$$\|\overline{y}^{\alpha,k} - x^*\|_\infty < 0.1 \quad \text{or} \quad |\mathcal{F}(\overline{y}^{\alpha,k}) - \mathcal{F}(x^*)| < 0.01\,. \tag{4.9}$$

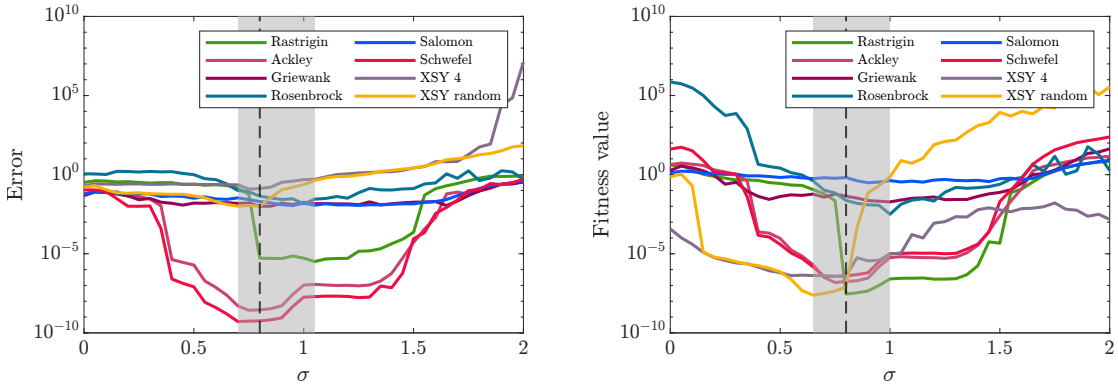

(a) $\|\overline{y}^{\alpha,k} - x^*\|_\infty$ (b) $\mathcal{F}(\overline{y}^{\alpha,k})$

Figure 4.1: Optimization on benchmark functions using CBO-ME. Behavior of the expectation error and fitness value for different values of σ. Here $\lambda = 0.01$ and α is adaptive, with $\alpha_0 = 10$. The particle population is $N = 200$. Gray bands (of values $[0.70, 1.05]$ for error and $[0.65, 1]$ for fitness) show the range in which the minima of the different benchmark functions fall. The dotted line marks the visually estimated pseudo-optimal value $\sigma = 0.8$. Results are averaged on 250 runs and obtained using $k_{\max} = 10^4$ iterations without stopping criterion (thus with no stall condition).

Table 4.1 reports success rate, final error given by $\|\overline{y}^{\alpha,k} - x^*\|_\infty$, mean objective function value and total number of iterations, averaged over 250 runs. In addition to the classic PSO method, where the acceleration coefficients are chosen to be equal $C_1 = C_2 = 1.49$, Table 4.1 also shows the results when only the alignment towards global best is considered in PSO ($C_1 = 0$).

While CBO already manages to find the global minimizer in most of the problems considered, we note that it sometimes fails when Rastrigin, Rosenbrock or XSY random functions are optimized. CBO-ME outperforms CBO in these objective functions. Standard PSO in many cases fails to solve the problem, see e.g. Rastrigin, Salomon or XSY 4 functions. PSO success rate is also lower among all problems, with the exception of the Schwefel 2.20 benchmark problem. Considering only global adjustment seems to show advantages except in the case of Ackley where setting $C_1 = 0$ decreases the success rate or, in the case of XSY 4, Salomon or Rastrigin, where convergence is not achieved even for $C_1 = 0$. Consensus methods, however, perform better in terms of both success rate and speed up. In addition, for most problems, the population size N seems not to play a significant role in the algorithms performance. This further motivates the introduction of the random selection strategy described in the Section 4.1.1 in order to save computational costs.

In the third experiment, we test the proposed random selection mechanism (4.4) for different values of the parameter μ. We recall that with $\mu = 0$ we have no particles removal, while as μ increases, more particles are likely to be discarded when the system

		CBO ($\sigma = \sqrt{2}/2$)			CBO-ME ($\sigma = 0.8$)			PSO			PSO ($C_1 = 0$)		
		$N = 50$	$N = 100$	$N = 200$	$N = 50$	$N = 100$	$N = 200$	$N = 50$	$N = 100$	$N = 200$	$N = 50$	$N = 100$	$N = 200$
Ackley	Rate	99.8%	100.0%	100.0%	100.0%	100.0%	100.0%	17.1%	41.2%	54.3%	4.2%	16.2%	40.1%
	Error	4.22e-06	2.14e-06	3.55e-06	2.42e-06	1.89e-06	1.56e-06	6.17e-09	8.86e-11	2.01e-12	2.23e-08	1.80e-10	8.65e-13
	$\mathcal{F}$	1.18e-04	5.81e-05	7.30e-05	1.54e-04	4.96e-05	4.99e-05	6.24e-09	7.65e-11	1.94e-12	2.06e-08	1.70e-10	8.01e-13
	Iterations	912.3	718.1	623.2	977.2	703.3	622.2	501.8	424.2	341.3	502.3	421.2	321.2
Griewank	Rate	100.0%	100.0%	100.0%	100.0%	100.0%	100.0%	46.0%	48.6%	55.3%	50.0%	58.7%	78.0%
	Error	2.20e-02	2.21e-02	2.24e-02	2.13e-02	2.16e-02	2.25e-02	7.34e-02	1.56e-02	9.45e-03	1.17e-01	1.10e-01	8.96e-02
	$\mathcal{F}$	5.26e-02	5.31e-02	5.47e-02	4.95e-02	5.15e-02	5.82e-02	3.23e-03	4.11e-03	3.78-03	3.73e-03	3.71e-03	2.90e-03
	Iterations	922.1	723.3	633.2	911.2	778.3	635.4	512.2	403.1	399.2	432.1	391.2	311.2
Rastrigin	Rate	12.1%	34.3%	62.7%	23.2%	69.7%	89.1%	0.0%	0.0%	0.0%	0.0%	0.0%	0.0%
	Error	1.28e-04	1.83e-04	2.34e-04	9.73e-05	1.27e-04	1.76e-04	-	-	-	-	-	-
	$\mathcal{F}$	4.51e-06	9.03e-06	1.46e-05	2.54e-06	4.31e-06	8.28e-06	-	-	-	-	-	-
	Iterations	1083.0	933.7	819.8	1007.6	922.5	769.9	10000.0	10000.0	10000.0	10000.0	10000.0	10000.0
Rosenbrock	Rate	65.3%	86.7%	100.0%	70.1%	94.2%	100.0%	9.3%	22.6%	36.6%	46.7%	60.7%	76.7%
	Error	1.84e-02	2.43e-02	1.42e-02	3.60e-02	4.01e-02	1.82e-02	6.19e-04	2.56e-04	1.67e-04	4.44e-02	4.45e-02	4.46e-02
	$\mathcal{F}$	6.13e-03	7.57e-03	2.40e-03	1.26e-02	1.42e-02	2.65e-03	3.80e-02	3.76e-02	2.56e-02	2.56e-03	8.95e-04	3.71e-04
	Iterations	5773.2	5423.2	5233.1	5933.2	4956.2	4155.2	4822.2	3823.2	3026.3	5924.2	3834.1	2933.3
Schwefel 2.20	Rate	100.0%	100.0%	100.0%	100.0%	100.0%	100.0%	100.0%	100.0%	100.0%	100.0%	100.0%	100.0%
	Error	5.79e-06	8.23e-07	2.44e-07	8.42e-06	1.03e-06	2.76e-07	8.34e-10	1.97e-12	4.58e-14	1.68e-07	3.41e-10	8.03e-14
	$\mathcal{F}$	1.04e-03	2.15e-04	8.36e-05	1.50e-03	3.12e-04	9.37e-05	1.94e-09	6.36e-12	1.52e-13	2.44e-07	6.48e-10	2.46e-13
	Iterations	822.2	682.2	622.1	655.2	544.2	455.2	491.2	434.2	399.1	578.2	467.2	423.2
Salomon	Rate	100.0%	100.0%	100.0%	100.0%	100.0%	100.0%	0.0%	0.0%	0.0%	0.0%	0.0%	0.0%
	Error	3.12e-02	2.14e-02	1.87e-02	5.28e-02	4.49e-02	3.91e-02	-	-	-	-	-	-
	$\mathcal{F}$	3.14e-01	2.15e-01	1.88e-01	2.44e-01	1.86e-01	1.91e-01	-	-	-	-	-	-
	Iterations	10000.0	10000.0	10000.0	8872.2	9021.2	5356.5	10000.0	10000.0	10000.0	10000.0	10000.0	10000.0
XSY random	Rate	52.3%	81.7%	92.6%	100.0%	100.0%	100.0%	3.2%	17.1%	31.2%	100.0%	100.0%	100.0%
	Error	2.64e-02	1.62e-02	9.80e-03	3.06e-02	1.86e-02	1.15e-02	2.25e-01	9.56e-02	8.42e-02	6.23e-02	5.12e-02	2.34e-02
	$\mathcal{F}$	6.95e-08	3.54e-08	2.13e-08	2.21e-06	4.85e-08	3.17e-08	3.35e-04	2.28e-04	1.34e-04	8.22e-04	4.11e-04	3.45e-04
	Iterations	10000.0	10000.0	10000.0	10000.0	10000.0	10000.0	10000.0	10000.0	10000.0	10000.0	10000.0	10000.0
XSY 4	Rate	27.2%	89.3%	100.0%	25.2%	91.2%	100.0%	0.0%	0.0%	0.0%	0.0%	0.0%	0.0%
	Error	8.10e-01	7.12e-01	7.89e-01	8.01e-01	7.55e-01	6.17e-01	-	-	-	-	-	-
	$\mathcal{F}$	4.79e-07	3.78e-07	3.46e-07	1.58e-06	8.56e-07	5.43e-07	-	-	-	-	-	-
	Iterations	10000.0	10000.0	10000.0	9733.2	9531.1	8733.2	10000.0	10000.0	10000.0	10000.0	10000.0	10000.0

Table 4.1: Comparison between classical CBO, CBO-ME and standard PSO with and without alignment towards personal best on benchmark problems. The solver `particleswarm` available in the MATLAB Global Optimisation Toolbox was used for the results concerning the PSO method. Optimal choice of parameters, different for each method, are used for the CBO algorithms. Same stopping criterion and definition of success, see (4.9), were used. Performance metric considered: success rate (see (4.9)), error $\|\overline{y}^{\alpha,k} - x^*\|_\infty$, fitness value $\mathcal{F}(\overline{y}^{\alpha,k})$ and number of iterations. Results are averaged over 250 runs.

		$\mu = 0$	$\mu = 0.05$	$\mu = 0.1$	$\mu = 0.2$
Ackley	Rate	100.0%	100.0%	100.0%	100.0%
	Error	1.89e-06	2.78e-06	6.12e-06	2.29e-05
	$\mathcal{F}$	9.21e-05	5.77e-05	2.12e-04	5.12e-04
	w_{iter}	688.2	502.3	387.2	178.2
	CTS	-	31.3%	52.1 %	70.2%
Griewank	Rate	100.0%	100.0%	100.0%	100.0%
	Error	2.12e-02	2.13e-02	2.18e-02	2.21e-02
	$\mathcal{F}$	5.80e-02	5.12e-02	5.90e-02	5.21e-02
	w_{iter}	634.2	400.1	202.3	191.2
	CTS	-	31.3%	58.0%	71.6%
Schwefel 2.20	Rate	100.0%	100.0%	100.0%	100.0%
	Error	2.16e-07	8.89e-07	8.12e-07	2.34e-08
	$\mathcal{F}$	9.11e-05	3.02e-05	1.23e-05	3.22e-05
	w_{iter}	465.2	360.1	320.2	191.1
	CTS	-	24.7%	33.2%	62.1%
Salomon	Rate	100.0%	100.0%	100.0%	100.0%
	Error	4.13e-02	3.37e-02	2.77e-02	1.69e-02
	$\mathcal{F}$	4.21e-01	4.22e-01	4.10e-01	3.67e-01
	w_{iter}	2455.1	1551.1	1242.3	892.3
	CTS	-	38.2%	50.2%	66.2%
XSY random	Rate	100.0%	100.0%	100.0%	100.0%
	Error	1.54e-02	8.34e-02	8.90e-02	9.23e-02
	$\mathcal{F}$	6.34e-07	2.05e-05	6.34e-05	2.33e-04
	w_{iter}	10000.0	2821.3	1921.7	1167.2
	CTS	-	70.2%	85.3%	89.7%
XSY 4	Rate	100.0%	100.0%	100.0%	100.0%
	Error	5.37e-01	3.90e-01	1.55e-01	1.67e-01
	$\mathcal{F}$	1.19e-05	6.23e-06	3.67e-06	3.99e-06
	w_{iter}	8945.1	3967.3	1923.4	1055.7
	CTS	-	50.2%	69.3%	85.6%

Table 4.2: CBO-ME algorithm with random selection of particles tested against different benchmark functions with different values of μ, which regulates the random selection mechanism. The system is initialized with $N_0 = 200$ particles and $\sigma = 0.8$. Performance metric considered: success rate (see (4.9)), error $\|\overline{y}^{\alpha,k} - x^*\|_\infty$, fitness value $\mathcal{F}(\overline{y}^{\alpha,k})$, weighted iteration (4.10), and Computational Time Saved (CTS). Results are averaged over 250 runs.

variance decreases. The initial population is set to $N_0 = 200$, while the minimum number of particles to $N_{\min} = 10$. Results are reported in Tables 4.2 and 4.3 in terms of: success rate, error, objective value, weighted number of iterations, given by

$$w_{\text{iter}} = \sum_{k=0}^{k_{\text{end}}} \frac{N_k}{N_0}\,, \tag{4.10}$$

and percentage of Computational Time Saved (CTS). Results show that relative large values of μ allow to reach fast convergence without affecting the algorithm performance. In our experiments, the Rastrigin problem allows for larger values of μ, while the Rosenbrock one seems to be more sensitive to the selection mechanism with respect to the other objectives. This justifies the different values of μ considered in Tables 4.2 and 4.3. In both cases, a suitable value of μ reduces the computational time with almost no impact in terms of accuracy.

		$\mu = 0$	$\mu = 0.1$	$\mu = 0.2$	$\mu = 0.5$
Rastrigin	Rate	100.0%	100.0%	100.0%	100.0%
	Error	9.22e-05	7.76e-05	3.54e-05	1.34e-05
	$\mathcal{F}$	2.90e-06	2.99e-06	1.45e-06	1.12e-06
	w_{iter}	1150.3	720.6	250.5	106.3
	CTS	-	39.2%	78.9%	92.3%
		$\mu = 0$	$\mu = 0.01$	$\mu = 0.02$	$\mu = 0.05$
Rosenbrock	Rate	100.0%	100.0%	99.4%	99.0%
	Error	2.12e-02	2.21e-02	1.78e-02	1.45e-02
	$\mathcal{F}$	4.22e-03	5.67e-03	4.12e-03	4.45e-03
	w_{iter}	3189.3	840.3	350.3	102.3
	CTS	-	75.3%	90.2%	92.4%

Table 4.3: CBO-ME algorithm with particle reduction tested against Rastrigin and Rosenbrock functions with an higher diffusion parameter $\sigma = 1.1$ and for different values of μ, which regulates the random selection mechanism. The system is initialized with $N_0 = 200$ particles. Performance metric considered: success rate (see (4.9)), error ($\|\overline{y}^{\alpha,k} - x^*\|_\infty$), fitness value $\mathcal{F}(\overline{y}^{\alpha,k})$, weighted iteration (4.10), and Computational Time Saved (CTS).

Fig.s 4.2 and 4.3 show error and fitness value as a function of the number of fitness evaluations during the algorithm computation for Ackley and Rastrigin problems, respe idered mech Initial and p s. We as μ

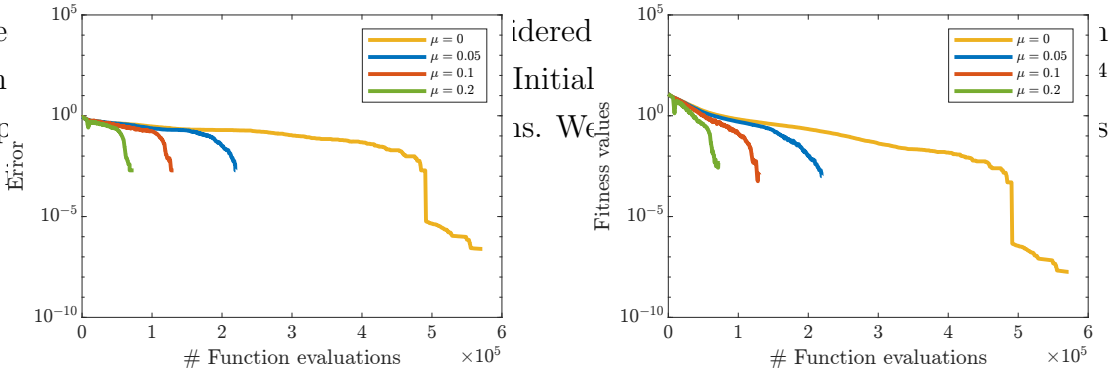

(a) Error: $\|\overline{y}^{\alpha,k} - x^*\|_\infty$ (b) Fitness value: $\mathcal{F}(\overline{y}^{\alpha,k})$

Figure 4.3: Optimization of Rastrigin function for different values of the random selection parameter μ where the initial particle population is $N_0 = 10^4$. We report error (on the left) and fitness values (on the right) as the number of function evaluations increases. Parameters are set as $\lambda = 0.01$, $\sigma = 1.1$, α adaptive starting from $\alpha_0 = 10$ and following the law $\alpha = \alpha_0 \cdot k \cdot \log_2(k)$. Results are averaged over 250 runs.

4.4 Theoretical analysis

A strength of CBO algorithms lays on the possibility of theoretically analyze the particle system by relying on a mean-field approximation of the dynamics. We will illustrate in this section how to derive such approximation and present the main theoretical result regarding the convergence of the particle system towards a solution to (1.1), in case of no selection mechanism. Next, we will study the impact of the random selection

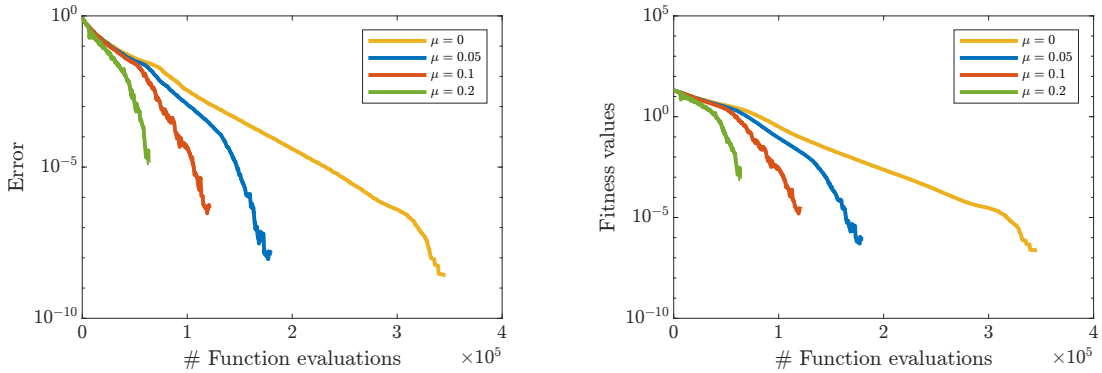

(a) Error: $\|\overline{y}^{\alpha,k} - x^*\|_\infty$ (b) Fitness value: $\mathcal{F}(\overline{y}^{\alpha,k})$

Figure 4.2: Optimization of Ackley function for different values of the random selection parameter μ, where the initial particle population is $N_0 = 10^4$. We report error (on the left) and fitness values (on the right) as the number of function evaluations increases. Parameters are set as $\lambda = 0.01$, $\sigma = 0.8$, α adaptive starting from $\alpha_0 = 10$ and following the law $\alpha = \alpha_0 \cdot k \cdot \log_2(k)$. Results are averaged over 250 runs.

strategy on the convergence properties of the algorithm. Technical details are left next section.

4.4.1 Mean-field approximation

First, we note that a simple update rule for the personal bests y_i^k is given by

$$y_i^{k+1} = y_i^k + \frac{1}{2}\left(x_i^{k+1} - y_i^k\right) S(x_i^{k+1}, y_i^k)\,, \quad \text{with} \quad S(x,y) = 1 + \operatorname{sign}\left(\mathcal{F}(y) - \mathcal{F}(x)\right)\,. \tag{4.11}$$

As in [50], we approximate it for $\beta \gg 1$ as

$$y_i^{k+1} = y_i^k + \frac{\nu}{2}\left(x_i^{k+1} - y_i^k\right) S^\beta(x_i^{k+1}, y_i^k)\,, \tag{4.12}$$

with $S^\beta(x,y)$ being a continuous approximation of $S(x,y)$ as $\beta \to \infty$. By choosing $\nu = 1$ we get (4.11) with the only difference of having S^β instead of S. As for $\overline{y}^\alpha$ with respect to $\overline{y}^\infty$, this is needed to make the update rule easier to handle mathematically, but it does have an impact on the performance for large values of β. We note that alternative ways of modeling the memory mechanisms have been suggested in the literature of PSO, see, for instance, [2] where fractional order calculus is used.

With the aim of deriving a continuous-in-time reformulation of (4.2) and (4.12), we introduce a single parameter $\Delta t > 0$ which controls the step length of all involved update mechanisms. By performing the rescaling

$$\lambda \leftarrow \lambda \Delta t\,, \quad \sigma \leftarrow \sigma\sqrt{\Delta t}\,, \quad \nu \leftarrow \nu \Delta t$$

to get the update rules

$$\begin{cases} x_i^{k+1} &= x_i^k + \lambda\Delta t \left(\overline{y}^{\alpha,k} - x_i^k\right) + \sigma\sqrt{\Delta t}\left(\overline{y}^{\alpha,k} - x_i^k\right) \otimes \vartheta_i^k \\ y_i^{k+1} &= y_i^k + (\nu\Delta t/2)\left(x_i^{k+1} - y_i^k\right) S^\beta(x_i^{k+1}, y_i^k) \end{cases} \tag{4.13}$$

which differ form the original formulation (4.2), (4.11) only due to the use of S^β instead of S.

As already noted in [50], the iterative process (4.13) corresponds to an Euler-Maruyama scheme applied to a system of Stochastic Differential Equations (SDEs). Indeed, (4.13) corresponds to a discretization of the system

$$\begin{cases} dX_t^i &= \lambda\left(\overline{y}^\alpha(\rho_t^N) - X_t^i\right)\, dt + \sigma\left(\overline{y}^\alpha(\rho_t^N) - X_t^i\right) \otimes dB_t^i \\ dY_t^i &= \nu(X_t^i - Y_t^i) S^\beta(X_t^i, Y_t^i)\, dt \end{cases} \tag{4.14}$$

where, for convenience, we underlined above the dependence of the consensus point on the empirical distribution $\rho_t^N = \sum_i \delta_{Y_t^i}$ (δ_y being the Dirac measure at $y \in \mathbb{R}^d$) by using

$$\overline{y}^\alpha(\rho) := \frac{\int y e^{-\alpha\mathcal{F}(y)} d\rho(y)}{\int e^{-\alpha\mathcal{F}(y)} d\rho(y)}, \tag{4.15}$$

defined for any Borel probability measure ρ over $\mathbb{R}^d$ ($\rho \in \mathcal{P}(\mathbb{R}^d)$). In this way, we generalized the definition introduced in (4.1) to any $\rho \in \mathcal{P}(\mathbb{R}^d)$, provided the above integrals exists. In (4.14), the random component of the dynamics is now described by N independent Wiener processes $(B_t^i)_{t>0}$. As before, we supplement the system with initial conditions $X_0^i \sim \rho_0, Y_0^i = X_0^i$ for some $\rho_0 \in \mathcal{P}(\mathbb{R}^d)$.

The continuous-in-time description (4.14) already simplifies the analytical analysis of the optimization algorithm, but still pays the price of a possible large number $\mathcal{O}(N)$ of equations. This issue is typically addressed by assuming that for large populations N, the particles become indistinguishable from one another and start behaving, in some sense, as a unique system. More precisely, let $F^N(t) \in \mathcal{P}(\mathbb{R}^{(2d)N})$ denote the joint probability distribution of N tuples (X_t^i, Y_t^i). We assume *propagation of chaos* [93] for large $N \gg 1$, that is, we assume that the joint probability distribution decomposes as $F^N(t) = f(t)^{\otimes N}$ for some $f(t) \in \mathcal{P}(\mathbb{R}^{2d})$. System (4.14) becomes independent on the index i and hence every particle moves according to the mono-particle process

$$\begin{aligned} d\overline{X}_t &= \lambda(\overline{y}^\alpha(\overline{\rho}_t) - \overline{X}_t)\, dt + \sigma\left(\overline{y}^\alpha(\overline{\rho}_t) - \overline{X}_t\right) \otimes d\overline{B}_t \\ d\overline{Y}_t &= \nu(\overline{X}_t - \overline{Y}_t) S^\beta(\overline{X}_t, \overline{Y}_t)\, dt \end{aligned} \tag{4.16}$$

where $\overline{\rho}_t = \mathrm{Law}(\overline{Y}_t)$.

Assume $(\overline{X}_t, \overline{Y}_t)$ are initially distributed according to $f_0 = \rho_0^{\otimes 2}$, by applying Itô formula we have that $f(t) = \mathrm{Law}(\overline{X}_t^i, \overline{Y}_t^i)$ satisfies

$$\partial_t f + \nabla_x \cdot (\lambda(\overline{y}^\alpha(\overline{\rho}) - x) f) + \nabla_y \cdot \big(\nu(x-y) S^\beta(x,y) f\big) = \sum_{\ell=1}^{d} \partial^2_{x_\ell} \left(\sigma(\overline{y}^\alpha(\overline{\rho}) - x)^2_\ell f\right) \quad (4.17)$$

and initial data $\lim_{t\to 0} f(t) = f_0$ in a weak sense. Dynamics (4.16), or, equivalently, (4.17), corresponds to the mean-field approximation of the particle system (4.14) as $N \to \infty$. We remark that the above derivation has only been possible thanks to the approximations $S \approx S^\beta$ and $\overline{y}^\infty \approx \overline{y}^\alpha$ for large α and β. Well-posedness of the system is also granted by such approximations, provided the objective function $\mathcal{F}$ satisfies the following assumptions (proof details are given in Appendix 4.5.2).

Assumption 4.4.1. *The objective function $\mathcal{F} : \mathbb{R}^d \to \mathbb{R}$ is bounded from below, $\inf \mathcal{F} > -\infty$, and there exist some constants $L_\mathcal{F}, c_u, c_l, R_l > 0$ such that*

$$|\mathcal{F}(x) - \mathcal{F}(x')| \le L_\mathcal{F} \left(\|x\|_2 + \|x'\|_2\right) \|x - x'\|_2 \qquad \text{for all} \quad x, x' \in \mathbb{R}^{\mathrm{d}},$$

and

$$\begin{aligned} &\mathcal{F}(x) - \inf \mathcal{F} \le c_u(1 + \|x\|_2^2) && \text{for all} \quad x \in \mathbb{R}^{\mathrm{d}}, \\ &\mathcal{F}(x) - \inf \mathcal{F} \ge c_l \|x\|_2^2 && \text{for all} \quad x \in \mathbb{R}^{\mathrm{d}} \, \|x\|_2 \ge R_l. \end{aligned}$$

Proposition 4.4.1 (Existence of solution to (4.16))**.** *Assume $\mathcal{F}$ satisfies Assumption 4.4.1. There exists a process $(\overline{X}, \overline{Y}) \in C([0,T], \mathbb{R}^{\mathrm{d}})$, $T > 0$ satisfying (4.14) with initial conditions $(\overline{X}_0, \overline{Y}_0)$ where $\overline{X}_0 \sim \rho_0 \in \mathcal{P}_4(\mathbb{R}^{\mathrm{d}})$ and $\overline{Y}_0 = \overline{X}_0$.*

Being mathematically tractable, we show next that the mean-field dynamics converges to a global solution to (1.1) if $\mathcal{F}, S^\beta$ satisfy suitable assumptions.

4.4.2 Convergence in mean-field law

We start by enunciating the necessary assumptions to the convergence result.

Assumption 4.4.2. *The objective function $\mathcal{F} \in C(\mathbb{R}^{\mathrm{d}}, \mathbb{R})$, satisfies:*

A1 *there exists uniquely $x^* \in \mathbb{R}^{\mathrm{d}}$ solution to (1.1);*

A2 *there exist $\eta, R_0 > 0$ and $\gamma \in (0, \infty)$ such that*

$$\begin{aligned} &\mathcal{F}(x) - \inf \mathcal{F} \ge \eta \|x - x^*\|_\infty^\gamma && \forall x \in \mathbb{R}^{\mathrm{d}}, \, \|x - x^*\|_\infty \le R_0 \\ &\mathcal{F}(x) - \inf \mathcal{F} \ge \eta R_0^\gamma && \forall x \in \mathbb{R}^{\mathrm{d}}, \, \|x - x^*\|_\infty > R_0 \, . \end{aligned}$$

A3 $\mathcal{F}$ *is convex in a (possibly small) neighborhood* $\{x \in \mathbb{R}^{\mathrm{d}} : \|x - x^*\|_\infty \leq R_1\}$ *of* x^* *for some* $R_1 < R_0$.

Assumption 4.4.3 (Assumptions on S^β)**.** *The function* $S^\beta \in C(\mathbb{R}^{2\mathrm{d}}, [0,2])$*, with* $\beta > 0$

A4 *has the following structure*

$$S^\beta(x,y) = 2\psi\left(\beta(\mathcal{F}(y) - \mathcal{F}(x))\right), \tag{4.18}$$

with $\psi \in C^1(\mathbb{R}, [0,1])$ *being a non-decreasing function with Lipschitz constant* $L_\psi = 1$.

A5 *The value* $S^\beta(x,y)$ *is positive only when* x *is strictly better than* y *in terms of objective value* $\mathcal{F}$*:*

$$S^\beta(x,y) \begin{cases} \geq 0 & \text{if} \quad \mathcal{F}(x) < \mathcal{F}(y) \\ = 0 & \text{else}\,. \end{cases}$$

Assuming uniqueness of global minimum is a typical assumption for analysis of CBO methods [42, 43] and it is due to the definition of the consensus point $\overline{y}^\alpha$ (or $\overline{x}^\alpha$ in the case without memory mechanism). Indeed, in presence of two global minima, $\overline{y}^\alpha$ may be placed between them, no matter how large α is. Assumption A1 ensure to avoid such situations. Furthermore, A2 also allows to give quantitative estimates on the difference between the global minimum and eventual local minima. In the literature, such property is known as *conditioning* [46]. Requirements A3 and A5 will be needed to ensure that if a personal best y_i^k enters such small neighborhood where $\mathcal{F}$ is convex, it will not leave it for the rest of the computation. For an intuition of A2 and A3 we refer to Figure 4.4, where the Rastrigin function is considered.

Theorem 4.1 (Convergence in mean-field law)**.** *Assume* $\mathcal{F}$ *satisfies Assumption 4.4.2 and* S^β *satisfies Assumption 4.4.3 for some* $\beta > 0$ *fixed. Let* $(\overline{X}_t, \overline{Y}_t)_{t\geq 0}$ *be a solution to (4.16) for* $t \in [0, T^*]$*, with initial data* $\overline{X}_0 \sim \rho_0 \in \mathcal{P}_4(\mathbb{R}^{\mathrm{d}}), \overline{Y}_0 = \overline{X}_0$ *such that* $x^* \in \mathrm{supp}(\rho_0)$.

Fix an accuracy $\varepsilon > 0$*. If* $2\lambda > \sigma^2$*, the expected* ℓ_2*-error satisfies*

$$\min_{t\in[0,T^*]} \mathbb{E}\left[\|\overline{X}_t - x^*\|_2^2\right] \leq \varepsilon \tag{4.19}$$

provided $T^*, \alpha > 0$ *are large enough.*

We refer to Appendix for a proof.

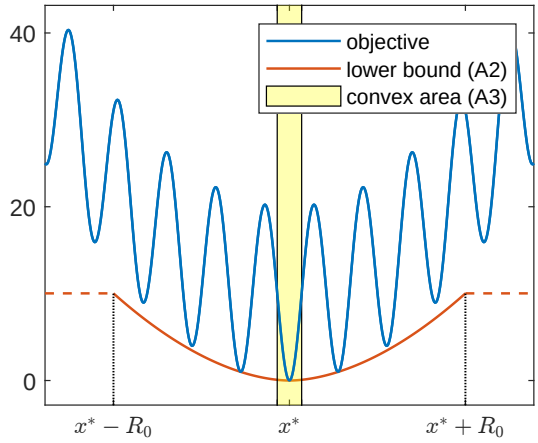

Figure 4.4: Assumptions 4.4.2 illustrated for Rastrigin function. For example, such objective function satisfies A2 with $\eta = 1$, $\gamma = 1.8$, $R_0 = 1.42$ and A3 with $R_1 = 0.25$.

Remark 4. *The mean-field mono-particle process (4.16) aims to approximate the algorithm iterative dynamics (4.13) for small time steps $\Delta t \ll 1$ and large particle populations $N \gg 1$. Therefore, convergence of the algorithm dynamics towards the global solution x^* can be proven by coupling Theorem 4.1 with error estimates of such approximation.*

For instance, assuming that all considered dynamics take place on a bounded set $\mathcal{D}$ ensures that the error introduced by the continuous-in-time approximation will be of order Δt thanks to classical results on Euler-Maruyama schemes [84]. Likewise, considering a bounded dynamics allows to prove that the error introduced by the mean-field approximation is of order N^{-1} (see e.g. [39, Theorem 3.1], [42, Proposition 16]). If such error rate holds, consider $\{(x_i^k, y_i^k)\}_{i=1}^N$ be given by (4.13), $\{(X_t^i, Y_t^i)\}_{i=1}^N$ be a solution (4.14) and $\{(\overline{X}_t^i, \overline{Y}_t^i)\}_{i=1}^N$ be N-copies of a solution to (4.16). Let $t^* \in [0, T^*]$ being a time minimizing the mean-field error in (4.19). Altogether, one obtains the following error decomposition for $k = \lfloor t^*/\Delta t \rfloor$,

$$\begin{aligned}\mathbb{E}\left[\frac{1}{N}\sum_{i=1}^N \|x_i^k - x^*\|_2^2\right] &\leq C\left(\mathbb{E}\left[\frac{1}{N}\sum_{i=1}^N \|x_i^k - X_{t^*}^i\|_2^2\right] + \mathbb{E}\left[\frac{1}{N}\sum_{i=1}^N \|X_{t^*}^i - \overline{X}_{t^*}^i\|_2^2\right]\right. \\ &\qquad \left. + \mathbb{E}\left[\frac{1}{N}\sum_{i=1}^N \|\overline{X}_{t^*}^i - x^*\|_2^2\right]\right) \\ &\leq C_{\mathrm{EM}}\Delta t + C_{\mathrm{MFA}}N^{-1} + \varepsilon\end{aligned}$$

where $C, C_{\mathrm{EM}}, C_{\mathrm{MFA}}$ are positive constant independent on $N, \Delta t$.

4.4.3 Random selection analysis

In this section, we analytically investigate the impact of randomly discarding particles during the computation. We are particularly interested in tracking the distance between a particle system $\{x_i^k, x_j^k\}_{i=1}^{N_0}$ evolving according to (4.13) where no particles are discarded, and a second system $\{\widehat{x}_i^k, \widehat{y}_i^k\}_{I_k}, |I_k| = N_k$ where $N_k - N_{k+1}$ particles are discarded after update rule (4.13). Clearly, we have that $N_{k+1} \leq N_k$ and $I_{k+1} \subseteq I_k \subseteq I_0 = \{1, \dots, N_0\}$ for all k. Similarly to the analysis carried out in [51, 52], we restrict to the simpler dynamics where, at every step k, the random variables ϑ_i^k and $\widehat{\vartheta}_i^k$ used to generate such systems are the same for all particles:

$$\vartheta_i^k = \widehat{\vartheta}_j^k = \vartheta^k \sim \mathcal{N}(0, \mathbf{I}_d) \quad \text{for all} \quad i \in I_k,\, j \in I_0. \tag{4.20}$$

To compare particle systems with a different number of particles, we rely on their representation as empirical probability measures and the notion of 2-Wasserstein distance. For $\{\widehat{x}_i^k\}_{i\in I_k}$ and $\{x_i^k\}_{i=1}^{N_0}$ we consider, respectively, the following probability measures

$$\rho_{N_k}^k := \frac{1}{N_k} \sum_{i\in I_k} \delta_{\widehat{x}_i^k} \quad \text{and} \quad \rho_{N_0}^k := \frac{1}{N_0} \sum_{i\in I_0} \delta_{x_i^k}. \tag{4.21}$$

Informally, the 2-Wasserstein distance $W_2(\rho_{N_k}^k, \rho_{N_0}^k)$ quantifies the minimal effort needed to move the mass from distribution $\rho_{N_k}^k$ into $\rho_{N_0}^k$ (or *vice versa*) [88]. Let w_{ij} denote the amount of mass leaving particle x_i^k and going into $\widehat{x}_i^k$: the cost of such movement is assumed to be given by $w_{ij}\|x_i^k - \widehat{x}_j^k\|_2^2$. Therefore, if we indicate the set of all admissible couplings between the two discrete probability measures as

$$\Gamma(\rho_{N_k}^k, \rho_{N_0}^k) = \left\{ w \in \mathbb{R}^{N_0 \times N_k} \,:\, \sum_{j=1}^{N_k} w_{ij} = \frac{1}{N_0},\, \sum_{i=1}^{N_0} w_{ij} = \frac{1}{N_k},\, w_{ij} \geq 0,\, \forall\, i, j \right\}, \tag{4.22}$$

the 2- Wasserstein distance is defined as

$$W_2(\rho_{N_k}^k, \rho_{N_0}^k) := \min_{w\in\Gamma(\rho_{N_k}^k, \rho_{N_0}^k)} \left(\sum_{i,j} w_{ij} \|x_i^k - \widehat{x}_j^k\|_2^2 \right)^{\frac{1}{2}} \tag{4.23}$$

see, for instance, [88, Section 6.4.1].

Before providing estimates on (4.22), let us present a more general result on the impact that the random selection strategy has on an arbitrary particle distribution.

Proposition 4.4.2 (Stability of random selection procedure). *Let $\mathbf{z} = \{z_i\}_{i\in I}, |I| = N$ be an ensemble of particles and $\{z_i\}_{j\in I_{\text{sel}}}$ with $I_{\text{sel}} \subseteq I, |I| = N_{\text{sel}}$ a random sub-set of such ensemble. Consider the associated empirical distributions μ_N and $\mu_{N_{\text{sel}}}$ (defined*

consistently to (4.21)), it holds

$$\mathbb{E}\left[W_2^2(\mu_N, \mu_{N_{\text{sel}}})\right] \leq 2\,\text{var}(\mathbf{z})\,\frac{N - N_{\text{sel}}}{N-1} \tag{4.24}$$

where the expectation is taken with respect to the random selection of I_{sel}.

We note how the system variance $\text{var}(\mathbf{z})$ enters the error estimate due to the randomness of the selection, similar to the Law of Large Number error for random variables. In particular, the smaller the particles variance is, the closer the reduced particle system will be to the original distribution. This justifies the choice of N_{k+1} proposed in Section 4.1.2 where we are allowed to discard particles only if the system shows a contractive behavior, see (4.4).

By iteratively applying Proposition 4.4.2 and by using suitable stability estimates of dynamics (4.13), we are able to bound the error introduced by the random selection procedure as follows.

Theorem 4.2. *Let* $\{x_i^k, y_i^k\}_{i=1}^{N_0}$ *be constructed according to (4.13) where particles are not discarded, and* $\{\widehat{x}_i^k, \widehat{y}_i^k\}_{I_k}, |I_k| = N_k$ *where* $N_k - N_{k+1}$ *particles are discarded after update rule (4.13). Assume (4.20) is satisfied and consider the probability measures (4.21). If* $\{x_i^k, y_i^k\}_{i=1}^{N_0}, \{\widehat{x}_i^k, \widehat{y}_i^k\}_{i\in I_k} \subset B_M(0)$ *at all step* k *for some* $M > 0$, *it holds*

$$\mathbb{E}\left[W_2^2\left(\rho_{N_k}^k, \rho_{N_0}^k\right)\right] \leq C \max_{h=1,\dots,k} \text{var}\left(\widetilde{\mathbf{z}}^h\right)\,\frac{N_0 - N_k}{N_k - 1} \tag{4.25}$$

where $C = C(\Delta t, \lambda, \sigma, \nu, \beta, \alpha, k, L_{\mathcal{F}}, M)$ *and* $\widetilde{\mathbf{z}}^h = \{(\widehat{x}_i^h, \widehat{y}_i^h)\}_{i\in I_{h-1}}$ *describes the particle system just before the random selection procedure at step* $h \leq k$. *The expectation is taken with respect to the sampling of* $\{\vartheta^h\}_{h=1}^k$ *and with respect to the selection procedure.*

We can directly apply the above result to relate the expected ℓ_2-errors of the two particle system, which we define as

$$\text{Err}(k) = \mathbb{E}\left[\frac{1}{N_0}\sum_{i\in I_0}\|x_i^k - x^*\|_2^2\right], \quad \text{Err}(k) = \mathbb{E}\left[\frac{1}{N_k}\sum_{i\in I_k}\|\widehat{x}_i^k - x^*\|_2^2\right],$$

that is, the discrete counterpart of the mean-field error $\mathbb{E}[\|\overline{X}_t^i - x^*\|_2^2]$ studied in Theorem 4.1. By definition of the Wasserstein-2 distance, we have

$$\text{Err}(k) = \mathbb{E}\left[W_2^2(\rho_{N_0}^k, \delta_{x^*})\right]$$

for any solution x^* to (1.1), and the same holds of $\mathrm{Err}_{\mathrm{sel}}(k)$. We then apply inequality

$$W_2^2(\rho^k_{N_k}, \delta_{x^*}) \leq 2\left(W_2^2(\rho^k_{N_k}, \rho^k_{N_0}) + W_2^2(\rho^k_{N_0}, \delta_{x^*})\right)$$

to obtain the following estimate.

Corollary 4.3. *Under the assumptions of Theorem 4.2, at all steps k, it holds*

$$\mathrm{Err}_{\mathrm{sel}}(k) \leq 2\left(\mathrm{Err}(k) + C \max_{h=1,\dots,k} \mathrm{var}(\widetilde{\mathbf{z}}^h)\, \frac{N_0 - N_k}{N_k - 1}\right). \tag{4.26}$$

Remark 5.

- *Proof of Theorem 4.2 can be adapted to any other particle system with random selection, provided that the update rule is stable with respect to the 2-Wasserstein distance. In the proposed method, such stability was proved thanks to the approximation of the global best $\overline{y}^{\infty,k}$ with $\overline{y}^{\alpha,k}$ for $\alpha \gg 1$ (see (4.1)) and $S(x,y)$ with $S^\beta(x,y)$ for $\beta \gg 1$ in the personal best update (4.12).*

- *Quantitative estimates on the variance decay can be used, if available, to improve the error bound in Theorem 4.2.*

- *The error introduced by a sub-sampling technique in a Monte Carlo integral approximation is expected to be of order*

$$2\,\mathrm{var}(\mathbf{z})\left(\frac{1}{N-1} - \frac{1}{N_{\mathrm{sel}}-1}\right) = 2\,\mathrm{var}(\mathbf{z})\,\frac{N - N_{\mathrm{sel}}}{(N-1)(N_{\mathrm{sel}}-1)}, \tag{4.27}$$

  see e.g. [64]. Therefore, an additional factor of order $1/(N_{\mathrm{sel}}-1)$ seems to be missing in Proposition 4.4.2. We remark, though, that Proposition 4.4.2 does not concern the Monte Carlo approximation of an integral quantity, but rather consider the 2-Wasserstein distance between discrete measures. Numerical simulations suggest that estimates of order (4.27) do not hold on in this case, see Fig.4.5.

4.5 Proofs

4.5.1 Notation and auxiliary lemmas

We will use the following notation. For any $a \in \mathbb{R}$, $|a|$ indicates the absolute value. For a given vector $b \in \mathbb{R}^d$, $\|b\|_p$ indicates its p-norm, $p \in [1,\infty]$; $(b)_\ell$ its ℓ-th component; while $\mathrm{diag}(b) \in \mathbb{R}^{d\times d}$ is the diagonal matrix with elements of b on the main diagonal.

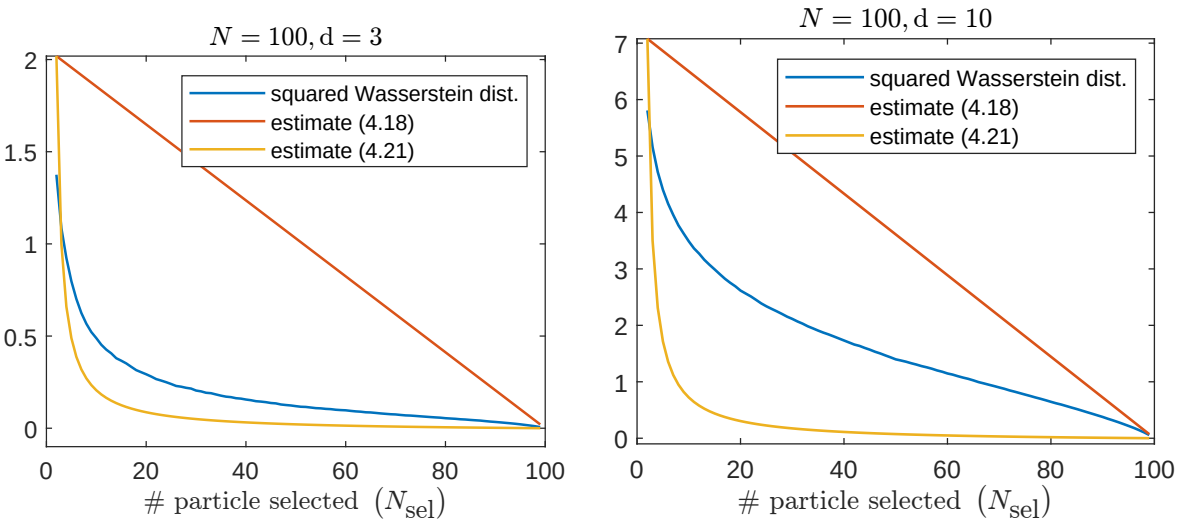

Figure 4.5: Numerical validation of Proposition 4.4.2 with different dimensions $\mathrm{d} = 3, 10$. $N = 100$ points are randomly, uniformly sampled over $[0,1]^{\mathrm{d}}$ to construct the empirical distribution μ_N and $N_{\mathrm{sel}} \in [2, N-1]$ are discarded to obtain $\mu_{N_{\mathrm{sel}}}$. The experiment is repeated 500 times for all N_{sel} to obtain an approximation of $\mathbb{E}\left[W_2^2(\mu_N, \mu_{N_{\mathrm{sel}}})\right]$ (blue line). In red, estimate provided by Proposition 4.4.2 (RHS of (4.24)), in yellow the one given equation (4.27). Wasserstein distances are computed with the `ot.emd` function provided by the Python Optimal Transport library [37].

Let $a, b \in \mathbb{R}^d$, $\langle a, b\rangle$ denotes the scalar product in $\mathbb{R}^d$. For a given closed convex set $A \subset \mathbb{R}^d$, $\mathcal{N}(A, x), \mathcal{T}(A, x)$ denote the Clarke normal and the tangential cone at $x \in A$ respectively. The ℓ^p-ball, $p \in [1, \infty]$, of radius r centered at $x \in \mathbb{R}^d$ is indicated with $B_r^p(x) = \{x \in \mathbb{R}^d \,|\, \|x\|_p \leq r\}$. All considered stochastic processes are assumed to take their realizations over the common probability space $(\Omega, \overline{\mathcal{F}}, \mathbb{P})$. $\mathcal{P}(\mathbb{R}^d)$ is the set of Borel probability measures over $\mathbb{R}^d$ and $\mathcal{P}_q(\mathbb{R}^d) = \{\mu \in \mathcal{P}(\mathbb{R}^d) \,|\, \int \|x\|_2^q d\mu < \infty\}$ which we equip with the Wasserstein distance W_q, $q \geq 1$, see [88]. For a random variable X, $X \sim \mu$, $\mu \in \mathcal{P}(\mathbb{R}^d)$ indicates a sampling procedure such that $\mathbb{P}(X \in A) = \mu(A)$ for any Borel set $A \subset \mathbb{R}^d$. With $\mathrm{Unif}(A) \in \mathcal{P}(\mathbb{R}^d)$ we denote the uniform probability measure over a bounded Borel set A. Throughout the computations, C will denote an arbitrary positive constant, whose value may vary from line to line. Dependence on relevant parameters or variables, will be underlined.

Lemma 4.4 ([20, Lemma 3.2])**.** *Let $\mathcal{F}$ satisfy Assumption 4.4.1 and $\rho_1, \rho_2 \in \mathcal{P}_4(\mathbb{R}^d)$ with*

$$\int \|x\|_2^4 \, d\rho_1 \,, \quad \int \|x\|_2^4 \, d\rho_2 \leq M \,.$$

Then, the following stability estimate holds

$$\|\overline{y}^\alpha(\rho_1) - \overline{y}^\alpha(\rho_2)\|_2 \leq C \, W_2(\rho_1, \rho_2)$$

for a constant $C = C(\alpha, L_{\mathcal{F}}, M)$.

Lemma 4.5. *Under Assumptions 4.4.1 and 4.4.3, for any* $x_1, x_2, y_1, y_2 \in B_M^2(0)$, *it holds*

$$\|(x_1 - y_1)S^\beta(x_1, y_1) - (x_2 - y_2)S^\beta(x_2, y_2)\|_2 \leq C\ (\|x_1 - y_1\|_2 + \|x_2 - y_2\|_2)$$

where $C = C(\beta, L_{\mathcal{F}}, M)$.

Proof. We note that function S^β is locally Lipschitz continuous thanks to the locally Lipschitz continuity of $\mathcal{F}$ (Assumption 4.4.1) and the Lipschitz continuity of ψ (Assumption 4.4.3):

$$\begin{aligned}
|S^\beta(x_1, y_1) - S^\beta(x_2, y_2)| &= |2\psi\left(\beta(\mathcal{F}(y_1) - \mathcal{F}(x_1)\right) - 2\psi(\beta(\mathcal{F}(y_2) - \mathcal{F}(x_2))\,| \\
&\leq 2\beta\,|\mathcal{F}(y_1) - \mathcal{F}(x_1) - \mathcal{F}(y_2) + \mathcal{F}(x_2)| \\
&\leq 4\beta L_{\mathcal{F}} M\,(\|x_1 - x_2\|_2 + \|y_1 - y_2\|_2)\ .
\end{aligned}$$

Next, we have

$$\begin{aligned}
&\|(x_1 - y_1)S^\beta(x_1,y_1) - (x_2 - y_2)S^\beta(x_2, y_2)\|_2 \\
&\qquad \leq \|(x_1 - y_1)S^\beta(x_1, y_1) - (x_2 - y_2)S^\beta(x_1, y_1)\|_2 \\
&\qquad\quad + \|(x_2 - y_2)S^\beta(x_1, y_1) - (x_2 - y_2)S^\beta(x_2, y_2)\|_2 \\
&\qquad \leq \|(x_1 - x_2 + y_2 - y_1)S^\beta(x_1, y_1)\|_2 + \|(x_2 - y_2)\left(S^\beta(x_1, y_1) - S^\beta(x_2, y_2)\right)\|_2 \\
&\qquad \leq 2\,(\|x_1 - x_2\|_2 + \|y_1 - y_2\|_2) + 2M|S^\beta(x_1, y_1) - S^\beta(x_2, y_2)| \\
&\qquad \leq C\,(\|x_1 - x_2\|_2 + \|y_1 - y_2\|_2)
\end{aligned}$$

with $C = C(\beta, L_{\mathcal{F}}, M)$, where we used the proved locally Lipischitz continuity of S^β in the last inequality. □

4.5.2 Proof of Proposition 4.4.1

Proof of Proposition 4.4.1. The proof is based on the Leray–Schauder fixed point theorem [47, Chapter 11], and we follow the proof of [20, Theorem 3.2].

Step 1. For any $\xi \in C([0, T], \mathbb{R}^{\mathrm{d}})$ there exists a unique process $(\widehat{X}_t, \widehat{Y}_t) \in C([0, T], \mathbb{R}^d)$ satisfying

$$\begin{aligned}
d\widehat{X}_t &= \lambda(\xi(t) - \widehat{X}_t)\,dt + \sigma(\xi(t) - \widehat{X}_t) \otimes d\widehat{B}_t \\
d\widehat{Y}_t &= \nu(\widehat{X}_t - \widehat{Y}_t)S^\beta(\widehat{X}_t, \widehat{Y}_t)\,dt
\end{aligned}$$

with $\mathrm{Law}(\widehat{X}_0) = \mathrm{Law}(\widehat{Y}_0) = \rho_0 \in \mathcal{P}(\mathbb{R}^d)$, by locally Lipschitz continuity and linear growth of the coefficients (thanks to Lemma 4.5). As a consequence, we also have that $f(t) := \mathrm{Law}(\widehat{X}_t, \widehat{Y}_t)$ satisfies

$$\frac{d}{dt}\int \varphi\, df(t) = \int \left(-\lambda\langle \nabla_x \varphi, \xi(t) - x\rangle + \frac{1}{2}\sigma \sum_{\ell=1}^{\mathrm{d}} \frac{\partial^2 \varphi}{\partial x_\ell^2}(\xi(t) - y)_\ell^2 - \nu S^\beta \langle \nabla_y \varphi, y - x\rangle \right) df(t)$$

for all $\varphi \in C_b^2(\mathbb{R}^{2d})$ by applying Itô's formula. Therefore, let $\overline{\rho}(t) = \mathrm{Law}(\widehat{Y}_t)$, we can set $\mathcal{T}\xi := \overline{y}^\alpha(\overline{\rho}(\cdot)) \in C([0,T],\mathbb{R}^d)$ to define

$$\mathcal{T} : C([0,T],\mathbb{R}^d) \to C([0,T],\mathbb{R}^d).$$

Step 2. We prove now compactness of $\mathcal{T}$. Thanks to $\rho_0 \in \mathcal{P}_4(\mathbb{R}^d)$ and standard results for SDEs (see [5, Chapter 7]) we have boundedness of the forth moments

$$\mathbb{E}\left[\|\widehat{X}_t\|_2^4 + \|\widehat{Y}_t\|_2^4\right] \leq c_1 \left(1 + \mathbb{E}[\|\widehat{X}_0\|_2^4 + \|\widehat{Y}_0\|_2^4] e^{c_2 t}\right)$$

for some $c_1, c_2 > 0$. Therefore, we can apply Lemma 4.4 to obtain for any $0 < s < t < T$,

$$\|\overline{y}^\alpha(\overline{\rho}(t)) - \overline{y}^\alpha(\overline{\rho}(s))\|_2 \leq C W_2\left(\overline{\rho}(t), \overline{\rho}(s)\right) \leq \widetilde{C}|t-s|^{1/2}$$

for some constants $C, \widetilde{C} > 0$, from which Hölder continuity of $t \mapsto \overline{y}^\alpha(\overline{\rho}(t))$ follows. Compactness of $\mathcal{T}$ follows by

$$\mathcal{T}(C([0,T],\mathbb{R}^d)) \subset C^{0,\frac{1}{2}}([0,T],\mathbb{R}^d) \hookrightarrow C([0,T],\mathbb{R}^d)\,.$$

Step 3. Consider $\xi \in C([0,T],\mathbb{R}^d)$ satisfying $\xi = \tau\mathcal{T}\xi$, for $\tau \in [0,1]$. Thanks to [20, Lemma 3.3] and boundedness of second moments, we obtain compactness of the set

$$\{\xi \in C([0,T],\mathbb{R}^d) \,:\, \xi = \tau\mathcal{T}\xi, \tau \in [0,1]\}$$

and by Leray–Schauder fixed point theorem there exists a fixed point for the mapping $\mathcal{T}$ and hence a solution to (4.16).

□

4.5.3 Proof of Theorem 4.1

Having proved there exists a solution $(\overline{X}_t, \overline{Y}_t)_{t\in[0,T]}$ to the mean-field process (4.16) we are here interested in studying the expected ℓ_2-error given by

$$\mathbb{E}\|\overline{X}_t - x^*\|_2^2$$

where x^* is the unique solution to the minimization problem (1.1) (uniqueness is given by Assumption 4.4.2). We do so by means of the following quantitative version of the Laplace principle.

Proposition 4.5.1 (Quantitative Laplace principle [43, Proposition 1])**.** *Let $\rho \in \mathcal{P}(\mathbb{R}^d)$ be such that $x^* \in \mathrm{supp}(\rho)$ and fix $\alpha > 0$. For any $r > 0$, define $\mathcal{F}_r := \sup_{x\in B_r^\infty(x^*)} \mathcal{F}(x) - \mathcal{F}(x^*)$.*

Then, under Assumption 4.4.2, for any $r \in (0, R_0]$ and $q > 0$ such that $q + \mathcal{F}_r \leq \mathcal{F}_\infty := \eta R_0^\gamma$, it holds

$$\|\overline{y}^\alpha(\rho) - x^*\|_2 \leq \frac{\sqrt{d}(q+\mathcal{F}_r)^\gamma}{\eta} + \frac{\sqrt{d}\exp(-\alpha q)}{\rho(B_r^\infty(x^*))}\int \|x - x^*\|_2 \, d\rho(x). \tag{4.28}$$

We remark that RHS of (4.28) can be made arbitrary small by taking large values of α and small values of q, r provided the integral is bounded.

Lemma 4.6. *Let $(\overline{X}_t, \overline{Y}_t)_{t\in[0,T]}$ be a solution to (4.16) and initial data $\overline{X}_0 = \overline{Y}_0$ and $x^* \in \mathbb{R}^d$. For any $t \in [0,T]$, it holds*

$$\mathbb{E}[\|\overline{Y}_t - x^*\|_2^2] \leq 2e^{\nu t} \sup_{s\in[0,t]} \mathbb{E}[\|\overline{X}_s - x^*\|_2^2]\,. \tag{4.29}$$

Proof. Due to (4.16) and chain rule, it holds

$$\begin{aligned}
\frac{d}{dt}\|\overline{Y}_t - x^*\|_2^2 &= 2\nu\langle \overline{Y}_t - x^*, \overline{X}_t - \overline{Y}_t\rangle S^\beta(\overline{X}_t, \overline{Y}_t)dt \\
&= 2\nu\langle \overline{Y}_t - x^*, \overline{X}_t - x^*\rangle S^\beta(\overline{X}_t, \overline{Y}_t)dt - 2\nu\|\overline{Y}_t - x^*\|_2^2 S^\beta(\overline{X}_t, \overline{Y}_t)dt \\
&\leq \nu\left(\|\overline{Y}_t - x^*\|_2^2 + \|\overline{X}_t - x^*\|_2^2\right)dt
\end{aligned}$$

By taking the expectation and applying Grönwall's inequality, we have

$$\mathbb{E}[\|\overline{Y}_t - x^*\|_2^2] \leq \mathbb{E}[\|\overline{Y}_0 - x^*\|_2^2]e^{\nu t} + \int_0^t \mathbb{E}[\|\overline{X}_s - x^*\|_2^2]e^{\nu(t-s)}ds\,.$$

Estimate (4.29) can be obtained after noting that $\mathbb{E}[\|\overline{Y}_0 - x^*\|_2^2] = \mathbb{E}[\|\overline{X}_0 - x^*\|_2^2]$ due to choice of the initial data, and by taking the supremum over all times $s \in [0,t]$. □

To apply Proposition 4.5.1 to all $\overline{\rho}(t) = \mathrm{Law}(\overline{Y}_t)$, we need though to provide lower bounds on $\overline{\rho}(t)(B_r^\infty(x^*))$ for any small radius r and times $t \in [0,T]$.

Lemma 4.7. *Let $\overline{\rho}(t) = \mathrm{Law}(\overline{Y}_t)$, with $\overline{Y}_t$ evolving according to (4.16) and $\lim_{t\to 0}\overline{\rho}(t) = \rho_0$ with $x^* \in \mathrm{supp}(\rho_0)$. Under Assumptions 4.4.2 and 4.4.3 , it holds $\overline{\rho}(t)(B_r^\infty(x^*)) \geq m_r > 0$, for all $t \in [0,T]$ and for all $r \leq R_0$.*

Proof. Let $\delta = \eta \min\{R_1, r\}^\gamma$, we start by proving that the mass in the set

$$L_\delta = \{x \in \mathbb{R}^{\mathrm{d}} \mid \mathcal{F}(x) \leq \inf \mathcal{F} + \delta\}$$

is non-decreasing. We note that for this choice of δ, L_δ is convex due to Assumption 4.4.2. Consider now $(\Omega, \overline{\mathcal{F}}, \mathbb{P})$ to be the common probability space over which the considered processes take their realization and define $\Omega_\delta = \{\omega : \overline{Y}_0(\omega) \in L_\delta\}$. By Assumption 4.4.3, $S^\beta(\overline{X}_t(\omega), \overline{Y}_t(\omega)) = 0$ whenever $\overline{X}_t(\omega) \notin L_\delta$. Therefore, it holds

$$\left\langle (\overline{X}_t(\omega) - \overline{Y}_t(\omega)) S^\beta(\overline{X}_t(\omega), \overline{Y}_t(\omega)) \, , \, n(\overline{Y}_t(\omega)) \right\rangle \begin{cases} = 0 & \text{if } \overline{X}_t(\omega) \notin L_\delta \\ \leq 0 & \text{if } \overline{X}_t(\omega) \in L_\delta \end{cases} \quad \text{for} \quad \overline{Y}_t(\omega) \in \partial L_\delta$$

for any $n(\overline{Y}_t(\omega)) \in \mathcal{N}(L_\delta, x)$ from which follows that $\overline{Y}_t(\omega)$ solves

$$\overline{Y}_t(\omega) = \overline{Y}_0(\omega) + \int_0^t \Pi_{\mathcal{T}(L_\delta, \overline{Y}_s(\omega))} \left((\overline{X}_s(\omega) - \overline{Y}_s(\omega)) S^\beta(\overline{X}_s(\omega), \overline{Y}_s(\omega)) \right) ds$$

for all $\omega \in \Omega_\delta$. As a consequence, if $\overline{Y}_0(\omega) \in L_\delta$, $\overline{Y}_t(\omega) \in L_\delta$ for all $t \geq 0$ and so

$$\overline{\rho}(t)(B_r^\infty(x^*)) = \mathbb{P}(\overline{Y}_t \in L_\delta) \geq \mathbb{P}(\overline{Y}_0 \in L_\delta) =: m_r$$

for all $t \geq 0$. We conclude by noting that $m_r > 0$ since $x^* \in \mathrm{supp}(\rho_0)$. □

Next, we study the evolution of the error $\mathbb{E}\|\overline{X}_t - x^*\|_2^2$ and, in particular, we try to bound it in terms of $\|\overline{y}^\alpha(\overline{\rho}(s)) - x^*\|_2$ and $\mathbb{E}\|\overline{X}_t - x^*\|_2$ itself for $s \in [0,t]$.

Proposition 4.5.2. *[43, Lemma 1] Let $(\overline{X}_t, \overline{Y}_t) \in C([0,T], \mathbb{R}^{2\mathrm{d}})$ satisfy (4.16) with initial datum $\overline{X}_0 \sim \rho_0, \rho_0 \in \mathcal{P}_4(\mathbb{R}^{\mathrm{d}}), \overline{Y}_0 = \overline{X}_0$ for some time horizon $T > 0$.*

Set $\mathcal{V}(\rho(t)) := (1/2)\mathbb{E}\|\overline{X}_t - x^*\|_2^2$ with $\rho(t) \in \mathrm{Law}(\overline{X}_t)$. For all $t \in [0,T]$, it holds

$$\frac{d}{dt}\mathcal{V}(\rho(t)) \leq -(2\lambda-\sigma^2)\mathcal{V}(\rho(t)) + \sqrt{2}(\lambda+\sigma^2)\sqrt{\mathcal{V}(\rho(t))}\,\|\overline{y}^\alpha(\overline{\rho}(t)) - x^*\|_2 + \frac{\sigma^2}{2}\|\overline{y}^\alpha(\overline{\rho}(t)) - x^*\|_2^2\,. \quad (4.30)$$

where $\overline{\rho}(t) = \mathrm{Law}(\overline{Y}_t)$.

Proof of Theorem 4.1. The above result, together with Lemma 4.7, leads to the convergence in mean-field law of the dynamics towards the solution to (1.1). The proof can be carried out exactly as in [43, Theorem 12] and we summarize here the main steps for completeness.

For notational simplicity, we introduce $\mathrm{Err}(t) := \mathbb{E}[\|\overline{X}_t - x^*\|_2^2]$. We start by setting the time horizon $T^* = -2\log(\varepsilon/\mathrm{Err}(0))/(2\lambda-\sigma^2)$. We apply Proposition 4.5.2 and, since $\mathcal{V}(\rho(t)) = \mathrm{Err}(t)/2$, we have for all $t \in [0, T^*]$

$$\frac{d}{dt}\mathrm{Err}(t) \leq -(2\lambda-\sigma^2)\mathrm{Err}(t) + (\lambda+\sigma^2)\sqrt{\mathrm{Err}(t)}\|\overline{y}^\alpha(\overline{\rho}(t)) - x^*\|_2 + \sigma^2\|\overline{y}^\alpha(\overline{\rho}(t)) - x^*\|_2^2\,.$$

Let $T \geq 0$ be given by

$$T := \sup\left\{t \in [0,T^*] \,:\, \mathrm{Err}(t') > \varepsilon \text{ and } \|\overline{y}^\alpha(\overline{\rho}(t')) - x^*\|_2^2 < C(t') \quad \forall t' \in [0,t]\right\}$$

with

$$C(t) := \min\left\{\frac{1}{4}\frac{2\lambda-\sigma^2}{\lambda+\sigma^2}\,,\, \sqrt{\frac{1}{4}\frac{2\lambda-\sigma^2}{\sigma^2}}\right\}\sqrt{\mathrm{Err}(t)}\,.$$

For this particular choice of T, we have that for all $t \in [0,T]$

$$\frac{d}{dt}\mathrm{Err}(t) \leq -\frac{1}{2}(2\lambda-\sigma^2)\mathrm{Err}(t) \quad \Rightarrow \quad \mathrm{Err}(t) \leq \mathrm{Err}(0)\,e^{-\frac{1}{2}(2\lambda-\sigma^2)t} \quad (4.31)$$

where we applied Grönwall's inequality. Now, we consider three possible scenarios.

Case $T = T^*$. By definition of T^* and decay estimate (4.31), we have $\mathrm{Err}(T^*) = \varepsilon$.

Case $T < T^*$ and $\mathrm{Err}(T) = \varepsilon$. Nothing to prove in this case.

Case $T < T^*$ and $\|\overline{y}^\alpha(\overline{\rho}(s)) - x^*\|_2^2 \geq C(T)$. We will show that if α is large enough, this case cannot occur. From Proposition 4.5.1 and Lemma 4.7 we have

$$\|\overline{y}^\alpha(\overline{\rho}(T)) - x^*\|_2 \leq \frac{\sqrt{\mathrm{d}}(q+\mathcal{F}_r)^\gamma}{\eta} + \frac{\sqrt{\mathrm{d}}\exp(-\alpha q)}{m_r}\mathbb{E}[\|\overline{Y}_T - x^*\|_2]$$

Now, by continuity of $\mathcal{F}$, we can take q, r small small enough such that the first term on the right-hand side is strictly smaller than $C(T)/2$. Thanks to Lemma 4.29 and

bound (4.31), it holds

$$\mathbb{E}[\|\overline{Y}_T - x^*\|_2] \leq \left(\mathbb{E}[\|\overline{Y}_T - x^*\|_2^2]\right)^{1/2} \leq \sqrt{2}e^{\frac{1}{2}\nu T}(\sup_{t\in[0,T]} \mathrm{Err}(t))^{1/2} \leq \sqrt{2}e^{\frac{1}{2}\nu T}\sqrt{\mathrm{Err}(0)}\,.$$

Therefore, we can take α sufficiently large such that

$$\frac{\sqrt{\mathrm{d}}\exp(-\alpha q)}{m_r}\mathbb{E}[\|\overline{Y}_T - x^*\|_2] \leq \frac{\sqrt{\mathrm{d}}\exp(-\alpha q)}{m_r}\sqrt{2}e^{\frac{1}{2}\nu T}\sqrt{\mathrm{Err}(0)} < \frac{C(T)}{2}\,, \tag{4.32}$$

from which follows

$$\|\overline{y}^\alpha(\overline{\rho}(T)) - x^*\|_2 < C(T)\,.$$

Therefore, we have a contradiction and we can conclude that this third case can be avoided by taking α sufficiently large. □

4.5.4 Proof of Proposition 4.4.2 and Theorem 4.2

We start by collecting a preliminary result.

Lemma 4.8. *Let $\{x_{1,i}^k, y_{1,i}^k\}_{i=1}^{N_1}$ and $\{x_{2,j}^k, y_{2,j}^k\}_{j=1}^{N_2}$ be two particle populations generated through update rules (4.13) with $\vartheta_{1,i}^k = \vartheta_{2,j}^k = \vartheta^k$ for all i, j and $k \in \mathbb{Z}_+$. At any iteration step k and for any couple of indexes (i, j), it holds*

$$\mathbb{E}\left[\|x_{1,i}^{k+1} - x_{2,j}^{k+1}\|_2^2 + \|y_{1,i}^{k+1} - y_{2,j}^{k+1}\|_2^2\right] \leq C\mathbb{E}\left[\|x_{1,i}^k - x_{2,j}^k\|_2^2 + \|y_{1,i}^k - y_{2,j}^k\|_2^2 + \|\overline{y}^\alpha(\overline{\rho}_1^k) - \overline{y}^\alpha(\overline{\rho}_2^k)\|_2^2\right]$$

where $C = C(\Delta t, \lambda, \sigma, \nu, \beta)$ is a positive constant and $\overline{\rho}_1^k, \overline{\rho}_2^k$ are the empiricial distributions associated with $\{y_{1,i}^k\}_{i=1}^{N_1}$ and $\{y_{2,j}^k\}_{j=1}^{N_2}$ respectively.

Proof. For all $k \in \mathbb{Z}_+$ and i, j

$$\begin{aligned}
\mathbb{E}\|x_{1,i}^{k+1} - x_{2,j}^{k+1}\|_2^2 \leq \mathbb{E}\Big\| & x_{1,i}^k + \lambda\Delta t\left(\overline{y}^\alpha(\overline{\rho}_1^k) - x_{1,i}^k\right) + \sigma\sqrt{\Delta t}\left(\overline{y}^\alpha(\overline{\rho}_1^k) - x_{1,i}^k\right)\otimes\vartheta_{1,i}^k \\
& - \left(x_{2,j}^k + \lambda\Delta t\left(\overline{y}^\alpha(\overline{\rho}_2^k) - x_{2,j}^k\right) + \sigma\sqrt{\Delta t}\left(\overline{y}^\alpha(\overline{\rho}_2^k) - x_{2,j}^k\right)\otimes\vartheta_{2,j}^k\right)\Big\|_2^2 \\
\leq\ & 2\mathbb{E}\left\|\left(1 - \lambda\Delta t - \sigma\sqrt{\Delta t}\,\mathrm{diag}(\vartheta^k)\right)(x_{1,i}^k - x_{2,j}^k)\right\|_2^2 \\
& + 2\mathbb{E}\left\|\left(\lambda\Delta t + \sigma\sqrt{\Delta t}\,\mathrm{diag}(\vartheta^k)\right)\left(\overline{y}^\alpha(\overline{\rho}_1^k) - \overline{y}^\alpha(\overline{\rho}_2^k)\right)\right\|_2^2 \\
\leq\ & 2(1 + \lambda^2\Delta t^2 + \sigma^2\Delta t)\mathbb{E}\|x_{1,i}^k - x_{2,j}^k\|_2^2 \\
& + 2(\lambda^2\Delta t^2 + \sigma^2\Delta t)\mathbb{E}\|\overline{y}^\alpha(\overline{\rho}_1^k) - \overline{y}^\alpha(\overline{\rho}_2^k)\|_2^2\,,
\end{aligned} \tag{4.33}$$

where we also used that $\mathbb{E}[(\vartheta^k)_\ell^2] = 1$ for all $\ell = 1, \ldots, d$. We now bound $\|y_{1,i}^{k+1} - y_{2,j}^{k+1}\|_2^2$

as

$$\begin{aligned}\mathbb{E}\|y_{1,i}^{k+1} - y_{2,j}^{k+1}\|_2^2 \leq \mathbb{E}\Big\| & y_{1,i}^k + (\nu\Delta t/2)\left(x_{i,1}^{k+1} - y_{1,i}^k\right) S^\beta(x_{1,i}^{k+1}, y_{1,i}^k) \\ & - \left(y_{2,j}^k + (\nu\Delta t/2)\left(x_{2,j}^{k+1} - y_{2,j}^k\right) S^\beta(x_{2,j}^{k+1}, y_{2,j}^k)\right)\Big\|_2^2 \\ & \leq C\mathbb{E}\left[\|x_{i,1}^{k+1} - x_{j,2}^{k+1}\|_2^2 + \|y_{i,1}^k - y_{j,2}^k\|_2^2\right] \end{aligned} \tag{4.34}$$

where we used Lemma 4.5 and $C = C(\Delta t, \beta, \nu)$. By combining (4.33) and (4.34) we get the desired estimate. □

Next, we show how the particle update rule (4.13) is stable with respect to the 2-Wasserstein distance.

Proposition 4.5.3 (Stability of update rule (4.13))**.** *Let $\{x_{1,i}^k, y_{1,i}^k\}_{i=1}^{N_1}, \{x_{2,j}^k, y_{2,j}^k\}_{j=1}^{N_2} \subset B_M(0)$, for some $M > 0$, be two particle populations generated through the update rules (4.13) with $\vartheta_{1,i}^k = \vartheta_{2,j}^k = \vartheta^k$ for all i, j and $k \in \mathbb{Z}_+$. Let $\mu_1^k, \mu_2^k \in \mathcal{P}(\mathbb{R}^{2d})$ the empirical probability measures defined as*

$$\mu_1^k := \frac{1}{N_1}\sum_{i=1}^{N_1} \delta_{(x_{1,i}^k, y_{1,i}^k)}\,, \quad \mu_2^k := \frac{1}{N_2}\sum_{j=1}^{N_2} \delta_{(x_{2,j}^k, y_{2,j}^k)}\,.$$

Under Assumptions 4.4.1 and 4.4.3, it holds

$$\mathbb{E}\left[W_2^2(\mu_1^{k+1}, \mu_2^{k+1})\right] \leq C_1\,\mathbb{E}\left[W_2^2(\mu_1^k, \mu_2^k)\right]\,,$$

where $C_1 = C_1(\Delta, \lambda, \sigma, \nu, \alpha, \beta, L_{\mathcal{F}}, M)$ is positive constant.

Proof. Let $\mathbb{E}_{\vartheta^k}[\cdot]$ denote the expectation taken with respect to the sampling of ϑ^k only and $w \in \mathbb{R}^{N_1 \times N_2}$ be the optimal coupling between μ_1^k, μ_2^k (see (4.22) and (4.23)). Being w a sub-optimal coupling for μ_1^{k+1}, μ_2^{k+1}, it holds

$$\begin{aligned}\mathbb{E}_{\vartheta^k}[W_2^2(\mu_1^{k+1}, \mu_2^{k+1})] &\leq \mathbb{E}_{\vartheta^k} \sum_{i,j} w_{ij}\left(\|x_{1,i}^{k+1} - x_{2,j}^{k+1}\|_2^2 + \|y_{1,i}^{k+1} - y_{2,j}^{k+1}\|_2^2\right) \\ &\leq C\sum_{i,j} w_{ij}\left(\|x_{1,i}^k - x_{2,j}^k\|_2^2 + \|y_{1,i}^k - y_{2,j}^k\|_2^2\right) + \|\overline{y}^\alpha(\overline{\rho}_1^k) - \overline{y}^\alpha(\overline{\rho}_2^k)\|_2^2\end{aligned}$$

where we used the linearity of the expectation, estimates given by Lemma 4.8 and, to take the last term out of the sum, the fact that $\sum_{ij} w_{ij} = 1$.

To estimate the distance between the two consensus points, we use Lemma 4.4 and note that the coupling w is sub-optimal for $\overline{\rho}_1^k, \overline{\rho}_2^k$ with respect to the optimal transport.

By Lemma 4.4, it follows

$$\|\overline{y}^{\alpha}(\overline{\rho}_1^k) - \overline{y}^{\alpha}(\overline{\rho}_2^k)\|_2^2 \leq \; CW_2^2(\overline{\rho}_1^k, \overline{\rho}_2^k) \; \leq C \sum_{i,j} w_{ij} \|y_{1,i}^k - y_{2,j}^k\|^2 \,.$$

Therefore,

$$\mathbb{E}_{\vartheta^k}[W_2^2(\mu_1^{k+1}, \mu_2^{k+1})] \leq C_1 \sum_{i,j} w_{ij} \left(\|x_{1,i}^k - x_{2,j}^k\|_2^2 + \|y_{1,i}^k - y_{2,j}^k\|_2^2 \right) = C_1 \, W_2^2(\mu_1^k, \mu_2^k) \,,$$

thanks to the optimality of w, with $C_1 = C_1(\Delta, \lambda, \sigma, \nu, \alpha, \beta, L_{\mathcal{F}}, M)$ being a positive constant. One can conclude by taking the expectation of the above inequality with respect to the sampling of $\vartheta^h, h < k$. □

We now quantify the impact of the particle discarding step.

Proof of Proposition 4.4.2. For notational simplicity, let us introduce $z_i = (x_i, y_i) \in \mathbb{R}^{2d}$. As in (4.23), the 2-Wasserstein distance is given by an optimal coupling between the full particle system $\{z_i\}_{i \in I}$ and the reduced one $\{z_j\}_{j \in I_{\text{sel}}}$. We consider the following transportation of mass from μ_N to $\mu_{N_{\text{sel}}}$: if particle i has not been discarded, all its mass remains in x_i, otherwise the mass is uniformly distributed among the selected particles to generate an admissible coupling $w \in \mathbb{R}^{N \times N_{\text{sel}}}$. This means that w is given by

$$w_{ij} = \begin{cases} 1/N & \text{if } j = i, i \in I_{\text{sel}} \\ 1/(N \cdot N_{\text{sel}}) & \text{if } i \in I \setminus I_{\text{sel}}, j \in I_{\text{sel}} \\ 0 & \text{else} \,. \end{cases} \tag{4.35}$$

We note that such coupling w satisfies the coupling conditions

$$\sum_{j \in I_{\text{sel}}} w_{ij} = \frac{1}{N} \quad \sum_{i \in I} w_{ij} = \frac{1}{N_{\text{sel}}}, \quad \forall \, i \in I, j \in I_{\text{sel}} \tag{4.36}$$

and that this choice will be in general sub-optimal. Therefore, it holds

$$\begin{aligned} W_2^2(\mu_N, \mu_{N_{\text{sel}}}) &\leq \sum_{i \in I, \, j \in I_{\text{sel}}} w_{ij} \|z_i - z_j\|_2^2 \\ &= \frac{1}{N} \sum_{i \in I_{\text{sel}}} \|z_i - z_i\|_2^2 + \frac{1}{N \cdot N_{\text{sel}}} \sum_{i \in I \setminus I_{\text{sel}}, \, j \in I_{\text{sel}}} \|z_i - z_j\|_2^2 \\ &= \frac{1}{N \cdot N_{\text{sel}}} \sum_{i,j \in I} \|z_i - z_j\|_2^2 \, \mathbf{1}_{i \in I \setminus I_{\text{sel}}} \, \mathbf{1}_{j \in I_{\text{sel}}} \end{aligned}$$

where $\mathbf{1}_{i \in A} = 1$ if $i \in A$ and $\mathbf{1}_{i \in A} = 0$ if $i \notin A$.

Now, the probability of having $i \in I \setminus I_{\text{sel}}$ is given by $(N - N_{\text{sel}})/N$, while the probability of having $j \in I_{\text{sel}}$ (condition $i \in I \setminus I_{\text{sel}}$) is given by $N_{\text{sel}}/(N-1)$. Hence, we have

$$\mathbb{E}\left[\mathbf{1}_{i\in I\setminus I_{\text{sel}}}\,\mathbf{1}_{j\in I_{\text{sel}}}\right] = \mathbb{P}\left[i \in I \setminus I_{\text{sel}}, j \in I_{\text{sel}}\right] = \frac{(N - N_{\text{sel}})N_{\text{sel}}}{N(N-1)}\,,$$

from which follows

$$\begin{aligned}\mathbb{E}\left[W_2^2(\mu_N, \mu_{N_{\text{sel}}})\right] &\leq \frac{1}{N \cdot N_{\text{sel}}} \sum_{i,j\in I} \|z_i - z_j\|_2^2\, \mathbb{E}\left[\mathbf{1}_{i\in I\setminus I_{\text{sel}}}\,\mathbf{1}_{j\in I_{\text{sel}}}\right] \\ &= \frac{1}{N \cdot N_{\text{sel}}} \cdot \frac{(N - N_{\text{sel}})N_{\text{sel}}}{N(N-1)} \sum_{i,j\in I} \|z_i - z_j\|_2^2\,.\end{aligned}$$

The desired estimates is then obtained by noting that the variance can be computed as $\text{var}(\mathbf{z}) = 1/(2N^2)\sum_{i,j\in I}\|z_i - z_j\|_2^2$, see definition (4.3).

□

Finally, we are ready to provide a proof of Theorem 4.2.

Proof of Theorem 4.2. Let $\{(x_i^k, y_i^k)\}_{i\in I_k}, |I_k| = N_k$ be the sequence of particles generated by iteration (4.13) where additionally $N_{k+1} - N_k$ particles are discarded after each step $k \geq 0$. We denote with $\mu_{N_k}^k \in \mathcal{P}(\mathbb{R}^{2\text{d}})$ the empirical measure associated with such particle system given by

$$\mu_{N_k}^k = \frac{1}{N_k} \sum_{i\in I_k} \delta_{(x_i^k, y_i^k)}\,.$$

We also introduce the measures $\mu_{N_0}^k, k \geq 0$ corresponding to a particle system generated with the same initial conditions $\mu_{N_0}^0$ but where no particle reduction occurs. Consistently, we define $\mu_{N_k}^h$, $h > k$ to represent the particle system generated starting from $\mu_{N_k}^k$, after $h - k$ iterations, with no random selection. The relation between such

measures is summarized in the following diagram

$$\begin{array}{ccccccccc}
\mu^0_{N_0} & \to & \mu^1_{N_0} & \to & \mu^2_{N_0} & \to & \dots & \to & \mu^k_{N_0} \\
 & & \vdots & & & & & & \\
 & & \mu^1_{N_1} & \to & \mu^2_{N_1} & \to & \dots & \to & \mu^k_{N_1} \\
 & & & & \vdots & & & & \\
 & & & & \mu^2_{N_2} & \to & \dots & \to & \mu^k_{N_2} \\
 & & & & & & \ddots & & \vdots \\
 & & & & & & & & \mu^k_{N_k}
\end{array} \tag{4.37}$$

where $\to$ indicates an iteration step (4.13) while $\dashrightarrow$ a particle reduction procedure. Therefore, we are interested in studying the distance between the main diagonal of such diagram $\mu^k_{N_k}$, corresponding to the system with particle reduction, and the first row $\mu^k_{N_0}$ where particle reduction is never performed.

We note that the 2-Wasserstein distance between subsequent rows can be estimated thanks to Proposition 4.5.3 and Proposition 4.4.2. Let $\widetilde{\mathbf{z}}^{h+1}$ denote the set of particles associated with the probability measure $\mu^{h+1}_{N_h}$, that is, the particle systems before the selection procedure (upper diagonal elements in scheme (4.37)). By first applying Proposition 4.5.3 and, subsequently, Proposition 4.4.2 to $\widetilde{\mathbf{z}}^{h+1}$, we obtain that for some constant $C > 0$

$$\begin{aligned}
\mathbb{E}\left[W_2^2(\mu^k_{N_k}, \mu^k_{N_0})\right] &\le C \sum_{h=0}^{k-1} \mathbb{E}\left[W_2^2\left(\mu^k_{N_h}, \mu^k_{N_{h+1}}\right)\right] \\
&\le C \sum_{h=0}^{k-1} C_1^{k-h+1}\, \mathbb{E}\left[W_2^2\left(\mu^{h+1}_{N_h}, \mu^{h+1}_{N_{h+1}}\right)\right] \\
&\le 2\, C \sum_{h=0}^{k-1} C_1^{k-h+1}\, \mathrm{var}\left(\widetilde{\mathbf{z}}^{h+1}\right) \frac{N_h - N_{h+1}}{N_h - 1} \\
&\le C_2 \max_{h=1,\dots,k} \mathrm{var}\left(\widetilde{\mathbf{z}}^{h}\right) \frac{1}{N_k - 1} \sum_{h=0}^{k-1} N_h - N_{h+1} \\
&= C_2 \max_{h=1,\dots,k} \mathrm{var}\left(\widetilde{\mathbf{z}}^{h}\right) \frac{N_0 - N_k}{N_k - 1}
\end{aligned}$$

with $C_2 = C_2(\Delta t, \lambda, \sigma, \nu, \beta, \alpha, k, M)$. Finally, the desired estimate follows after noting

that

$$W_2^2(\rho_{N_k}^k, \rho_{N_0}^k) \leq W_2^2(\mu_{N_k}^k, \mu_{N_0}^k)$$

since $\|x_i^k - x_j^k\|_2^2 \leq \|(x_i^k, y_i^k) - (x_j^k, y_j^k)\|_2^2$ for all couples of particles (i, j). □

4.6 Concluding remarks

This chapter has been devoted to the analysis of a consensus-based optimization algorithm with memory effects and random selection for global optimization. While sharing common features with PSO methods, CBO-ME differs in the way the particle system explores the search space and in the random selection process which greatly improves the performance of the method. We compared CBO-ME with CBO without memory effects and with classical PSO on several benchmark problems and showed how the introduction of personal bests or the release of parameters from each other improves the performance of the algorithm. A convergence analysis was conducted based on an approximation of the mean field of the particle system and error estimates were provided.

Chapter 5

Applications to image segmentation and machine learning

In this chapter, we consider some applications of the CBO algorithm with memory effects (CBO-ME) and random selection studied in the previous chapter. In realistic applications such as machine and deep learning or image recognition, the dimensionality of the problem is typically very high, and it is necessary to find methods that do not suffer from the curse of dimensionality and are capable of dealing with a wide range of problems. In Chapter 4, we showed with numerical tests on high-dimensionality benchmark functions how memory effects combined with random selection lead to advantages over the classical CBO method in terms of speed of convergence; moreover, it is evident that this method also outperforms PSO methods, which, by not decoupling the alignment and exploration terms, in some cases have limitations in solving the most challenging problems.

Once we have tested the capabilities of the method in optimizing the benchmark functions, in this chapter we can employ the method in some applications by setting the parameters in their best configuration previously studied. First, we consider image segmentation by threshold selection, where the size of the problem increases with the number of thresholds to be searched. Otsu's multi-threshold segmentation technique was used to perform it. As a next application, we propose to train a neural network (NN) with the purpose of approximating functions. The goal is to minimize the distance between the original function and the solution predicted by the network, and this involves a large number of parameters. The functions to be approximated may be difficult due to an oscillatory nature or the presence of some discontinuities. The last numerical application we performed concerns the MNIST database and the recognition of handwritten digits. The data processed lead to a highly dimensional and rather complex optimization problem, so it is important to show how acceptable results can

be obteineded with a rather small number of particles. The results obtained here are preliminary and are comparable to methods already known in the literature.

5.1 Image segmentation

To perform image segmentation, we use a threshold detection technique, namely, the multidimensional Otsu algorithm [81, 97] in order to compare the results to similar optimization algorithm, such as the Modified PSO in [94].

In the Otsu algorithm, every pixel of the image is assigned to one of the possible L grayscale values. We denote with η_i the number of pixel with gray level i, $1 \leq i \leq L$ and $N_{pix} = \sum_{i=1}^{L} \eta_i$ the total number of pixels [81]. Then, the image is divided into object C_0 with gray-level $[1, \dots, l]$ and background C_1 with gray-level $[l+1, \dots, L]$ by inserting a threshold l. The probabilities of class occurrence and the class mean level for the object, respectively, are given by

$$\omega_0(l) = \sum_{i=1}^{l} p_i, \quad p_i = \frac{\eta_i}{N_{pix}}$$
$$\mu_0(l) = \sum_{i=1}^{l} \frac{i p_i}{\omega_0(k)}.$$

For the background, the class occurrence probabilities and the class mean level are given by

$$\omega_1(l) = \sum_{i=l+1}^{L} p_i, \quad p_i = \frac{\eta_i}{N_{pix}}$$
$$\mu_1(l) = \sum_{i=l+1}^{L} \frac{i p_i}{\omega_1(k)}.$$

As in [81], the best threshold l^* is obtained when the variance formula

$$f(l) = \omega_0(l)\ \omega_1(l)\ (\mu_0(l) - \mu_1(l))^2 \tag{5.1}$$

between object group and background reaches its maximum value, i.e. $l^* = \text{argmax}_l f(l)$. The problem is then reduced to a threshold problem, which we can solve with optimization methods.

Since segmentation is a trivial one-dimensional problem, we consider an extension of Otsu's technique to the multidimensional case [97] to test capabilities of method. Assuming we want to optimize the choice of d thresholds, we require $d+1$ classes

of different gray-scales $(C_0, \dots, C_d)$ with relative probabilities of occurrence classes defined as

$$\omega_0(l_1) = \sum_{i=1}^{l_1} p_i \ , \dots , \ \omega_d(l_d) = \sum_{i=l_d+1}^{L} p_i, \quad p_i = \frac{\eta_i}{N_{pix}}$$

and classes mean levels

$$\mu_0(l_1) = \frac{\sum_{i=1}^{l_1} i p_i}{\omega_0} \ , \dots , \ \mu_d(l_d) = \frac{\sum_{i=l_{d+1}}^{L} i p_i}{\omega_d},$$

The optimal thresholds $(\widehat{l}_1, \dots, \widehat{l}_d)$ are those that satisfy $\widehat{l}_1 < \dots < \widehat{l}_d$ and maximise

$$f(l_1, \dots l_d) = \sum_{i=1}^{d} \omega_i(l_i)\mu_i^2(l_i) \tag{5.2}$$

For the experiment, we chose $d = 5$ thresholds and compare the segmentation performed by Otsu's method, solved with both standard PSO and CBO-ME, with segmentation obtained by dividing the greyscale into $d+1$ uniformly spaced intervals. For PSO, we use to the default parameters in the `particleswarm` function in the MATLAB Global Optimization Toolbox, while for CBO-ME we used optimal parameters found in Appendix A1 and exploit the random selection technique to speed up the algorithm.

We report the results on three sample images, Fig.s 5.1, 5.2 and 5.3. We fix the maximum number of iterations at 10^3 and average results over 250 runs. As in [6], we evaluate multi-thresholding segmentation through the Peak Signal to Noise Ratio ($PSNR$) computed as:

$$PSNR = 20 \cdot \log_{10}\left(\frac{255}{RMSE}\right)$$

where $RMSE$ is the Root Mean-Squared Error, defined as

$$RMSE = \sqrt{\frac{1}{N_{pix}} \sum_{i=1}^{N_{row}} \sum_{j=1}^{N_{col}} [I(i,j) - S(i,j)]^2}$$

where $N_{pix} = N_{row} \cdot N_{col}$, I is the original image and S is the associated segmented image. The higher the value of $PSNR$ is, the greater the similarity between the clustered image and the original image is. From Fig.s 5.1,5.2,5.3, we note that the most accurate segmentation on details is obtained by the CBO-ME method. This is quantitatively confirmed by the $PSNR$ values reported in Table 5.1.

(a) Original (b) Standard segmentation (c) Otsu segmentation, PSO solver (d) Otsu segmentation, CBO-ME solver

Figure 5.1: Image segmentation of `darkhair woman` image (256×256 pixels) with standard segmentation and Otsu segmentation solved by PSO and by CBO-ME ; results are averaged over 250 runs, with an initial population of $N_0 = 10^3$ particles.

(a) Original (b) Standard segmentation (c) Otsu segmentation, PSO solver (d) Otsu segmentation, CBO-ME solver

Figure 5.2: Image segmentation of `lake` image (256×256 pixels) with standard segmentation and Otsu segmentation solved by PSO and by CBO-ME; results are averaged over 250 runs, with an initial population of $N_0 = 10^3$ particles.

(a) Original (b) Standard segmentation (c) Otsu segmentation, PSO solver (d) Otsu segmentation, CBO-ME solver

Figure 5.3: Image segmentation of `cameraman` image (256×256 pixels) with standard segmentation and Otsu segmentation solved by PSO and by CBO-ME ; results are averaged over 250 runs, with an initial population of $N_0 = 10^3$ particles.

	cameraman	lake	lena	peppers	woman darkhair
Standard segmentation	22.83	21.72	24.35	27.24	25.33
Otsu segmentation solved by PSO	34.62	32.33	38.19	38.03	37.14
Otsu segmentation solved by CBO-ME	**37.22**	**35.44**	**38.72**	**38.28**	**39.57**

Table 5.1: $PSNR$ values obtained for 5 sample images known in literature. We compared the Otsu segmentation solved by the proposed CBO-ME method with the classical PSO method and with equispaced thresholding segmentation. Experiments are performed with d = 5 thresholds.

5.2 Approximating functions with NN

In this section, we use the proposed CBO-ME algorithm to train a NN architecture into approximating a function $u : I \to \mathbb{R}, I \subset \mathbb{R}$ with low regularity. As in [24], we use a fully-connected NN with m layers

$$f(x;\vartheta) = (L_m \circ \dots L_2 \circ L_1)(x) \tag{5.3}$$

where each layer is given by

$$L_i = \sigma(W^i x + b^i)$$

with $\sigma(x) = 1/(1+\exp(-x))$ being the sigmoid function. We use internal layers of dimension n, so $W^1 \in \mathbb{R}^{n\times 1}, b^1 \in \mathbb{R}$, $W^m \in \mathbb{R}^{1\times n}, b^m \in \mathbb{R}^d$ and $W^i \in \mathbb{R}^{n\times n}$ for all $i = 2,\dots,m-1$. In (5.3), all DNN parameters are collected in $\vartheta = \{W^i, b^i\}_{i=1}^m$.

As loss function which need to be minimized, we consider the L^2-norm between the target function u and its NN approximation $f(\cdot\,;\vartheta)$

$$\mathcal{F}(\vartheta) := \|f(\cdot\,;\vartheta) - u\|_{L^2(I)}\,. \tag{5.4}$$

Again, similarly to [24], we test the method against the following three functions:

$$u_1(x) = \sin(2\pi x) + \sin(8\pi x^2) \tag{5.5}$$

$$u_2(x) = \sin(4\pi x^4) \tag{5.6}$$

$$u_3(x) = \begin{cases} 1 & \text{if } x < -\frac{7}{8}, -\frac{1}{8} < x < \frac{1}{8}, x > \frac{7}{8} \\ -1 & \text{if } \frac{3}{8} < x < \frac{5}{8}, -\frac{5}{8} < x < -\frac{3}{8}, \\ 0 & \text{otherwise}\,. \end{cases} \tag{5.7}$$

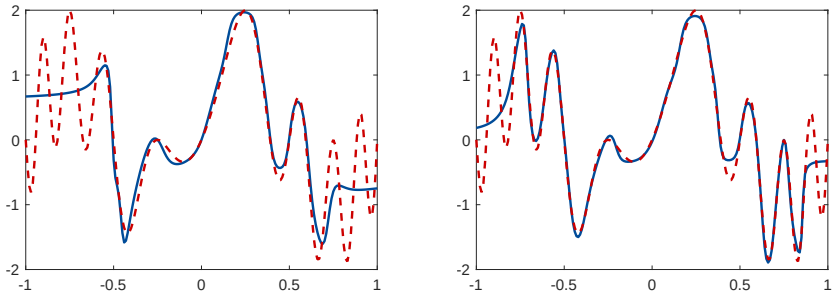

(a) 2000 epochs (b) 3000 epochs

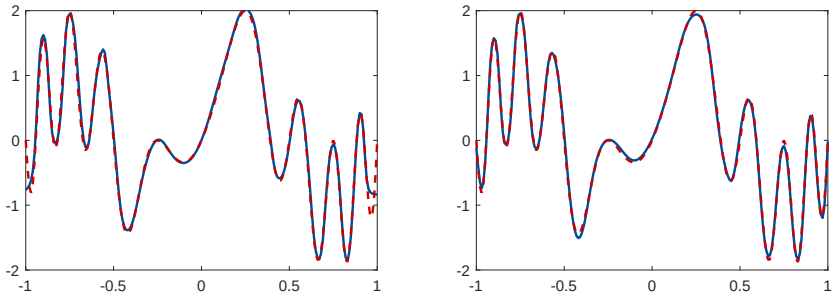

(c) 5000 epochs (d) 8000 epochs

Figure 5.4: Approximating smooth function u_1 (5.5) using a network with $n = 50$ and $m = 3$. We initially use $N_0 = 500$ particles and we set $\lambda = 0.01$, $\sigma = 0.8$. Parameter α is adaptive, starting from $\alpha_0 = 10$.

We note that u_1 and u_2 are smooths, while u_3 is discontinuous. Parameters of the CBO-ME algorithm have been set to $\lambda = 0.01, \sigma = 0.8$, as in the previous sections. Parameter α is adapted during the computation as in 4.8 and random selection mechanism is used. We employ $m = 3$ layers with internal dimension $n = 50$. Results are displayed in Fig.s 5.4, 5.5 and 5.6. We note that smooth functions u_1 and u_2 are well-approximated already after 5000 epochs, while convergence is slower for the discontinuous step function u_3.

5.3 Application on MNIST dataset

We now employ the proposed algorithm to train a NN architecture to solve a image classification task. We will consider the MNIST dataset [70] composed of handwritten digits in gray scale with 28×28 pixels. For better comparability with CBO methods without memory effects, we follow the experiment settings used in the literature [9, 23, 43, 87], which we summarize below.

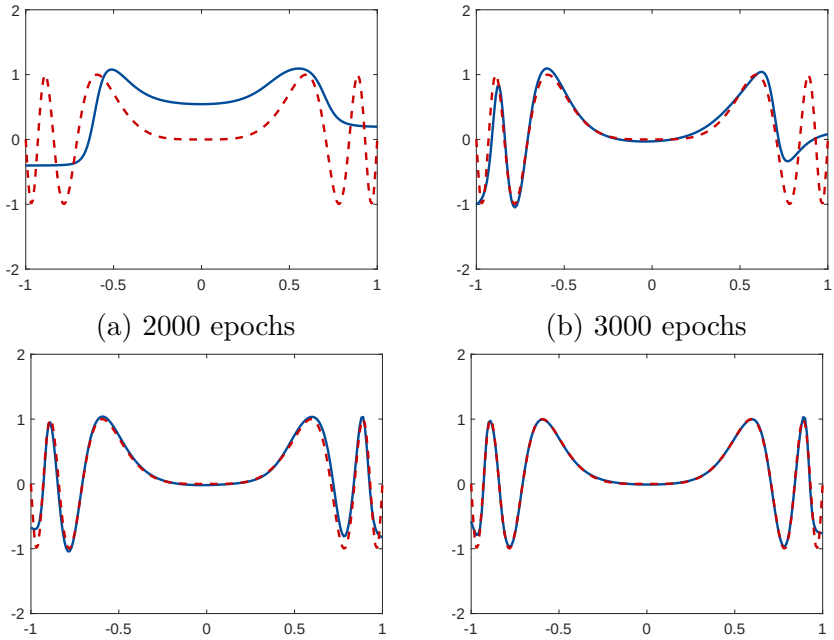

(a) 2000 epochs (b) 3000 epochs

(c) 5000 epochs (d) 8000 epochs

Figure 5.5: Approximating smooth u_2 (5.6) function using a network with $n = 50$ and $m = 3$. We initially use $N_0 = 500$ particles and we set $\lambda = 0.01$, $\sigma = 0.8$. Parameter α is adaptive, starting from $\alpha_0 = 10$.

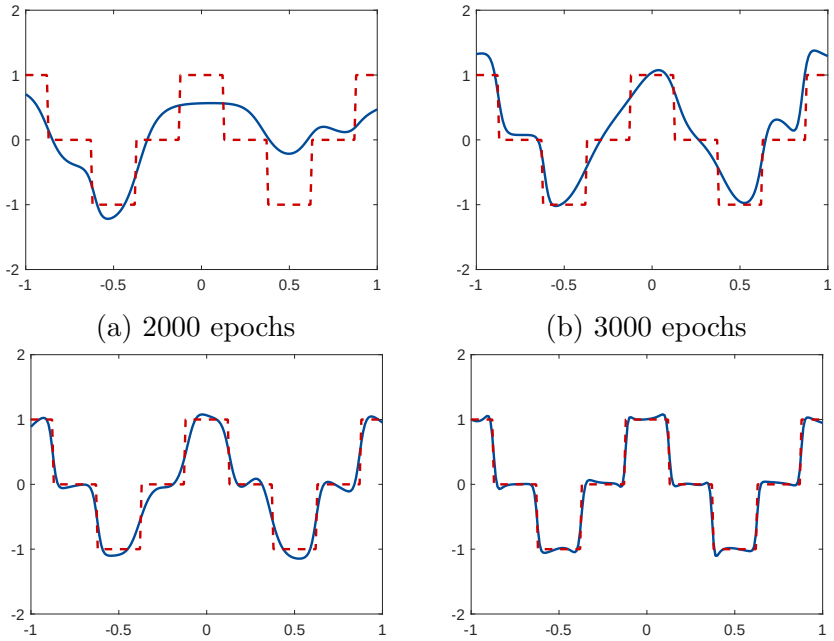

(a) 2000 epochs (b) 3000 epochs

(c) 5000 epochs (d) 8000 epochs

Figure 5.6: Approximating non-smooth u_3(5.7) function using a network with $n = 50$, $m = 3$.We initially use $N_0 = 500$ particles and we set $\lambda = 0.01$, $\sigma = 0.8$. Parameter α is adaptive, starting from $\alpha_0 = 10$.

Figure 5.7: Sample images from MNIST test dataset

We consider a 1-layer NN where input images $x \in \mathbb{R}^{28\times 28}$ are first vectorized $x \mapsto \mathrm{vec}(x) \in \mathbb{R}^{784}$ and then processed through a fully-connected layer with parameters $\vartheta = \{W, b\}$, where $W \in \mathbb{R}^{10\times 784}, b \in \mathbb{R}^{10}$. That is, the network is given by

$$f^{\mathrm{SNN}}(x;\vartheta) = \mathrm{softmax}\left(\mathrm{ReLU}\left(W\,\mathrm{vec}(x) + b\right)\right), \tag{5.8}$$

where $\mathrm{ReLU}(z) = \max\{z, 0\}$ (component-wise) and $\mathrm{softmax}(z) = (e^{z_1}, \dots, e^{z_n})/(\sum_i e^{z_i})$ are the commonly used activation functions. During the training, batch regularization is performed after ReLU is applied in order to speed up convergence. Given a training set $\{(x^m, \ell^m)\}_{m=1}^M$, $x_m \in \mathbb{R}^{28\times 28}, \ell_m \in \{0,1\}^{10}$ made of M image-label tuples, we train the model by minimizing the categorical cross-entropy loss

$$\mathcal{F}(\vartheta) = \frac{1}{M}\sum_{m=1}^{M}\left(-\sum_{i=1}^{10}\ell_i^m \log(f_i(x^m,\vartheta))\right). \tag{5.9}$$

The entire training set is made of 60,000 images, 6,000 per class, but we divide it in batches of size $M = 120$, and consider a different batch at each algorithm iteration to evaluate (5.9).

The initial population of N_0 particles is sampled from the standard normal distribution $\mathcal{N}(0, \mathbf{I}_d)$ and we employ the particle reduction strategy given by (4.4) with $N_{\min} = 100$. Differently from previous experiments, though, we compute the new number of particles N_{k+1} based on the variance of the personal bests $\{y_i^k\}_{i\in N_k}$, rather then considering the particle positions $\{x_i^k\}_{i\in N_k}$. This is because, in this application, the variance of the particle positions shows an oscillatory behavior (see Fig. 5.9).

Following the mini-batch approach suggested in [23], at each algorithm iteration we divide the particle population in mini-batches of size $n_N = 20$ (the last one being

eventually smaller) and independently perform the update within the different mini-batches. Particles are re-ordered after each update step, so that the mini-batches always vary during the computation.

Fig. 5.8a, shows the algorithm performance when $N_0 = 1000$ particles are initially used and random selection is performed with different parameters μ. We note that, in terms of accuracy and loss, the performance is comparable. The random selection strategy sensibly reduces the number of function evaluations needed, especially when the particle system has already formed consensus. The number of particles per iteration is displayed in Fig. 5.9, further showing how the computational complexity of an update step decays during the computation.

We also compare the algorithm performance when different initial population sizes $N_0 = 500, 1000, 2000$ are considered, with same random selection strength $\mu = 0.1$. In this case, the best balance between computational cost and accuracy is given by $N_0 = 1000$. We note in particular how starting with a larger population size of 2000 particles leads to a marginal improvement of the algorithm performance, while requiring a much higher number of loss evaluations.

In the last experiment, we compare algorithms CBO-ME and CBO without memory effects. We also consider a third heuristic proposed in [23] and further tested in [43]. In this CBO variant, no memory is employed, but, whenever $\|\overline{x}^{\alpha,k+1} - \overline{x}^{\alpha,k}\|_\infty \leq \delta$, particles are randomly perturbed before the CBO iteration, by adding Gaussian noise:

$$x_i^k \leftarrow x_i^k + \sigma \widetilde{\vartheta}_i^k \quad \text{with} \quad \widetilde{\vartheta}_i^k \sim \mathcal{N}(0, \mathbf{I}_\mathrm{d})\,. \tag{5.10}$$

In our experiment, we also consider the above variant with $\delta = 10^{-5}$ and $\overline{x}^{\alpha,k}$ computed among the whole particle system.

Fig. 5.10 illustrates the performance of the different algorithms for three different choices of parameter α: increasing, fixed to $\alpha = 50$ and fixed to $\alpha = 5 \cdot 10^4$. The drift parameter is set to $\lambda = 0.1$ while we set $\sigma = \sqrt{0.1}$ for CBO-ME and CBO without random perturbations and $\sigma = \sqrt{0.04}$ for CBO when random noise is added. Initial populations of $N_0 = 1000$ with selection parameter $\mu = 0.2$ are used when there is no additional noise, while we use $N_0 = 250$ and no particle selection when we perform random perturbations. This is motivated by the fact that the particle variance, whenever noise is added, shows an oscillatory behavior which is not compatible with the mechanism of random selection.

We note that CBO-ME performs better when lower values of α are used, while the effect of memory is reduced for larger values of α. A low value of sigma, together with random perturbations, typically slow down the convergence of the particle system.

Remark 6.

- *In CBO literature, an additional parameter* Δt *is typically used to define step size* $\lambda = \widetilde{\lambda}\Delta t$ *and the diffusion strength* $\sigma = \widetilde{\sigma}\sqrt{\Delta t}$*, for some* $\widetilde{\lambda}, \widetilde{\sigma}$*. This is because the particles update rule is interpreted as a numerical scheme solving a time-continuous dynamics, as we will see in the next Section. We decided here to avoid using* Δt *for better comparability with PSO algorithms. We note how choosing, for instance,* $\lambda = 0.1, \sigma = \sqrt{0.1}$ *is equivalent to the parameters choice* $\widetilde{\lambda} = 1, \widetilde{\sigma} = 1$ *with* $\Delta t = 0.1$*.*

- *Experiments show how both CBO and CBO-ME converges towards a solution in less than an epoch. This is coherent with other population-based algorithms, such as Ensemble Kalman Filter [103]. Moreover, we note how adding noise during the computation sensibly reduces the convergence speed, see Fig. 5.10.*

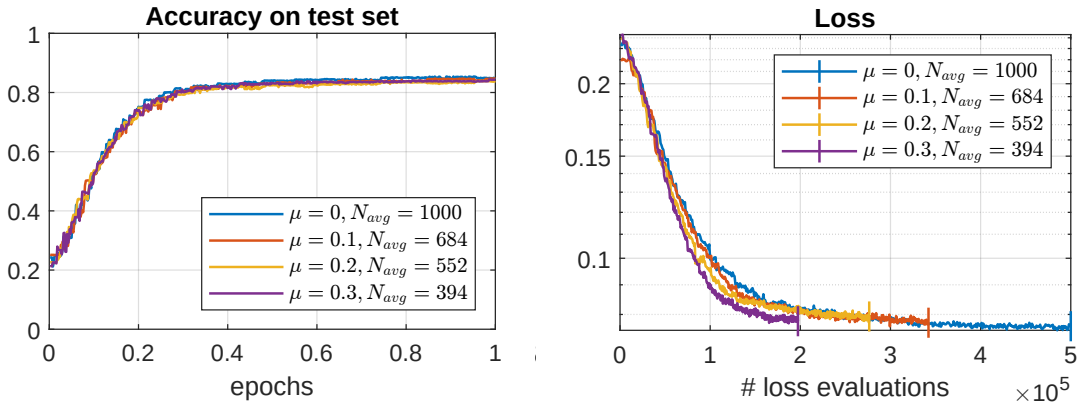

(a) Different random selection parameters μ, same initial population size $N_0 = 1000$

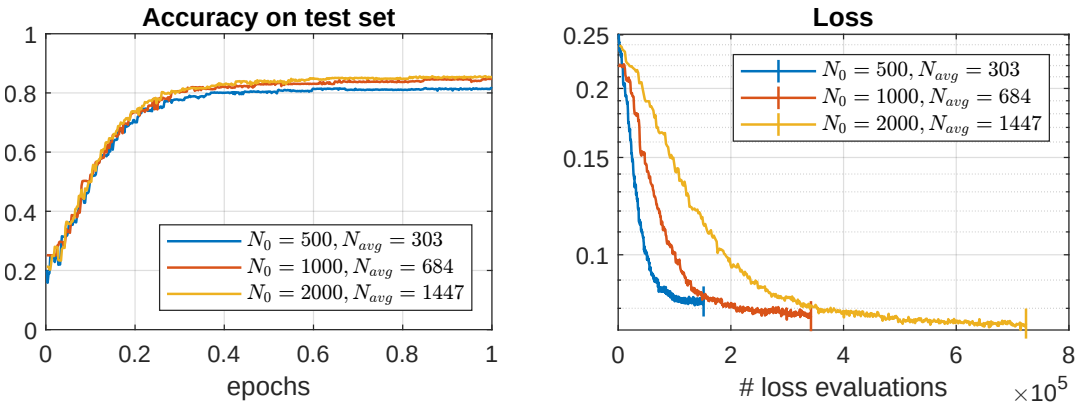

(b) Different initial population sizes N_0, same random selection parameter $\mu = 0.1$

Figure 5.8: Performance of CBO-ME algorithm in training a shallow NN for MNIST classification. Experiment with different combinations of random selection parameter μ and initial population sizes are considered. Plots on the left display accuracy as a function of the amount of training data considered. On the right, the loss is displayed as a function of the number of loss evaluations. Clearly, when less particles are employed (either due to large μ or to small N_0), fewer loss evaluations are needed. The average number of particles is denoted by N_{avg}. Algorithm parameters are set to $\lambda = 0.1, \sigma = \sqrt{0.1}, \alpha = 5 \cdot 10^4$

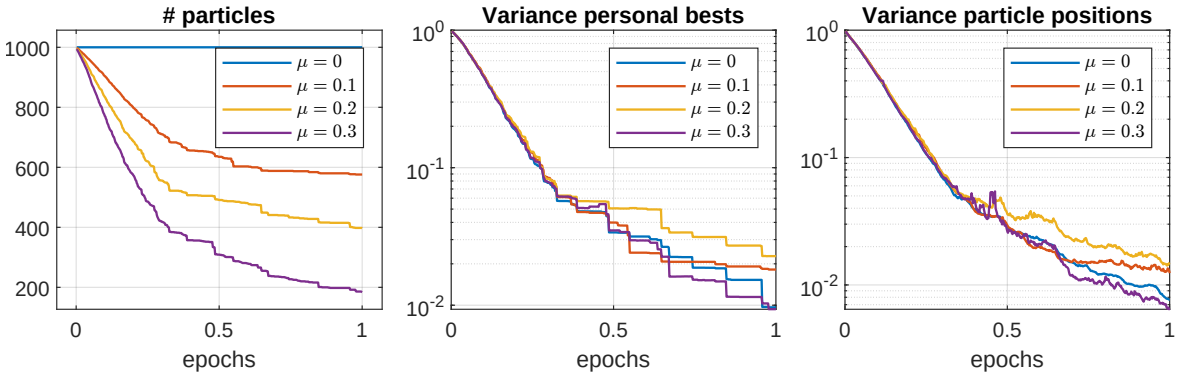

Figure 5.9: Population statistics during the training of shallow NN with CBO-ME method. Experiments with different random selection parameters μ and initial population sizes $N_0 = 1000$. Algorithm parameters are set to $\lambda = 0.1, \sigma = \sqrt{0.1}, \alpha = 5 \cdot 10^4$

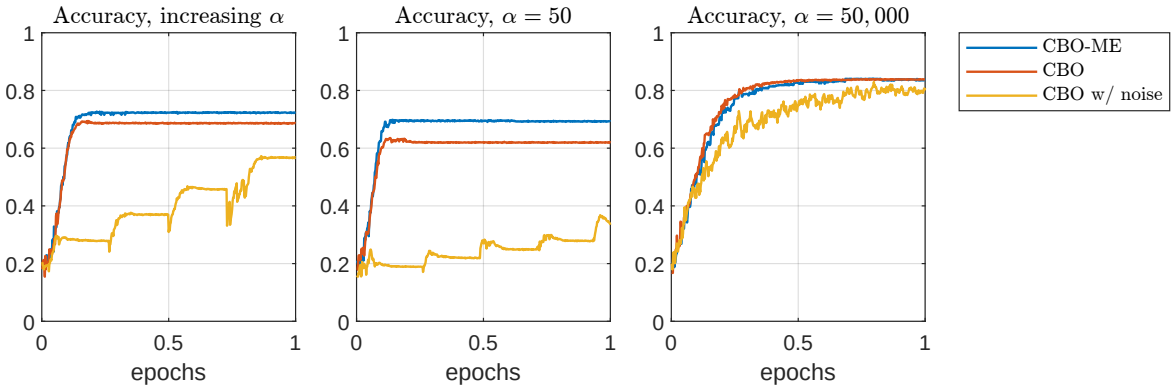

Figure 5.10: Performance comparison between different consensus algorithms in training of shallow NN. We consider the proposed CBO-ME algorithm, the plain CBO algorithm and the CBO algorithm with random perturbation (5.10), as proposed in [23]. For the first two algorithms we set $\sigma = \sqrt{0.1}$, while for the third one $\sigma = \sqrt{0.04}$. We set $\lambda = 0.1$ and consider three different strategies for α: $\alpha_k = 5 \cdot k, \alpha_k = 50$ and $\alpha_k = 5 \cdot 10^4$

5.4 Concluding remarks

In this lastchapter, we explored the performance of the various CBO methods in realistic problems including several test cases in machine learning. We compared the standard CBO method with the CBO that includes memory and particle selection. This variant of CBO showed better performance compared to the standard method, and in most test cases, it led to a significant computational speed up. The memory and particle selection mechanism allow the algorithm to remember successful steps taken in the optimization process and prioritize those steps in subsequent iterations. Overall, the results of this study suggest that the modified CBO method with memory and par-

ticle selection is a promising approach for optimizing complex machine learning models and other real-world problems, potentially saving significant computational resources.

Appendices

A1 Benchmark functions

In this Appendix we report the global optimization test functions that were used in the article to validate the performance of the algorithms below. Each function is reported within the typical search domain and, if $B, C = 0$, has the global minima located at $x^* = (0, \ldots, 0)$ with $\mathcal{F}(x^*) = 0$.

1. **Ackley function** (Continuous, Differentiable, Non-convex, Non-Separable, Multimodal)

$$\mathcal{F}(x) = 20 + \exp(1) - 20 \exp\left(-0.2\sqrt{\frac{1}{d}\sum_{i=1}^{d}(x_i - B)^2} \right) - \exp\left(\frac{1}{d}\sum_{i=1}^{d}\cos\left(2\pi(x_i - B)\right) \right) + C, \tag{A.1}$$

   subject to $-32 \leq x \leq 32$.

2. **Griewalk function** (Continuous, Differentiable, Non-convex, Separable, Unimodal)

$$\mathcal{F}(x) = 1 + \sum_{i=1}^{d}\frac{(x_i - B)^2}{4000} - \prod_{i=1}^{d}\cos\left(\frac{x_i - B}{i}\right) + C, \tag{A.2}$$

   subject to $-600 \leq x \leq 600$.

3. **Rastrigin function** (Continuous, Differentiable, Convex, Separable, Multimodal)

$$\mathcal{F}(x) = 10d + \sum_{i=1}^{d}\left[(x_i - B)^2 - 10\cos\left(2\pi(x_i - B)\right)\right] + C, \tag{A.3}$$

   subject to $-5.12 \leq x \leq 5.12$.

4. **Rosenbrock function** (Continuous, Differentiable, Non-convex, Non-Separable, Unimodal)

$$\mathcal{F}(x) = \sum_{i=1}^{d-1} \left[100\ ((x_{i+1} - B) - (x_i - B)^2)^2 + (x_i - B - 1)^2\right] + C, \tag{A.4}$$

subject to $-5 \leq x_i \leq 10$. The global minimum is $x^* = (1, \ldots, 1) \in \mathbb{R}^d$ for $B = 0$ with $\mathcal{F}(x^*) = 0$ for $C = 0$.

5. **Salomon function** (Continuous, Differentiable, Non-Convex, Non-Separable, Multimodal)

$$\mathcal{F}(x) = 1 - \cos\left(2\pi\sqrt{\sum_{i=1}^{d}(x_i - B)^2}\right) + 0.1\sqrt{\sum_{i=1}^{d}(x_i - B)^2} + C, \tag{A.5}$$

subject to $-100 \leq x \leq 100$.

6. **Schwefel function** (Continuous, Non-Differentiable, Convex, Separable, Unimodal)

$$\mathcal{F}(x) = \sum_{i=1}^{d} |x_i - B| + C, \tag{A.6}$$

subject to $-100 \leq x \leq 100$.

7. **Xin She-Yang random function** (Random, Non-Differentiable, Non-convex, Separable, Multimodal)

$$\mathcal{F}(x) = \sum_{i=1}^{d} \eta_i |x_i - B|^i + C \tag{A.7}$$

with $\eta_i, i = 1, \ldots, d$ random variable uniformly distributed in $[0, 1]$. The standard domain size is $-5 \leq x \leq 5$.

8. **Xin She-Yang 4 function** (Non-Differentiable, Non-convex, Non-Separable, Multimodal)

$$\mathcal{F}(x) = \left(\sum_{i=1}^{d} \sin^2(x_i - B) - e^{-\sum_{i=1}^{d}(x_i - B)^2}\right) e^{-\sum_{i=1}^{d} \sin^2\sqrt{|x_i - B|}} + C, \tag{A.8}$$

subject to $-10 \leq x_i \leq 10$. The global minimum is $x^* = (0, \ldots, 0) \in \mathbb{R}^d$ for $B = 0$ with $\mathcal{F}(x^*) = -1$ for $C = 0$.

Name	**Function $\mathcal{F}(x)$**	**Range**	x^*	$\mathcal{F}(x^*)$	**Sketch in 2D**
Ackley	$-20\,\exp\left(-0.2\sqrt{\frac{1}{d}\sum_{i=1}^{d}(x_i)^2}\right) - \exp\left(\frac{1}{d}\sum_{i=1}^{d}\cos\left(2\pi(x_i)\right)\right) + 20 + e$	$[-32, 32]^d$	$(0, \ldots, 0)$	0	
Griewank	$1 + \sum_{i=1}^{d}\frac{(x_i)^2}{4000} - \prod_{i=1}^{d}\cos\left(\frac{x_i}{i}\right)$	$[-600, 600]^d$	$(0, \ldots, 0)$	0	
Rastrigin	$10d + \sum_{i=1}^{d}\left[(x_i)^2 - 10\cos\left(2\pi(x_i)\right)\right]$	$[-5.12, 5.12]^d$	$(0, \ldots, 0)$	0	
Rosenbrock	$1 - \cos\left(2\pi\sqrt{\sum_{i=1}^{d}(x_i)^2}\right) + 0.1\sqrt{\sum_{i=1}^{d}(x_i)^2}$	$[-5, 10]^d$	$(1, \ldots, 1)$	0	
Salomon	$1 - \cos\left(2\pi\sqrt{\sum_{i=1}^{d}(x_i)^2}\right) + 0.1\sqrt{\sum_{i=1}^{d}(x_i)^2}$	$[-100, 100]^d$	$(0, \ldots, 0)$	0	
Schwefel 2.20	$\sum_{i=1}^{d}\lvert x_i\rvert$	$[-100, 100]^d$	$(0, \ldots, 0)$	0	
XSY random	$\sum_{i=1}^{d}\eta_i\lvert x_i\rvert^i, \qquad \eta_i \sim \mathcal{U}(0,1)$	$[-5, 5]^d$	$(0, \ldots, 0)$	0	
XSY 4	$\left(\sum_{i=1}^{d}\sin^2(x_i) - e^{-\sum_{i=1}^{d}(x_i)^2}\right) e^{-\sum_{i=1}^{d}\sin^2\sqrt{\lvert x_i\rvert}}$	$[-10, 10]^d$	$(0, \ldots, 0)$	-1	

Table A.1: Summary table of prototype test functions for global optimization.

References

[1] E. Aarts and J. Korst, *Simulated annealing and Boltzmann machines: A stochastic approach to combinatorial optimization and neural computing*, John Wiley & Sons, Inc., 1989.

[2] S M. Abedi Pahnehkolaei, A. Alfi, and J A. Tenreiro Machado, *Analytical stability analysis of the fractional-order particle swarm optimization algorithm*, Chaos, Solitons & Fractals **155** (2022), 111658.

[3] J-A. Acebrón and R. Spigler, *Adaptive frequency model for phase-frequency synchronization in large populations of globally coupled nonlinear oscillators*, Physical Review Letters **81** (1998), no. 11, 2229–2232.

[4] G. Albi and L. Pareschi, *Binary interaction algorithms for the simulation of flocking and swarming dynamics*, Multiscale Modeling & Simulation **11** (2013), no. 1, 1–29.

[5] L. Arnold, *Stochastic differential equations: Theory and applications*, first ed., Wiley Interscience, 1974, Structure-preserving algorithms for ordinary differential equations.

[6] S. Arora, J. Acharya, A. Verma, and P K. Panigrahi, *Multilevel thresholding for image segmentation through a fast statistical recursive algorithm*, Pattern Recognition Letters **29** (2008), no. 2, 119–125.

[7] C. Audet and W. L. Hare, *Derivative-free and blackbox optimization*, Springer, 2017.

[8] N. Bellomo and S Y. Ha, *A quest toward a mathematical theory of the dynamics of swarms*, Mathematical Models and Methods in Applied Sciences **27** (2017), no. 4, 745–770.

[9] A. Benfenati, G. Borghi, and L. Pareschi, *Binary interaction methods for high dimensional global optimization and machine learning*, Applied Mathematics & Optimization (2022), 1–41.

[10] P. Billingsley, *Convergence of probability measures*, John Wiley & Sons, 2013.

[11] C.M. Bishop, *Pattern recognition and machine learning*, Springer, 2006.

[12] F. Bolley, J A. Canizo, and J A. Carrillo, *Stochastic mean-field limit: non-Lipschitz forces and swarming*, Mathematical Models and Methods in Applied Sciences **21** (2011), no. 11, 2179–2210.

[13] E. Bonabeau, M. Dorigo, and G. Theraulaz, *Swarm intelligence: From natural to artificial system*, Oxford University Press, 1999.

[14] G. Borghi, S. Grassi, and L. Pareschi, *Consensus based optimization with memory effects: random selection and applications*, Preprint ArXiv:2301.13242 (2023).

[15] G. Borghi, M. Herty, and L. Pareschi, *A consensus-based algorithm for multi-objective optimization and its mean-field description*, Proceedings of, the 61st IEEE Conference on Decision and Control (2022), 4131–4136.

[16] ———, *Constrained consensus-based optimization*, SIAM Journal on Optimization **33** (2023), no. 1, 10.1137.

[17] V. Bruned, A. Mas, and S. Wlodarczyk, *Weak convergence of particle swarm optimization*, arXiv preprint arXiv:1811.04924 (2019).

[18] J A. Carrillo and Y-P. Choi, *Mean-field limits: From particle descriptions to macroscopic equations*, Arch. Ration. Mech. Anal. **241** (2021), no. 3, 1529–1573. MR 4284530

[19] J A. Carrillo, Y-P. Choi, and S. Salem, *Propagation of chaos for the Vlasov-Poisson-Fokker-Planck equation with a polynomial cut-off*, Commun. Contemp. Math. **21** (2019), no. 4, 1850039, 28. MR 3957154

[20] J A. Carrillo, Y-P. Choi, C. Totzeck, and O. Tse, *An analytical framework for consensus-based global optimization method*, Mathematical Models and Methods in Applied Sciences **28** (2018), no. 6, 1037–1066.

[21] J A. Carrillo, M. Fornasier, G. Toscani, and F. Vecil, *Particle, kinetic, and hydrodynamic models of swarming*, Mathematical modeling of collective behavior in socio-economic and life sciences, Springer, 2010, pp. 297–336.

[22] J A. Carrillo, F. Hoffmann, A M. Stuart, and U. Vaes, *Consensus-based sampling*, Studies in Applied Mathematics **148** (2022), no. 3, 1069–1140.

[23] J A. Carrillo, J. Shi, L. Lei, and Z. Yuhua, *A consensus-based global optimization method for high dimensional machine learning problems*, ESAIM: COCV **27** (2021), S5.

[24] J. Chen, S. Jin, and L. lyu, *A consensus-based global optimization method with adaptive momentum estimation*, Communications in Computational Physics **31** (2022), no. 4, 1296–1316.

[25] Y-P. Choi and S. Salem, *Cucker-Smale flocking particles with multiplicative noises: Stochastic mean-field limit and phase transition*, Kinetic & Related Models **12** (2019), no. 3, 573–592.

[26] Y-P. Choi and O. Tse, *Quantified overdamped limit for kinetic vlasov–fokker–planck equations with singular interaction forces*, Journal of Differential Equations **330** (2022), 150–207.

[27] C. Cipriani, H. Huang, and J. Qiu, *Zero-inertia limit: from particle swarm optimization to consensus-based optimization*, SIAM Journal on Mathematical Analysis **54** (2022), no. 3, 3091–3121.

[28] R. Courant, K. Friedrichs, and H. Lewy, *On the partial difference equations of mathematical physics*, IBM journal of Research and Development **11** (1967), no. 2, 215–234.

[29] F. Cucker and S. Smale, *Emergent behavior in flocks*, IEEE Trans. Automat. Control **52** (2007), no. 5, 852–862. MR 2324245

[30] G. Da Prato and J. Zabczyk, *Stochastic equations in infinite dimensions*, Cambridge university press, 2014.

[31] T. Dantzig and J. Mazur, *Number: The language of science*, Penguin, 2007.

[32] A. Dembo, *Large deviations techniques and applications*, Springer, 2009.

[33] M. Dorigo and C. Blum, *Ant colony optimization theory: A survey*, Theoretical computer science **344** (2005), no. 2-3, 243–278.

[34] M H. Duong, A. Lamacz, M A. Peletier, and U. Sharma, *Variational approach to coarse-graining of generalized gradient flows*, Calculus of variations and partial differential equations **56** (2017), no. 4, 65–100.

[35] R. Durrett, *Stochastic calculus: a practical introduction*, CRC press, 2018.

[36] H M. Emara and H A A. Fattah, *Continuous swarm optimization technique with stability analysis*, Proceedings of the 2004 American control conference, vol. 3, IEEE, 2004, pp. 2811–2817.

[37] R. Flamary, N. Courty, A. Gramfort, M.Z. Alaya, A. Boisbunon, S. Chambon, L. Chapel, A. Corenflos, K. Fatras, N. Fournier, L. Gautheron, N T H. Gayraud, H. Janati, A. Rakotomamonjy, I. Redko, A. Rolet, A. Schutz, V. Seguy, D J. Sutherland, R. Tavenard, A. Tong, and T. Vayer, *POT: Python Optimal Transport*, Journal of Machine Learning Research **22** (2021), no. 78, 1–8.

[38] D B. Fogel, *Evolutionary computation: toward a new philosophy of machine intelligence*, John Wiley & Sons, 2006.

[39] M. Fornasier, H. Huang, L. Pareschi, and P. Sünnen, *Consensus-based optimization on hypersurfaces: Well-posedness and mean-field limit*, Mathematical Models and Methods in Applied Sciences **30** (2020), no. 14, 2725–2751.

[40] ———, *Consensus-based optimization on the sphere: Convergence to global minimizers and machine learning*, The Journal of Machine Learning Research **22** (2021), no. 1, 10722–10776.

[41] ———, *Anisotropic diffusion in consensus-based optimization on the sphere*, SIAM Journal on Optimization **32** (2022), no. 3, 1984–2012.

[42] M. Fornasier, T. Klock, and K. Riedl, *Consensus-based optimization methods converge globally*, arXiv:2103.15130 (2021).

[43] ———, *Convergence of anisotropic consensus-based optimization in mean-field law*, Applications of Evolutionary Computation: 25th European Conference, EvoApplications 2022, Held as Part of EvoStar 2022, Madrid, Spain, April 20–22, 2022, Proceedings, Springer, 2022, pp. 738–754.

[44] H. Fumio, *Econometrics*, Princeton University Press, 2000.

[45] A H. Gandomi, G J. Yun, Yang. X-S., and S. Talatahari, *Chaos-enhanced accelerated particle swarm optimization*, Communications in Nonlinear Science and Numerical Simulation **18** (2013), no. 2, 327–340.

[46] G. Garrigos, L. Rosasco, and S. Villa, *Convergence of the forward-backward algorithm: beyond the worst-case with the help of geometry*, Mathematical Programming (2022).

[47] D. Gilbarg and N.S. Trudinger, *Elliptic partial differential equations of second order*, Classics in Mathematics, Springer Berlin Heidelberg, 2001.

[48] F. Golse, *The mean-field limit for the dynamics of large particle systems*, Journées équations aux dérivées partielles (2003), 1–47.

[49] S. Grassi, H. Huang, L. Pareschi, and J. Qiu, *Mean-field particle swarm optimization*, Modeling and Simulation for Collective Dynamics, IMS Lecture Notes Series **40** (2023), 127–194.

[50] S. Grassi and L. Pareschi, *From particle swarm optimization to consensus based optimization: stochastic modeling and mean-field limit*, Mathematical Models and Methods in Applied Sciences **31** (2021), no. 08, 1625–1657.

[51] S Y. Ha, S. Jin, and D. Kim, *Convergence of a first-order consensus-based global optimization algorithm*, Mathematical Models and Methods in Applied Sciences **30** (2020), no. 12, 2417–2444.

[52] S-Y. Ha, S. Jin, and D. Kim, *Convergence and error estimates for time-discrete consensus-based optimization algorithms*, Numerische Mathematik **147** (2021), no. 2, 255–282.

[53] W K. Hastings, *Monte Carlo sampling methods using Markov chains and their applications*, Biometrika **57** (1970), no. 1, 97–109.

[54] J H. Holland, *Adaptation in natural and artificial systems: an introductory analysis with applications to biology, control, and artificial intelligence*, MIT press, 1992.

[55] R. Holley and D. Stroock, *Simulated annealing via sobolev inequalities*, Communications in Mathematical Physics **115** (1988), no. 4, 553–569.

[56] E H. Houssein, A G. Gad, K. Hussain, and P N. Suganthan, *Major advances in particle swarm optimization: Theory, analysis, and application*, Swarm and Evolutionary Computation **63** (2021), 100868.

[57] H. Huang, *A note on the mean-field limit for the particle swarm optimization*, Applied Mathematics Letters **117** (2021), 107133.

[58] H. Huang, J-G. Liu, and P. Pickl, *On the mean-field limit for the Vlasov-Poisson-Fokker-Planck system*, J. Stat. Phys. **181** (2020), no. 5, 1915–1965. MR 4179791

[59] H. Huang and J. Qiu, *On the mean-field limit for the consensus-based optimization*, Mathematical Methods in the Applied Sciences **45** (2022), no. 2, 7814–7831.

[60] H. Huang, J. Qiu, and K. Riedl, *On the global convergence of particle swarm optimization methods*, arXiv preprint arXiv:2201.12460 (2022).

[61] P-E. Jabin, *A review of the mean field limits for Vlasov equations*, Kinetic & Related Models **7** (2014), no. 4, 661.

[62] P-E. Jabin and Z. Wang, *Mean field limit for stochastic particle systems*, Active Particles, Volume 1, Springer, 2017, pp. 379–402.

[63] M. Jamil and X S. Yang, *A literature survey of benchmark functions for global optimisation problems*, International Journal of Mathematical Modelling and Numerical Optimisation **4** (2013), no. 2, 150–194.

[64] S. Jin, L. Li, and J G. Liu, *Random Batch Methods (RBM) for interacting particle systems*, Journal of Computational Physics **400** (2020), 108877.

[65] J. Kennedy, *The particle swarm: social adaptation of knowledge*, Proceedings of 1997 IEEE International Conference on Evolutionary Computation (ICEC'97), IEEE, 1997, pp. 303–308.

[66] ———, *Particle swarm optimization*, Springer US, Boston, MA, 2010.

[67] J. Kennedy and R. Eberhart, *Particle swarm optimization*, Proceedings of ICNN'95-international conference on neural networks, vol. 4, IEEE, 1995, pp. 1942–1948.

[68] S. Kirkpatrick, C D. Gelatt Jr, and M P. Vecchi, *Optimization by simulated annealing*, Science **220** (1983), no. 4598, 671–680.

[69] J. Larson, M. Menickelly, and S M. Wild, *Derivative-free optimization methods*, Acta Numerica **28** (2019), 287–404.

[70] Y. LeCun and C. Cortes, *MNIST handwritten digit database*, (2010).

[71] C. Li, Y. Liu, A. Zhou, L. Kang, and H. Wang, *A fast particle swarm optimization algorithm with cauchy mutation and natural selection strategy*, Advances in Computation and Intelligence (Berlin, Heidelberg) (L. Kang, Y. Liu, and S. Zeng, eds.), Springer Berlin Heidelberg, 2007, pp. 334–343.

[72] J D C. Little, K G. Murty, D W. Sweeney, and C. Karel, *An algorithm for the traveling salesman problem*, Operations research **11** (1963), no. 6, 972–989.

[73] B. Liu, L. Wang, Y-H. Jin, F. Tang, and D-X. Huang, *Improved particle swarm optimization combined with chaos*, Chaos, Solitons & Fractals **25** (2005), no. 5, 1261–1271.

[74] X. Mao, *Stochastic differential equations and applications*, Elsevier, 2007.

[75] J G. March, *Exploration and exploitation in organizational learning*, Organization science **2** (1991), no. 1, 71–87.

[76] H P. McKean Jr, *A class of Markov processes associated with nonlinear parabolic equations*, Proceedings of the National Academy of Sciences of the United States of America **56** (1966), no. 6, 1907.

[77] S. Motsch and E. Tadmor, *Heterophilious dynamics enhances consensus*, SIAM Rev. **56** (2014), no. 4, 577–621. MR 3274797

[78] A. Neumaier, *Complete search in continuous global optimization and constraint satisfaction*, Acta Numerica **13** (2004), 271–369.

[79] A. Nickabadi, M M. Ebadzadeh, and R. Safabakhsh, *A novel particle swarm optimization algorithm with adaptive inertia weight*, Applied soft computing **11** (2011), no. 4, 3658–3670.

[80] I H. Osman and G. Laporte, *Metaheuristics: A bibliography*, 1996.

[81] N. Otsu, *A threshold selection method from gray-level histograms*, IEEE transactions on systems, man, and cybernetics **9** (1979), no. 1, 62–66.

[82] M E H. Pedersen, *Good parameters for particle swarm optimization*, Hvass Lab., Copenhagen, Denmark, Tech. Rep. HL1001 (2010), 1551–3203.

[83] R. Pinnau, C. Totzeck, O. Tse, and S. Martin, *A consensus-based model for global optimization and its mean-field limit*, Mathematical Models and Methods in Applied Sciences **27** (2017), no. 1, 183–204.

[84] E. Platen, *An introduction to numerical methods for stochastic differential equations*, Acta Numerica **8** (1999), 197–246.

[85] R. Poli, *Mean and variance of the sampling distribution of particle swarm optimizers during stagnation*, IEEE Transactions on Evolutionary Computation **13** (2009), no. 4, 712–721.

[86] R. Poli, J. Kennedy, and T. Blackwell, *Particle swarm optimization*, Swarm intelligence **1** (2007), no. 1, 33–57.

[87] K. Riedl, *Leveraging memory effects and gradient information in consensus-based optimization: On global convergence in mean-field law*, arXiv.2211.12184 (2022).

[88] F. Santambrogio, *Optimal transport for applied mathematicians*, Birkhäuser, 2015.

[89] B I. Schmitt, *Convergence analysis for particle swarm optimization*, FAU University Press, 2015.

[90] Y. Shi and R. Eberhart, *A modified particle swarm optimizer*, 1998 IEEE international conference on evolutionary computation proceedings. IEEE world congress on computational intelligence (Cat. No. 98TH8360), IEEE, 1998, pp. 69–73.

[91] R. Storn and K. Price, *Differential evolution–a simple and efficient heuristic for global optimization over continuous spaces*, Journal of global optimization **11** (1997), no. 4, 341–359.

[92] D J. Sumpter, *Collective animal behavior*, Princeton University Press, 2010.

[93] A S. Sznitman, *Topics in propagation of chaos*, Ecole d'été de probabilités de Saint-Flour XIX—1989, Springer, 1991, pp. 165–251.

[94] D. Tian and Z. Shi, *MPSO: Modified particle swarm optimization and its applications*, Swarm and evolutionary computation **41** (2018), 49–68.

[95] C. Totzeck, R. Pinnau, S. Blauth, and S. Schotthöfer, *A numerical comparison of consensus-based global optimization to other particle-based global optimization schemes*, PAMM **18** (2018), no. 1, 1–28.

[96] C. Totzeck and M T. Wolfram, *Consensus-based global optimization with personal best*, Mathematical Biosciences and Engineering **17** (2020), 6026–6044.

[97] C-Y. Tsai, T-Y. Liu, and W-C. Chen, *A novel histogram-based multi-threshold searching algorithm for multilevel colour thresholding*, International Journal of Advanced Robotic Systems **9** (2012), no. 5, 223.

[98] V. Vapnik, *Principles of risk minimization for learning theory*, Advances in neural information processing systems, 1991, pp. 831–838.

[99] D. Wang, D. Tan, and L. Liu, *Particle swarm optimization algorithm: an overview*, Soft computing **22** (2018), no. 2, 387–408.

[100] G. Xu and G. Yu, *On convergence analysis of particle swarm optimization algorithm*, Journal of Computational and Applied Mathematics **340** (2018), 709–717.

[101] X-S. Yang, *Nature-inspired optimization algorithms*, Academic Press, 2020.

[102] X-S. Yang, S. Deb, and S. Fong, *Accelerated particle swarm optimization and support vector machine for business optimization and applications*, Networked Digital Technologies (Berlin, Heidelberg) (Simon Fong, ed.), Springer Berlin Heidelberg, 2011, pp. 53–66.

[103] A. Yegenoglu, K. Krajsek, S D. Pier, and M. Herty, *Ensemble kalman filter optimizing deep neural networks: An alternative approach to non-performing gradient descent*, Machine Learning, Optimization, and Data Science (Cham), Springer International Publishing, 2020, pp. 78–92.

[104] Y. Zhang and X. Kong, *A particle swarm optimization algorithm with empirical balance strategy*, Chaos, Solitons & Fractals: X **10** (2023), 100089.

[105] Y. Zhang, S. Wang, and G. Ji, *A comprehensive survey on particle swarm optimization algorithm and its applications*, Mathematical problems in engineering **2015** (2015).